The influence of molecular parameters on the dimensional stability of injection moulded amorphous thermoplastics

Hut, M.G.T.

Award date:
1994

THE INFLUENCE OF MOLECULAR PARAMETERS ON THE DIMENSIONAL STABILITY OF INJECTION MOULDED AMORPHOUS THERMOPLASTICS.

By
Maarten G.T. Hut

WFW-REPORT 94.030.

Report of the graduate work for the Master Degree of Mechanical Engineering at the Eindhoven University of Technology.

Supervised by:

prof. dr. ir. H.E.H. Meijer
Department of Mechanical Engineering
Eindhoven University of Technology

dr. dipl. ing. R. Wimberger-Friedl
Philips Research Laboratories Eindhoven

Eindhoven, the Netherlands, March 1994

Dedicated to my father,
on the occasion of his 56th birthday.

Eindhoven, March 21st, 1994.

Summary

The scope of this work is to assess the influence of the weight-average molecular weight M_w, the molecular weight dispersion D and the entanglement molecular weight M_e on the dimensional stability of amorphous thermoplastics. Systematic differences in these properties are obtained by using copolycarbonates with varying M_e and polystyrene standards with variation in M_w and D. The material parameters are determined in oscillatory shear, gel permeation chromatography (GPC) and differential scanning calorimetry (DSC) experiments.
As a measure for the potential dimensional instability, the recoverable compliance J_e^0 is determined from oscillatory shear and in steady shear creep and recovery experiments.

The results indicate that the weight average molecular weight M_w does not influence the recoverable compliance significantly. However, J_e^0 was found to increase rapidly with increasing polydispersity, i.e. the width of the molecular weight distribution. A proportional relation between J_e^0 and M_e is observed.

It can be concluded that for a high dimensional stability a polymer should have a narrow molecular weight distribution, contain no low molecular weight additives and have a low M_e, i.e. high chain flexibility resulting in a dense entanglement network.

Samenvatting

De doelstelling van dit werk is het onderzoeken van de invloed van de gewichtsgemiddelde molecuul-massa M_w, de dispersiegraad D (de breedte van de molecuul-gewichtsverdeling) en de gemiddelde molecuul-massa tussen netwerk-knooppunten M_e op de dimensie stabiliteit van amorfe thermoplasten. Een systematische variatie in deze parameters is verkregen door het gebruik van copolycarbonaten met variërende M_e en polystyreen standaarden met variatie in M_w en D. De materiaal parameters zijn bepaald in dynamisch mechanische experimenten en met behulp van gel permeatie chromatografie (GPC) en *differential scanning calorimetry* (DSC).
Als maat voor de potentiële dimensie stabiliteit is de *recoverable compliance* J_e^0 bepaald uit dynamisch mechanische experimenten en uit kruip en reversibele kruip in afschuiving.

Uit de resultaten blijkt dat de gewichtsgemiddelde molecuul-massa M_w geen significante invloed heeft op de *recoverable compliance*. Echter, J_e^0 neemt snel toe met toenemende dispersiegraad. Daarnaast is een proportioneel verband gevonden tussen J_e^0 en M_e.

Aldus kan er geconcludeerd worden, dat voor een hoge dimensie stabiliteit een polymeer een smalle molecuul-gewichtsverdeling moet hebben, geen laag moleculaire additieven bevatten en een lage M_e hebben, i.e. een hoge keten-flexibiliteit resulterend in een hoge vernettingsgraad.

Preface

This study was performed at the Polymers and Organic Chemistry Group of the Philips Research Laboratories in Eindhoven, The Netherlands and took place from June 1993 to March 1994. This report represents the graduate work for the Master Degree of Mechanical Engineering at the Eindhoven University of Technology.

Graduation Committee:

prof. dr. ir. H.E.H. Meijer	Eindhoven University of Technology
dr. dipl. ing. R. Wimberger-Friedl	Philips Research Laboratories Eindhoven
dr. ir. G.W.M. Peters	Eindhoven University of Technology
dr. ir. L.E. Govaert	Eindhoven University of Technology
ir. P.P. Tas	Eindhoven University of Technology, DSM Research

Contents

Summary iii

Samenvatting iv

Preface v

List of Symbols viii

1 Introduction 1

1.1 Injection moulding of amorphous thermoplastics 1

1.2 Dimensional stability and free shrinkage above T_g 1

1.3 Molecular properties 3

1.3.1 The concept of entanglement coupling 4

1.4 Objectives of the project. 5

1.5 Materials with systematic variations in M_e, M_w and D 5

1.6 Outline 6

2 Linear viscoelastic behaviour 7

2.1 Introduction 7

2.2 Models of viscoelastic behaviour 7

2.3 Static deformation 9

2.3.1 Creep and elastic recovery 9

2.4 Dynamic deformation 10

2.4.1 Oscillatory shear 10

2.4.2 Time temperature superposition 12

2.4.2.1 The WLF equation 13

2.4.2.2 The Arrhenius equation 13

2.4.2.3 Temperature density correction 13

3 Experimental 14

3.1. Introduction 14

3.2 DSC and GPC measurements 14

3.3 Rheological Characterization 15
3.3.1 Oscillatory shear experiments 15
3.3.1.1 Determination of M_e 16
3.3.1.2 Determination of J_e^0 16
3.3.1.3 The Cox-Merz viscosity. 16
3.3.2 Steady shear experiments 17
3.3.2.1 Determination of J_e^0 from recovery 18
3.3.2.2 Determination of J_e^0 from creep 18
3.4. Simple extension 19

4 Results and discussion **21**
4.1 Oscillatory shear experiments 21
4.2 Steady shear experiments 23
4.3 Molecular property effects 24
4.3.1 The weight average molecular weight M_w 24
4.3.2 The dispersion *D* 25
4.3.3 The entanglement molecular weight M_e 28

5 Conclusions and recommendations **29**

Bibliography **31**

Appendix A: The Voigt model **34**

Appendix B: Dynamical spectra **36**

Appendix C: Creep and recovery results **59**

Appendix D: Creep and recovery plots **61**

Appendix E: A single Maxwell element **63**

Acknowledgements **65**

List of symbols

α	angular displacement	[rad]
$a_T(T,\omega)$	horizontal shift factor	[-]
$b_T(T,\omega)$	vertical shift factor	[-]
C_p	heat capacity	[J/K]
D	dispersion	[-]
$\delta(t)$	standard impulse function	
$\delta(\omega)$	loss angle	[rad]
ε	strain	[-]
ε_r	reversible strain; shrinkage	[-]
ε_s	creep strain	[-]
$\eta(t)$	viscosity	[Pa s]
η_0	steady state viscosity	[Pa s]
η^*	complex viscosity	[Pa s]
η_d	dynamic viscosity	[Pa s]
$\mathbf{F}$	deformation tensor	
F	force	[N]
$G(\omega)$	relaxation modulus	[Pa]
$G^*(\omega)$	complex modulus	[Pa]
$G_d(\omega)$	dynamic modulus	[Pa]
$G'(\omega)$	storage modulus	[Pa]
$G''(\omega)$	loss modulus	[Pa]
G_N^0	plateau modulus	[Pa]
$\gamma(t)$	shear strain	[-]
$\gamma_{21}(t)$	shear component of strain tensor	[-]
γ_0	shear strain amplitude	[-]
γ_r	maximum recoverable shear strain	[-]
$\dot{\gamma}$	shear rate; time derivative of $\gamma(t)$	[s^{-1}]
h	gap width; sample thickness	[m]
$J(t)$	compliance	[Pa^{-1}]
J_e^0	equilibrium recoverable compliance	[Pa^{-1}]
J_i	instantaneous compliance	[Pa^{-1}]
l	length	[m]

l_0	original length	[m]
l_1	length after creep	[m]
l_2	length after recovery	[m]
M_c	critical molecular weight	[kg/mol]
M_e	entanglement molecular weight	[kg/mol]
M_n	number-average molecular weight	[kg/mol]
M_w	weight-average molecular weight	[kg/mol]
ω	angular frequency	[rad/s]
Ψ_1	primary normal stress coefficient	[Pa s^2]
$\Psi_{1,0}$	limiting primary normal stress coefficient	[Pa s^2]
R	universal gas constant = 8,3144	[J/mol K]
R	sample radius	[m]
ρ	density	[kg/m^3]
S	torque	[N m]
σ	Cauchy stress tensor	
$\sigma(t)$	stress	[Pa]
σ_0, σ_A, σ_B	applied constant stress	[Pa]
σ_{21}	shear component of stress tensor	[Pa]
t	time	[s]
τ	time constant	[s]
τ_k	characteristic retardation time	[s]
T	temperature	[K]
T_0, T_{ref}	reference temperature	[K]
T_g	glass transition temperature	[K]
Θ	angle between cone and plate	[rad]

Chapter 1

Introduction

§ 1.1 Injection moulding of amorphous thermoplastics

Quality demands on injection moulded products are continuously increasing. Injection moulding is a powerful production process that makes it possible to manufacture complexly shaped plastic products in large numbers at short cycle times. An intrinsic problem of this process is, however, that large temperature and pressure gradients occur in time and space and that both the processing parameters and the polymer properties determine the ultimate long term performance of a product. Thermoplastics are attractive materials for injection moulding purposes, because of their good processability [2]. Amorphous thermoplastics are transparent to visible light. They can replace traditional inorganic materials in a number of optical applications such as compact discs, collimator lenses, etc. [3]. For these products high precision and constant (optical) properties are essential. Due to the nature of the materials and the injection moulding process, products show dimensional instabilities in time, caused by mechanisms such as volume relaxation, water absorption and recovery of frozen-in strains. Whereas much attention has been paid to a number of these aspects (e.g. [7, 8, 9, 10]), this report will only focus on the recovery of frozen-in strains.

§ 1.2 Dimensional stability and shrinkage above T_g

In the melt state, i.e. at temperatures high above the glass transition temperature T_g, the long chain molecules of an amorphous thermoplastic are considered to be randomly coiled, without showing any structural order. In this equilibrium state the polymer is unoriented (see Figure 1.1a) and the entropy of the molecules is maximal. To visualize this situation, some authors refer to it as the 'cooked spaghetti' model (Arridge [6]). During the injection stage of the moulding process the melt flows into the mould at high shear rates. The polymer molecules become oriented by the flow field (Figure 1.1b). This molecular orientation is partially frozen-in, because relaxation is prevented by rapid cooling. In time the deformed molecules will tend to return slowly to their equilibrium state, causing dimensional changes. At room temperature, far below T_g, the mobility of the chain molecules is very low so that this process may take several years, thereby making it hardly accessible for experimental investigations. Increasing the temperature accelerates these changes.

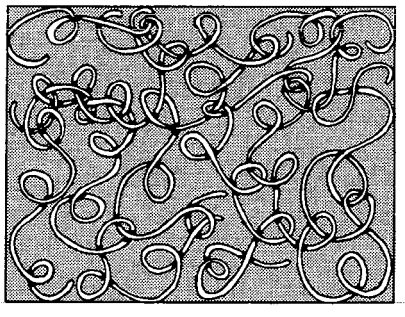

Figure 1.1a
Schematic diagram of an unoriented amorphous polymer [5].

Bringing the temperature of a polymeric solid above its T_g will cause the dimensional changes to take place within an experimentally reasonable time scale. Thus, by examining the free shrinkage above T_g, the frozen-in strain can be determined and the potential dimensional instability of a product can be quantified.

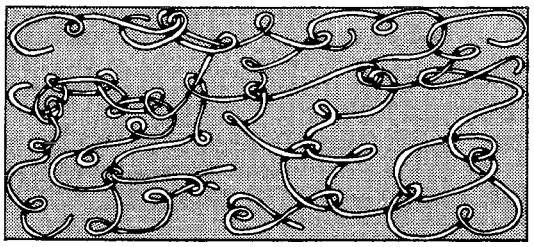

Figure 1.1b
Schematic diagram of an oriented amorphous polymer [5].

The thermo-mechanical history (that entirely determines the momentary state after moulding) is different for each material point of an injection moulded product [3]. It depends on processing conditions, specific material parameters and the geometry of the mould. This results in complicated spatial distributions of the polymer properties within a sample. At Philips, the dimensional stability of injection moulded flat plates has recently been studied by Schennink [9] and Beerens [30] (Figure 1.2). It was found that the relaxation of frozen-in orientation determines to a great extent the long-term dimensional stability of a product. Therefore the control of this orientation, causing anisotropic shrinkage, is crucial.

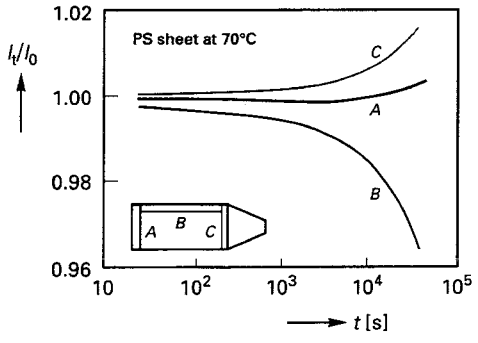

Figure 1.2
Relative dimensional changes (l_t/l_0) vs. time t for an injection moulded flat plate at elevated temperature [9].

The long-term performance of injection moulded products can be influenced by changing process conditions, or by modifying specific material properties; this study aims at the latter.
To assess influences of single molecular properties in a reproducible manner, effects of processing conditions and mould geometry should be excluded. To determine intrinsic material parameters which scale with the potential anisotropy of the dimensional changes of moulded products, well defined experiments have to be performed.

It has been stated [13] that simple shear flow is the most prominent type of deformation in injection moulding. Therefore simple unambiguous creep tests in shear and/or elongation are better suitable to generate orientation and frozen-in strain in a reproducible manner [11].
The maximum recoverable strain γ_r determined from a shrinkage or recovery experiment is a measure for the amount of frozen-in strain. The equilibrium recoverable compliance J_e^0 is defined as the recoverable strain γ_r per unit applied stress, assuming that this stress is uniform for all

material points of a sample. J_e^0 is then a material parameter which is only determined by the properties of the temporary network in the polymer.

By examining this recoverable compliance, a reproducible method has become available to investigate the relation between molecular parameters and the potential dimensional stability.

§ 1.3 Molecular properties

Polymers consist of long chain molecules that are built of small repeating monomeric units. Depending on the method of synthesis, the average chain length and the dispersion, i.e. a measure of the width of distribution of lengths, may vary greatly (Figure 1.3).

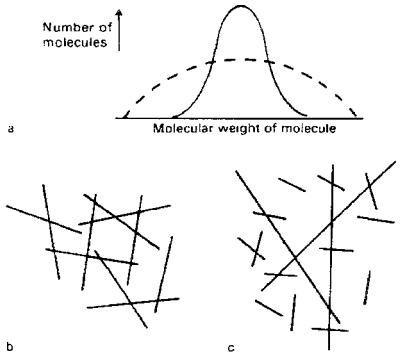

Figure 1.3
Schematic illustration of narrow (b) and broad (c) molecular weight distributions [20].

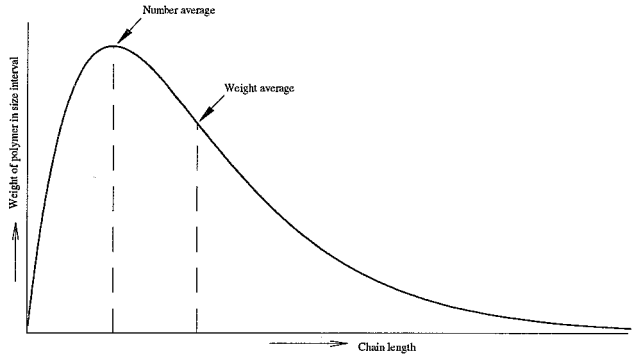

Figure 1.4
Typical molecular mass distribution in a polymer (after Flory [14]).

Both the chemical structure and the molecular mass distribution are fundamental characteristics of polymers. It has become clear that the processing behaviour and many end-use properties of polymers are influenced by both the average molecular mass and the molecular mass distribution [4]. Molecular weight can be defined in different ways, of which the weight average, M_w, and number average, M_n, are the most common (Figure 1.4):

$$M_w = \frac{\Sigma w_i M_i}{\Sigma w_i} \tag{1.1}$$

$$M_n = \frac{\Sigma n_i M_i}{\Sigma n_i} \tag{1.2}$$

M_i is the molar mass of the component molecules of kind i, w_i is the weight-fraction of the component molecules i and n_i is the number-fraction of the component molecules i.

The molecular weight dispersion D is then defined as:

$$D = \frac{M_w}{M_n} \tag{1.3}$$

Another aspect of importance is that the typical properties of polymers are to a great extent determined by the fact that the long chain molecules are physically entangled [15].

§ 1.3.1 The concept of entanglement coupling

Chemically cross-linked polymers are known to show a rubbery behaviour as it was described by Treloar [16]. In amorphous thermoplastics, where a cross-linked network is absent[1], a similar behaviour can be observed above a certain critical molecular weight M_c. This effect is attributed to entanglement coupling. Above M_c temporary physical cross-links occur, because of adjacent chains that become entangled (Figure 1.5).

In this network, junctions are constantly formed and broken up causing a constant concentration of topological constraints. From the dependence of viscosity η on molecular weight M, the critical molecular weight M_c can be determined (Figure 1.6).

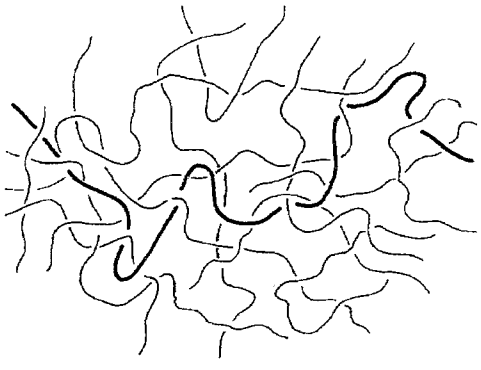

Figure 1.5
Polymer molecule entangled in a mesh of other polymer chains [12].

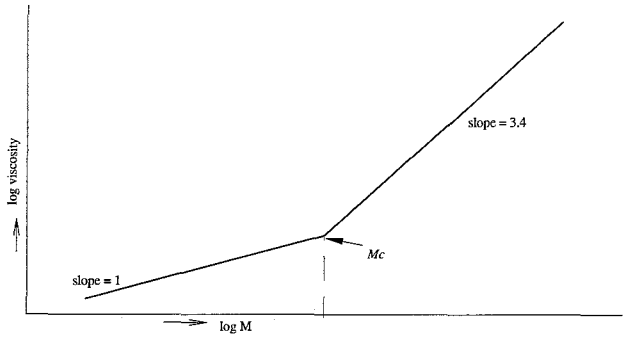

Figure 1.6
Dependence of viscosity on molecular weight. If $M \geq Mc$, then $\eta \propto M^{3,4}$.

M_c is equal to M at the point where the viscosity becomes proportional to $M^{3,4}$ [1].

This concept allows the definition of another important molecular parameter, the entanglement molecular weight M_e, which is considered to be the average molar mass between neighbouring entanglements on a chain molecule. According to the theory of Bueche [27], M_c is related to M_e in a rather complicated manner on the basis of the dragging of one molecule by another, but approximately $M_c \approx 2M_e$.

In his pseudotopological theory [15, 17, 18], Wu states that the chain length of an entanglement strand depends on chain structure through a characteristic ratio C_∞ by:

$$N_v = 3C_\infty^2 \tag{1.4}$$

where N_v is the number of elementary skeletal rotational units in an entanglement strand and C_∞ the characteristic ratio of a coiled chain. This latter parameter is defined as the ratio of the end-to-end distance and the total chain length of a polymer molecule according to:

$$C_\infty = \lim_{n_v \to \infty} \frac{\langle R_0^2 \rangle}{n_v \langle l_v^2 \rangle} \tag{1.5}$$

where $\langle R_0^2 \rangle$ is the mean-square end-to-end distance of an unperturbed chain, n_v the number of

[1] Amorphous thermoplastics are soluble in a suitable solvent.

statistical skeletal units and $<l_v^2>$ the mean-square length of a statistical skeletal bond.
When defined in this way, the characteristic ratio is a measure of the intrinsic stiffness of a coiled chain [15]. According to equation (1.4) it follows [29] that M_e is proportional to the square of the characteristic ratio:

$$M_e \propto C_\infty^2 \tag{1.6}$$

Although the analysis of Wu is theoretically speculative with respect to the physical reality, equation (1.6) has experimentally proven its validity [29]. As will be shown in a later section, the entanglement molecular weight M_e, can be determined from dynamic mechanical measurements in the rubbery state.

§ 1.4 Objectives of the project

Obviously, dimensional stability is an important requirement of injection moulded thermoplastics. Apart from the moulding conditions also the material choice is critical. Additional to existing selection criteria this study aims at addressing molecular properties which affect the dimensional stability.

In this report the influence of the weight-average molecular weight M_w, the molecular weight dispersion D and the entanglement molecular weight M_e on the dimensional stability of amorphous thermoplastics is investigated.
An attempt is made to apply systematic changes in the above mentioned properties and compare their influence on the dimensional stability by investigating the recoverable compliance J_e^0 from simple shear creep and recovery experiments.

For comparison, J_e^0 is also derived from dynamic mechanical experiments, which were performed for the determination of M_e.

§ 1.5 Materials with systematic variations in M_e, M_w and D

To achieve systematical variations in the weight-average molecular weight M_w and exclude dispersion influences at the same time, narrowly distributed ($D \approx 1.05$) polystyrene standards from Polymer Laboratories with molecular weights of about 96, 330, and 560 [kg/mol] are used in this study.

Effects of polydispersity were studied by including Styron 678E from Dow Chemical, a well known [e.g. 8, 9] broad disperse polystyrene with a molecular weight in the range of the above mentioned polystyrenes.

At the Philips Research Laboratories the principle described by equation (1.6), was used to synthesize several copolycarbonates with a systematic variation in the entanglement molecular weight M_e. By adding a restraining spiro-group in different percentages to Bisphenol-A polycarbonate molecules, different chain stiffnesses were obtained. Figure 1.7 shows the chemical structure of the resulting molecule.

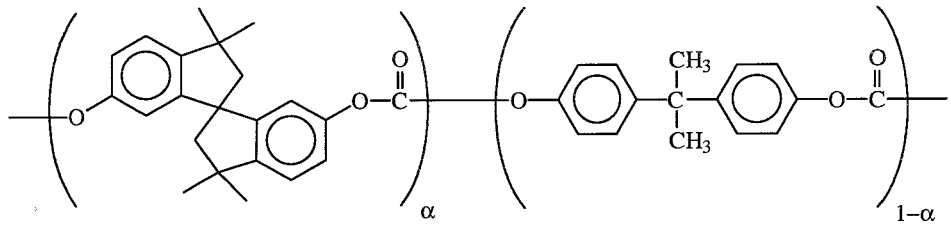

Figure 1.7
Chemical structure of copolycarbonate with spiro group.

The spiro-group suppresses rotation, which has an increasing effect on chain stiffness. The index α denotes the molar percentage of spiro-units.
For this project, copolycarbonates with respective α's of 27, 46, 65 and 86 % where used. For a reference, Makrolon CD2000 from Bayer (100 % Bisphenol-A) was added. Experimental results for this material are widely available [e.g. 8, 9]. For an extra comparison, a spiro copolycarbonate from General Electric and a tetramethylpolycarbonate (TMPC) from Bayer were included in the study.

§ 1.6 Outline

In the next chapter aspects of linear viscoelastic theory are reviewed, followed by a chapter on the experimental methods and the materials that were used in the investigations. In chapter 4 the results of these experiments are presented, compared to literature and discussed. Final conclusions and recommendations for future research are given in chapter 5.

Chapter 2

Linear viscoelastic behaviour

§ 2.1 Introduction

Polymeric systems are viscoelastic materials, that exhibit a combination of elastic and viscous behaviour. An interesting feature of amorphous thermoplastics is that the contribution of both shares is depending on temperature and the experimentally chosen time scale.
A general constitutive relation describing viscoelastic behaviour is given by [19]:

$$\sigma(\xi,t) = N\{\mathbf{F}(\xi,\tau) \,|\, \tau \le t\} \tag{2.1}$$

where σ represents the Cauchy stress, ξ the position of a material point, t the time and $\boldsymbol{F}$ denotes the deformation tensor. The equation shows that the stress in a material point only depends upon the deformation history of that point. In matrix representation, the stress tensor can be written as:

$$\sigma = \begin{bmatrix} \sigma_{11} & \sigma_{12} & \sigma_{13} \\ \sigma_{21} & \sigma_{22} & \sigma_{23} \\ \sigma_{31} & \sigma_{32} & \sigma_{33} \end{bmatrix} \tag{2.2}$$

Under assumption that the mechanical properties of the material are time invariant[1], the material behaviour is geometrically and physically linear and that the Boltzmann superposition principle[2] is valid, straight forward linear viscoelastic theories can be applied to describe the material behaviour. In the case of simple shear, the following equations for stress σ_{21} and strain γ_{21} can be derived:

$$\sigma_{21}(t) = \int_{\tau=-\infty}^{t} G(t-\tau)\dot{\gamma}_{21}(\tau)\,d\tau \tag{2.3}$$

$$\gamma_{21}(t) = \int_{\tau=-\infty}^{t} J(t-\tau)\dot{\sigma}_{21}(\tau)\,d\tau \tag{2.4}$$

where $G(t)$ is the relaxation modulus and $J(t)$ is the creep compliance, $\dot{\gamma}_{21}(t)$ and $\dot{\sigma}_{21}(t)$ are time derivatives of strain and stress respectively.

§ 2.2 Models of viscoelastic behaviour

To model viscoelasticity, use can be made of simple elastic and viscous elements, such as springs and dashpots. An ideal spring stores all deformation energy and returns it after the external forces

[1] Physical aging effects are negligible on the time scale that is considered.

[2] Proportionality and superposition in excitation and response.

are removed, by reverting exactly to its original length according to Hooke's law: $\sigma_{21} = G(t) \cdot \gamma_{21}$. An ideal dashpot flows irreversibly under the action of external forces and dissipates all energy, which is described by Newton's law: $\sigma_{21} = \eta(t) \cdot \dot{\gamma}_{21}$.

The most commonly used basic models for viscoelasticity consist of a single spring and a single dashpot, either in series[3] or in parallel[4]. Since real materials exhibit a range of relaxation times, multi-mode models are more appropriate to characterize them.
A discrete expression for the compliance *J(t)* of a viscoelastic liquid can be obtained by looking at a generalized Voigt model (retarded elastic response) in series with an instantaneous elasticity J_i and a dashpot accounting for the viscous contribution (Figure 2.1) .

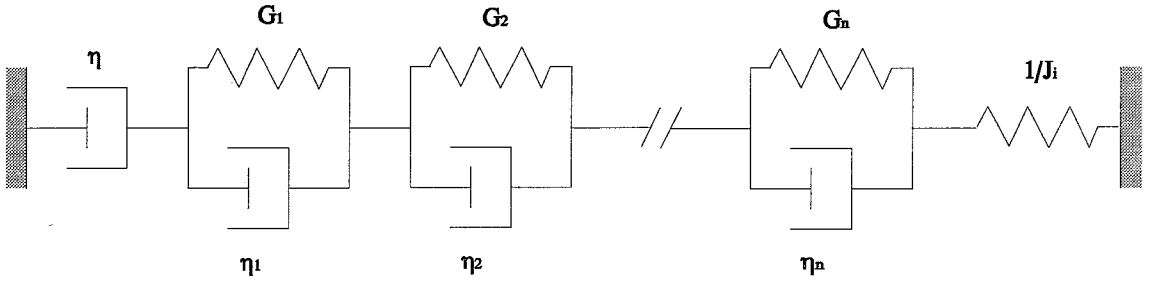

Figure 2.1
Generalized Voigt model, in series with a Maxwell model; also known as extended Burgers model [4].

In Appendix A the stress-strain relations for a single Voigt element are written down. For the multi-mode model it follows that:

$$J(t) = J_i + \sum_{k=1}^{N} f_k \left[1 - e^{-\frac{t}{\tau_k}}\right] + \frac{t}{\eta} \tag{2.8}$$

with f_k a constant equal to $1/G_k$, $\tau_k = \eta_k/G_k$ a characteristic retardation time and η the steady state viscosity. For an infinite number of elements, the Voigt model represents a continuous spectrum of retardation times, $f(\tau)$, defined by a continuous analogon of equation (2.8):

$$J(t) = J_i + \int_{\tau=0}^{\infty} f(\tau) \left[1 - e^{-\frac{t}{\tau}}\right] d\tau + \frac{t}{\eta} \tag{2.9}$$

where $f(\tau)$ is a function of f_k and a standard impulse function $\delta(t)$:

$$f(\tau) = \sum_{k=1}^{N} f_k \, \delta(\tau - \tau_k) \tag{2.10}$$

The compliance J_i is an hypothetical initial elasticity that must be added to allow for the possibility of a discrete contribution with $\tau = 0$. This compliance is experimentally hardly accessible, but must

[3] Also known as the Maxwell model, and often used to describe stress relaxation.

[4] Also known as the Kelvin or Voigt model, which is commonly used to describe creep.

be present, otherwise instantaneous deformation would require infinite stress. More details are given by Ferry [1] and Oomens [19].

§ 2.3 Static Deformation

Steady shear flow provides an elegant way to subject every element of a material to a well-defined history. Essentially two major variants are available to achieve steady state creep: applying a constant shear rate $\dot{\gamma}_{21}$, or a constant stress σ_0. The latter will be described in more detail below, for the case of a viscoelastic liquid.

§ 2.3.1 Creep and elastic recovery

Particularly interesting is the situation where a creep experiment has progressed for some time and the stress is then suddenly removed, causing a reverse deformation called creep recovery. This can be described as follows: a stress $\sigma_A = \sigma_0$ is applied at t = 0 followed by additional stress $\sigma_B = -\sigma_0$ at $t = t_2$, the total strain at time t is found according to equation (2.4):

$$\gamma(t) = \sigma_A J(t) + \sigma_B J(t - t_2) \tag{2.11}$$

For a viscoelastic liquid (amorphous polymer above T_g) the shear creep followed by recovery is shown schematically in Figure 2.2. After a sufficiently long time ($0 \ll t < t_2$) when a steady-state flow is reached, the creep strain is given by:

$$\gamma(t) = \sigma_0 \left(J_e^0 + \frac{t}{\eta_0}\right) \tag{2.12}$$

where J_e^0 is the steady-state compliance and η_0 a Newtonian viscosity. $\sigma_0 \cdot J_e^0$ represents the elastic part of the strain in the generalized Voigt model presented at the previous page for the case of constant stress and steady-state deformation. Accordingly, the viscosity $\eta = \eta_0$ accounts for the viscous contribution in equations (2.8) and (2.9). During recovery ($t > t_2$) the strain can be written as:

$$\gamma(t) = \sigma_0 \left(J_e^0 + \frac{t_2}{\eta_0} - J(t - t_2) \right) \tag{2.13}$$

The compliance J_e^0 is also called the equilibrium recoverable compliance. Together with the applied stress σ_0 it determines the final elastic response of a material.

Recording strain recovery after an instantaneous stress removal provides a simple way of measuring the elastic recovery. This recovery is directly related to the internal strain [20]. Suddenly removing the stress during steady-state creep in an isothermal experiment, can be considered similar to deforming above T_g, freezing in and subsequently releasing the frozen-in strain by free shrinkage above T_g.

An apparatus specifically designed to measure strain recovery after constant-stress deformation will be discussed in the next chapter.

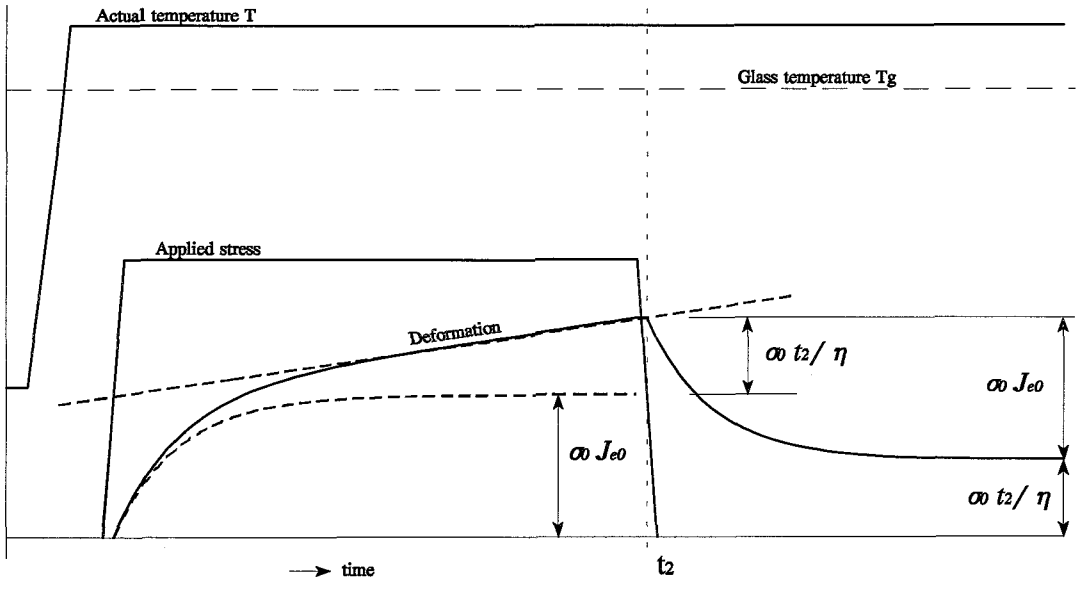

Figure 2.2
Shear creep and creep recovery shown schematically for a viscoelastic liquid, e.g. an uncrosslinked polymer (after Ferry [1]).

§ 2.4 Dynamic Deformation

Rheological properties describing the material behaviour of a molten polymer can be determined with oscillatory shear experiments. By imposing a small amplitude harmonic strain on a sample, a sinusoidal stress response (with a different amplitude and out of phase with the strain input) can be measured. In the next section the most important theoretical relations are given and it will be shown that some steady-state properties can be calculated from limiting values of dynamical properties for zero frequency.

§ 2.4.1 Oscillatory shear

An harmonic shear strain excitation can be written as:

$$\gamma(t) = \gamma_0 \cos(\omega t) = \gamma_0 \Re(e^{i\omega t}) \tag{2.14}$$

with γ_0 the dynamic strain amplitude and ω the angular frequency. The latter expression $\Re$ denotes the real part of a complex input signal with complex unity *i*. In the linear viscoelastic regime, the stress response will also be harmonic, but with a different amplitude and out of phase with the input (Figure 2.3):

$$\sigma_{21}(t) = \gamma_0 \Re(G^* e^{i\omega t}) = \gamma_0 G_d \Re(e^{i(\omega t + \delta)}) \tag{2.15}$$

where G^* is the complex modulus and $G_d = |G^*|$. The loss angle δ denotes the phase shift between stress and strain.

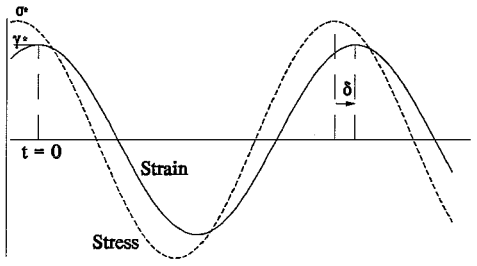

Figure 2.3
Stress response to harmonic strain excitation. σ^* is the stress amplitude and δ the phase lag.

Equation (2.15) can also be expressed in terms of a storage modulus G', which is in phase with γ and a loss modulus G'', which is $\pi/2$ radians out of phase with γ:

$$\sigma_{21}(t) = \gamma_0(G'\sin(\omega t) + G''\cos(\omega t)) \tag{2.16}$$

Dynamic modulus G_d and loss angle δ are respectively defined as:

$$G_d = \sqrt{(G')^2 + (G'')^2} \tag{2.17}$$

$$\tan(\delta) = \frac{G'}{G''} \tag{2.18}$$

When loss angle $\delta = 0$, the behaviour is purely elastic, for $\delta = \pi/2$ it is purely viscous

Analogously, a dynamical viscosity $\eta_d = |\eta^*|$ can be defined from the complex viscosity η^*:

$$\eta^* = \eta' - i\eta'' = \frac{G''}{\omega} - i\frac{G'}{\omega} \tag{2.19}$$

It follows directly that the limiting value of the dynamical viscosity for zero shear rate, is equal to:

$$\eta_0 = \lim_{\omega \to 0}\left(\frac{G''}{\omega}\right) \tag{2.20}$$

A consequence of shearing deformations is the appearance of normal stresses. For simple shear equation (2.2) becomes:

$$\sigma = \begin{bmatrix} \sigma_{11} & \sigma_{12} & 0 \\ \sigma_{21} & \sigma_{22} & 0 \\ 0 & 0 & \sigma_{33} \end{bmatrix} \tag{2.21}$$

Thus, even though the rate of strain tensor has only a $\dot{\gamma}_{12} = \dot{\gamma}_{21} = \dot{\gamma}$ component, the stress tensor has different diagonal elements.

Accordingly, the primary normal stress coefficient Ψ_1 can be defined as [1]:

$$\Psi_1 = \frac{(\sigma_{11} - \sigma_{22})}{\dot{\gamma}^2} \tag{2.22}$$

Coleman et al. [21] have predicted the limiting value of the primary normal stress coefficient for vanishing shear to be:

$$\Psi_{1,0} = \lim_{\omega \to 0}\left(\frac{2G'}{\omega^2}\right) \tag{2.23}$$

where several models [21, 22] predicted the following relation:

$$\Psi_{1,0} = 2\eta_0^2 J_e^0 \tag{2.24}$$

Combining equations (2.23) and (2.24), an expression for the recoverable compliance J_e^0 can be derived:

$$J_e^0 = \lim_{\omega \to 0}\left(\frac{G'}{(G'')^2}\right) \tag{2.25}$$

For $G'' \gg G'$, which is usually a reasonable assumption in the limiting zone, this equation corresponds to a relation given by others [23, 24]:

$$J_e^0 \equiv \lim_{\omega \to 0}\left(\frac{G'}{(G')^2 + (G'')^2}\right) \tag{2.26}$$

§ 2.4.2 Time temperature superposition

For viscoelastic materials, changes in time and temperature have an equivalent influence on shear moduli and viscosity [25]. This means that a set of isothermal curves of similar form that are measured in the same frequency range can be shifted onto one mastercurve by a horizontal shift along the frequency axis as shown schematically in Figure 2.4.

Thus by performing experiments at several different temperatures, the experimental time window can be broadened extensively. Materials for which this time temperature superposition principle is valid for all viscoelastic functions, are called thermorheologically simple.

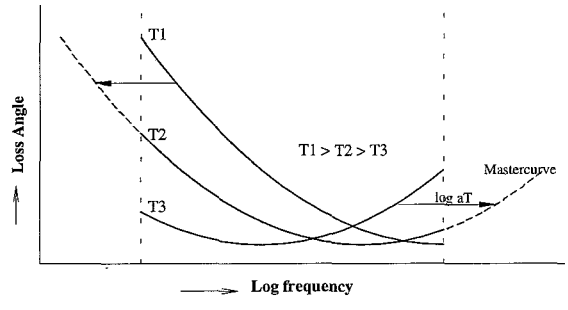

Figure 2.4
Time temperature equivalence. The curves shift without changing in shape.

The temperature dependent shiftfactor a_T is defined as follows:

$$\begin{aligned} \delta(\log\ \omega, T) &= \delta(\log\ \omega a_T, T_0) \\ G(\log\ \omega, T) &= b_T G(\log\ \omega a_T, T_0) \end{aligned} \tag{2.27}$$

where T_0 is the reference temperature, corresponding with the temperature of the mastercurve and b_T is a correction factor that accounts for changes in density with temperature. Both a_T and b_T are a function of T and T_0. First a_T is determined by horizontally shifting the loss angle δ. After a_T is applied to the viscoelastic function G, the vertical shiftfactor b_T can be determined.

This time-temperature equivalence principle can also be applied to creep behaviour in a similar way. For amorphous polymers above T_g several procedures governing the temperature dependence of the shiftfactor are available.

§ 2.4.2.1 The WLF equation

It was found by Williams, Landel and Ferry [26], that for amorphous polymers, in the range between T_g and 100 K above T_g, the shift factor a_T is governed by:

$$\log a_T = - \frac{c_1 (T - T_0)}{c_2 + T - T_0} \tag{2.28}$$

with material constants c_1 and c_2. The WLF equation is extensively described by Ferry [1].

§ 2.4.2.1 The Arrhenius equation

For temperatures above T_g + 100 K, an Arrhenius-type equation can be applied to model the temperature dependence of a_T:

$$\ln a_T = \frac{E_{act}}{R} \left(\frac{1}{T} - \frac{1}{T_0}\right) \tag{2.29}$$

where E_{act} is an activation energy and R is the universal gas constant. More details are given by van Krevelen [4].

§ 2.4.2.1 Temperature density correction

The vertical shift b_T in the melt state can be modelled by a temperature density correction [1] according to:

$$b_T = \frac{\rho\ T}{\rho_0\ T_0} \tag{2.30}$$

with temperature dependent density ρ. The index *0* refers to the reference temperature.

Chapter 3

Experimental

§ 3.1 Introduction

This chapter contains a description of the experiments performed for the material characterization and the rheological characterization. The methods that were followed for the determination of M_e and J_e^0 are reviewed. A section on simple extension is added.

§ 3.2 DSC and GPC measurements

Glass transition temperatures were determined on a Perkin Elmer DSC-7. At rates of 10 [K/min] samples were heated and cooled twice from at least 50 [K] below to about 100 [K] above the expected glass transition temperature. T_g was determined during the second heating stage from the sudden change in heat capacity C_p that occurs at the glass transition. The results of these measurements are given in Table 3.1. More details on differential scanning calorimetry are given by Turi [36].

Gel permeation chromatography measurements were performed to determine M_w, M_n and D. Narrow disperse polystyrene standards are used for calibration of the GPC column, so values are calculated relative to polystyrene. The results of these experiments are also shown in Table 3.1. The GPC method is described more extensively by Braam [37].

Table 3.1
Results of differential scanning calorimetry and gel permeation chromatography.

DSC & GPC Experiments	T_g [K]	$<M_w>$ [kg/mol]	$<M_n>$ [kg/mol]	D [-]	Remarks
PS678E	361.0	264	63.0	4.2	T_g=366 [K] [32]
PS96	376.2	94.3	90.7	1.04	GPC-data of PS standards as provided by manufacturer (Polymer Laboratories)
PS330	377.3	327	316	1.04	
PS560	378.7	555	553	1.06	
CD2000	414.6	32	13.0	2.4	T_g=412 [K] [32]
Spiro PC 27%	455.7	460	60.0	7.7	
Spiro PC 46%	471.1	460	92.0	5.0	
Spiro PC 65%	479.8	155	39.0	4.0	
Spiro PC 86%	490.3	59.0	48.5	1.22	
GE Spiro PC	478.5	64	9.0	7.1	Caudiform
TMPC	469.3	38	10.0	3.8	

Caudiform indicates the presence of a small low molecular peak in the chromatogram.

The relatively small value of D = 1.22 for the material with 86% spiro is caused by the fact that a low molecular fraction was removed to decrease the brittleness of this material.

§ 3.3 Rheological Characterization

All materials were vacuum dried at about 20 [K] below T_g and moulded into cylindrical samples in a Fonteyne flat plate press using a maximum compression force of about 100 [kN]. The discs were checked for residual stress before the experiments, by looking at birefringence. For most materials less than 5 [g] was available for testing. All experiments were carried out under nitrogen conditions.

§ 3.3.1 Oscillatory shear experiments

The linear viscoelastic properties are determined by oscillatory shear experiments, that were carried out on a Rheometrics Dynamic Spectrometer RDS-II at the Eindhoven University of Technology. Cylindrical samples were used in a plate-plate geometry.
By imposing a small amplitude sinusoidal shear strain on a sample above T_g, the response can be measured. First, a strain sweep at a set frequency was performed to determine the extent of the linear viscoelastic regime. This was followed by a number of isothermal frequency sweeps at different temperatures. A correction of 2 [μm/K] was applied to the gapwidth, accounting for expansion of the plates. Excess material at the outer edge of the plates was removed during the experiments, if possible.
Thermal instabilities of both oven and polymer melt significantly affect experimental results, especially for high T_g polymers. For this reason, frequency sweeps are usually started at high frequencies.

The first experiment is performed at the chosen reference temperature, followed by a number of experiments at lower temperatures. After the lowest temperature is reached ($T \approx T_g$ + 20 [K]), the temperature is raised to above the reference temperature.
Mastercurves are obtained, by applying the time temperature superpositon principle as described in § 2.4.2. First the loss angle δ is shifted horizontally along the frequency axis onto a mastercurve. After this horizontal shift is applied to the dynamic modulus G_d, the vertical shift can be determined.

The temperature dependence of the horizontal shiftfactor a_T is modelled by WLF and Arrhenius type fits, using equations (2.28) and (2.29). The vertical shiftfactor b_T was described by a temperature density correction according to equation (2.30).

The density ρ depends on the temperature as follows:

$$\rho = \rho_0 - \Delta T \cdot 9\alpha \tag{3.1}$$

where ρ_0 is the density at 293 [K], and α is the linear coefficient of thermal expansion. For polystyrene $\rho_0 = 1.05 \cdot 10^3$ [kg/m^3] and $\alpha = 7 \cdot 10^{-5}$ [K^{-1}] and for polycarbonate $\rho_0 = 1.20 \cdot 10^3$ [kg/m^3] and $\alpha = 6.8 \cdot 10^{-5}$ [K^{-1}] [39, 40]. For the temperature correction of polystyrene melts, an additional relation given by Wales [41] is available:

$$\rho T = 400 + 0.82(T - 398) \tag{3.2}$$

§ 3.3.1.1 Determination of M_e

According to a relation given by Wu [15], the entanglement molecular weight M_e can be calculated from the mastercurve of the storage modulus G' by:

$$M_e = \frac{\rho R T}{G_N^0} \tag{3.3}$$

with ρ the density, R the universal gas constant, T the absolute temperature and G_N^0 the plateau modulus, defined as:

$$G_N^0 = [G']_{\tan \delta \rightarrow \text{minimum}} \tag{3.4}$$

This method is illustrated in Figure 3.1.

§ 3.3.1.2 Determination of J_e^0

It appears that the G' and G'' curves at low frequencies show slopes of respectively 2 and 1 on double logarithmic scales [42]. This means that the ratio defined in equation (2.25) remains constant with decreasing frequency when these slopes are reached. Thus a method, which is depicted in Figure 3.2, for the determination of the recoverable compliance J_e^0 from dynamic measurements in the melt state has become available.

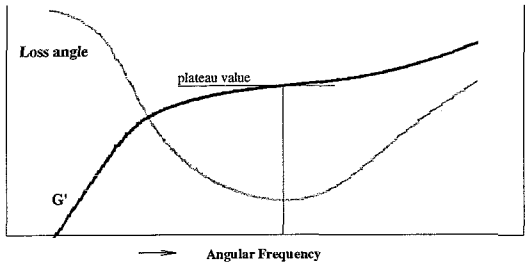

Figure 3.1
Schematical representation of the plateau modulus G_N^0.

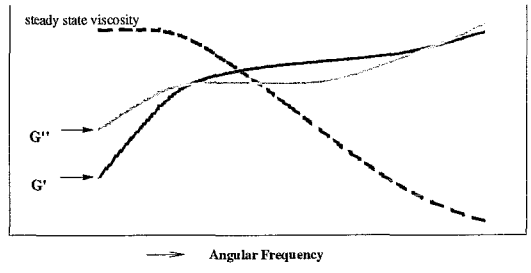

Figure 3.2
The recoverable compliance can be calculated from limiting values of G' and G'', if slopes 2 and 1 are reached.

§ 3.3.1.3 The Cox-Merz Viscosity

An empirical rule relating the absolute value of the complex viscosity to the viscosity measured in

a linear shear flow was derived by Cox and Merz [43]:

$$\eta(\dot{\gamma}) = |\eta^*(\omega)|_{\omega=\dot{\gamma}} = \sqrt{(\eta'(\omega))^2 + (\eta''(\omega))^2}\,|_{\omega=\dot{\gamma}} \tag{3.5}$$

where the index indicates that the angular frequency is equal to the shear rate.
This rule makes it possible to translate results from small amplitude oscillatory shear to large strain steady flow fields, which are dominating in processing. Figure 3.2 illustrates the frequency dependence of the complex viscosity. For low frequencies, the dynamic viscosity becomes equal to the steady state viscosity η_0.

§ 3.3.2 Steady shear experiments

At DSM Research a self constructed rheogoniometer, specifically designed to measure strain recovery after a steady shear flow, is in use. It consists of two parallel plates (Figure 3.3) in a small oven. While the lower one is fixed, the upper plate can rotate virtually frictionless by means of an air bearing. The angular displacement α of this plate can be recorded contactless with an optical encoder. The smallest displacement detectable is equal to $\alpha = 1.26 \cdot 10^{-4}$ [rad]. When a sample is put in between the two plates and a constant torque S is applied, as schematically shown in Figure 3.4, an experiment can be performed similar to the method described in § 2.3.1.

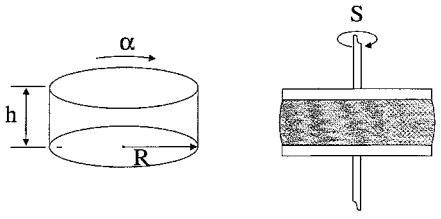

Figure 3.3
Torsion between parallel plates.

Relations of strain and stress, valid for small strains, are as follows [1]:

$$\gamma_{21} = \frac{\alpha R}{h} \tag{3.6}$$

$$\sigma_{21} = \frac{2S}{\pi R^3} \tag{3.7}$$

where R is the radius of the sample, h is its thickness and S is the torque applied.
For this study a cone and plate geometry (Figure 3.5) was preferred in order to subject every element of a sample to an identical and well defined history. Equations (3.6) and (3.7) then become:

$$\gamma_{21} = \frac{\alpha}{\Theta} \tag{3.8}$$

$$\sigma_{21} = \frac{3S}{2\pi R^3} \tag{3.9}$$

where Θ is the angle between cone and plate.

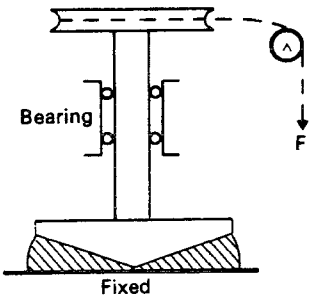

Figure 3.4
The principle of a constant stress rheogoniometer [20].

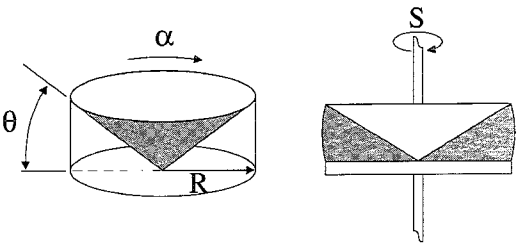

Figure 3.5
Torsion between cone and plate.

The constant stress rheogoniometer was originally designed to test low T_g polymers. At temperatures near 250 °C problems due to heat leakage and thermal expansion of the apparatus may arise. Furthermore normal forces can not be recorded and must be controlled manually.

Several methods that were used to determine the recoverable compliance from either creep or recovery are shortly discussed in the following sections.

§ 3.3.2.1 Determination of J_e^0 from recovery

When a recovery experiment has progressed for a sufficiently long time, J_e^0 can be determined directly from the limiting value of the recoverable strain γ_r, as was illustrated in Figure 2.2:

$$J_e^0 = \lim_{t \to \infty} \frac{\gamma_r}{\sigma_0} \tag{3.10}$$

where σ_0 is the constant stress that was applied during creep. The use of recoverable shear as the prime measure of elastic response has the additional advantage that, while it is being measured, it is the only thing which is happening [20]. Determined this way, J_e^0 is no longer influenced by start-up transients, but depends on long term processes. Using this method, the steady state viscosity η_0 still depends on the absolute value of the final creep strain

The time-scale at which final recovery takes place depends on a number of factors, including molecular weight and dispersity. However, for numerous reasons experimenting times are limited, which may cause underestimation of J_e^0. Here, recovery times in the range between 1000 and 2000 [s] were used.

§ 3.3.2.2 Determination of J_e^0 from creep

In this study two methods were applied to determine the recoverable compliance from the creep experiment. When, after a sufficiently long time the slope of the compliance $J(t)$ against time on a double logarithmic scale has become equal to 1, the behaviour is governed by linear viscoelasticity according to equation (2.12).

Figure 3.6 shows how J_e^0 can be determined from linear regression of $J(t)$ versus time on linear scales.

A similar method was introduced by Sherby and Dorn [33] and is illustrated in Figure 3.7. A plot of the shear rate (determined from the creep curve) against the shear strain, should approach to a constant value $\dot{\gamma}_0$. This constant shear rate accounts for the viscous contribution in time and if subtracted from the shear strain γ, the elastic contribution can be separated from the total strain.

This allows the determination of J_e^0, from the shear strain against time.

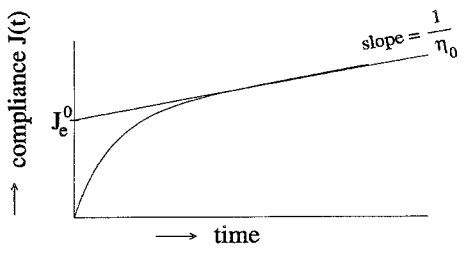

Figure 3.6
The recoverable compliance can be calculated from the intercept of a regression line at t=0.

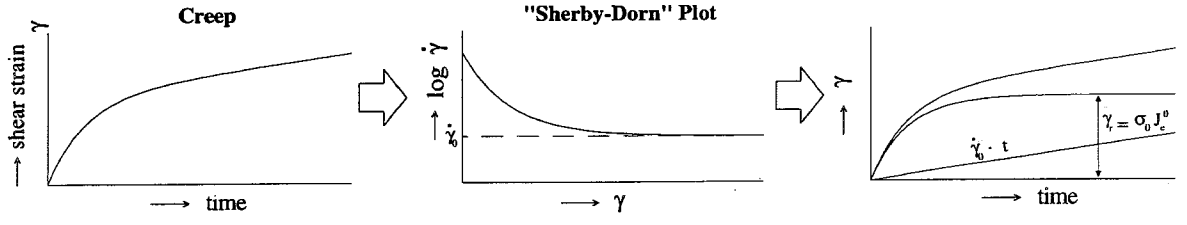

Figure 3.7
The elastic part of the total strain can be determined according to Sherby and Dorn [33]. As a result, the recoverable compliance J_e^0 can be calculated.

Even though long term constant rates may be achieved quite easily, results of these two methods are very sensitive to the accuracy of the apparatus. Transient phenomena during start-up have a direct influence on J_e^0 in this case, whereas η_0 only depends on long term processes.

§ 3.4 Simple extension

In an early stage of this project, several creep-recovery experiments in simple extension were performed with polystyrene 678E and polycarbonate CD2000. Flat strips (100 × 15 × 0.1 [mm]) were moulded and labelled with 15 markers at a mutual distance of d = 5.0 [mm] (see Figure 3.8). These strips were stretched under constant force in an oven at temperatures of 20 [K] above T_g for PS678E and at 30 and 40 [K] above T_g for CD2000. The procedure is shown in Figure 3.9. During creep, at time t_1 the oven is opened, causing the temperature to drop and the deformation to freeze in. The strain between markers can then be measured. At time t_2 the strip is put back in the oven, this time unloaded.

Recovery of frozen-in strain will then occur and after a sufficiently long time the strip can be removed and the distance between markers measured again.

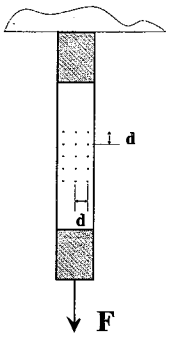

Figure 3.8
Illustration of flat strip. F is the applied force and d the distance between markers.

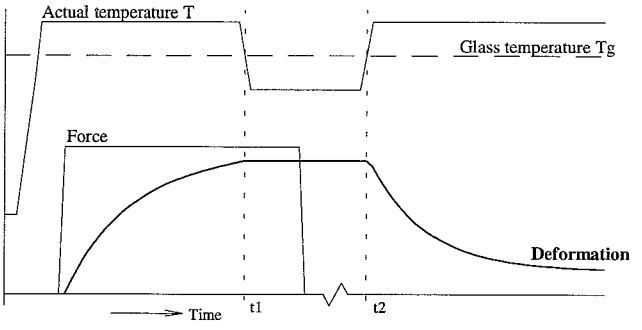

Figure 3.9
Temperature-loading program

The strain ε_s and subsequent shrinkage ε_r were respectively defined as:

$$\varepsilon_s = \frac{l_1 - l_0}{l_0} \cdot 100\% \tag{3.11}$$

$$\varepsilon_r = \frac{l_1 - l_2}{l_0} \cdot 100\% \tag{3.12}$$

where l_0 is the original length, l_1 is the length after creep and l_2 is the length after recovery.
A total number of 7 polystyrene strips were stretched, up to 320 % locally. It was found that they all fully recovered, in agreement with results of Schennink [9]. The complete experimental process was repeated by a different operator, giving the same results. For polycarbonate the results are given below in Figure 3.10 where the shrinkage ε_r is plotted against the applied strain ε_s for different initial stresses and temperatures. The true final stress for the maximum strain (± 900 %), was found to be in the range of 5 [MPa].
An explanation for the relatively high amount of recovery could be given by the fact that during creep the stress increases significantly. Consequently, the true stress is a function of elongation and no steady state is reached. An elegant method that deals with this problem and can be implemented quite easily, is illustrated is Figure 3.11 [37]. To support the sample and for efficient temperature transfer a silicon oil bath can be applied. During the creep experiment the load is decreased by using a cam.

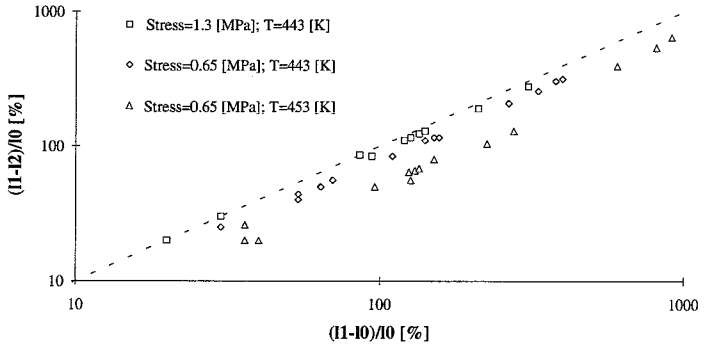

Figure 3.10
Results of creep and recovery experiments for polycarbonate CD2000. Maximum strains of over 900 % were reached. The dashed line indicates full recovery.

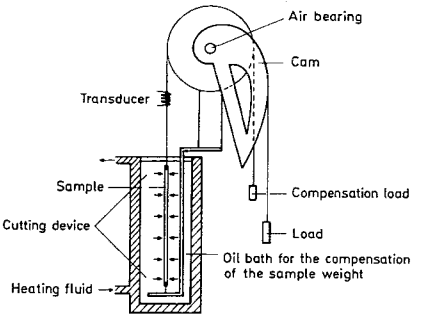

Figure 3.11
Schematical representation of extension test with virtually constant stress (after Janeschitz-Kriegl [37]).

Chapter 4

Results and discussion

In this chapter the results of the oscillatory and steady shear experiments are given and shortly discussed. Effects of the different molecular properties on the elastic response of the materials are subsequently reviewed.

§ 4.1 Oscillatory shear experiments

In Table 4.1 the results of the oscillatory shear experiments are summarized. T_0 is the chosen reference temperature. The plateau modulus G_N^0, the density ρ, the entanglement molecular weight M_e, the recoverable compliance J_e^0 and the steady state viscosity η_0 were determined according to the respective methods described in Chapter 3.

Table 4.1
Results of Oscillatory shear experiments performed on a Rheometrics RDS-II.

Oscillatory Shear Experiments	T_0 [K]	G_N^0 [MPa]	$\rho(T_0)$ 10^3 [kg/m^3]	M_e [kg/mol]	$J_e^0(T_0)$ 10^{-5} [Pa^{-1}]	$\eta_0(T_0)$ 10^4 [Pa s]	Remarks
PS678E	480	0.120	1.010	33.6	14.3	0.34	
PS96	473	0.210	1.012	19.0	0.978	0.098	
PS330	470	0.183	1.013	21.6	1.98	2.95	
PS560	470	0.188	1.013	21.1	3.67	16.3	
CD2000	462	2.00	1.166	2.24	0.551	6.75	
Spiro PC 27%	548	1.69	1.148	3.10	3.09	2.74	
Spiro PC 46%	563	1.02	1.445	6.63	6.41	2.23	slope log(G')≠2
Spiro PC 65%	573	0.717	1.143	7.60	4.79	1.04	
Spiro PC 86%	569	0.368	1.144	14.7	11.9	0.276	slope log(G')≠2
GE Spiro PC	541	0.780	1.149	6.63	1.47	1.06	
TMPC	538	0.871	1.150	5.91	3.26	0.545	slope log(G')≠2

The M_e values that were found agree reasonably well with available literature values that are given in Table 4.2 at the next page. For monodisperse polystyrene, Schausberger [42] has reported a critical molecular weight M_c of about 38 [kg/mol], which agrees with the M_e values ($M_c \approx 2M_e$) of the narrowly distributed polystyrenes used in this study.

Where the entanglement molecular weight of monodisperse polystyrenes is expected to be constant ($M \geq M_c$), it should increase for the copolycarbonates as the percentage spiro increases.
In Figure 4.1 the dependence of M_e and T_g on the percentage spiro is shown. Reference is PC CD2000 (100 % Bisphenol-A)

Table 4.2
Literature values for the entanglement molecular weight M_e.

Literature values	M_e [kg/mol]	Remarks
PS678E	30.0	[9,31]
PS678E	18.7	experimental [17]
	17.9	predicted [17]
CD2000	3.4	[9, 31]
CD2000	1.78	experimental [17]
	2.55	predicted [17]
TMPC	3.62	experimental [17]
	4.44	predicted [17]

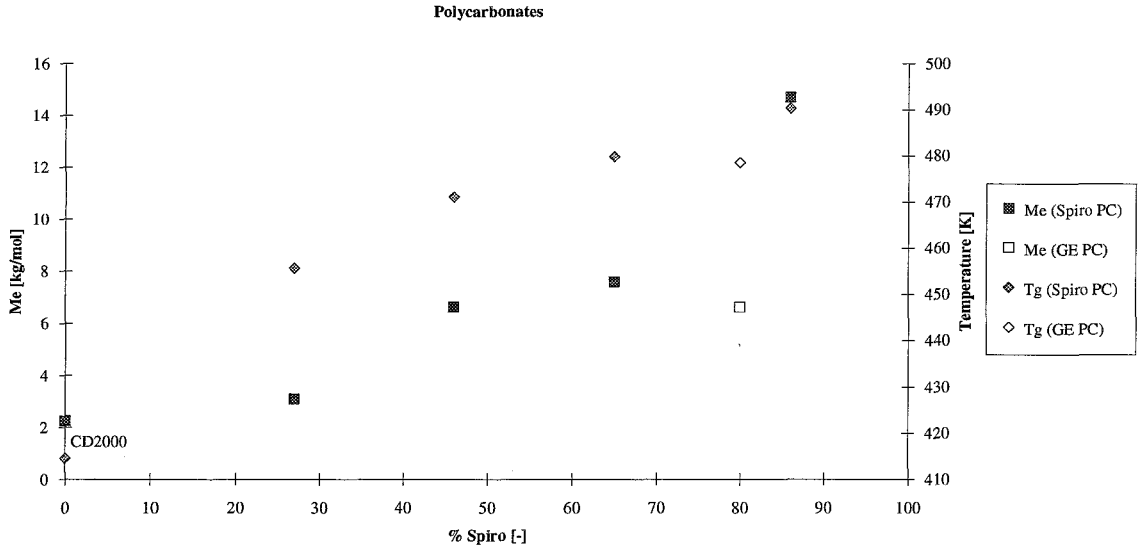

Figure 4.1
The entanglement molecular weight M_e and glass transition temperature T_g as a function of the molar percentage spiro in copolycarbonates.

As one can see from Figure 4.1, it seems that M_e of the polymer with 46 % spiro is overestimated. This is probably due to the fact that during the experiments performed with this material some fluctuations in the temperature occurred, causing a small rotation in the curves. This rotation, which can be seen in the spectrum of the loss angle makes the interpretation of the shiftfactors somewhat arbitrary.

In Appendix B mechanical spectra of loss angle δ and complex modulus G^*, together with mastercurves of G', G'' and η^* are given for each material. A plot of the shiftfactors and the different fitting methods is also included. In general, the WLF fit agrees reasonably well with the shiftfactors whereas the Arrhenius equation is not able to describe the temperature dependence of a_T satisfactory. The vertical shift b_T does not agree with the temperature density correction. This is mainly due to the shifting procedure that causes a number of experimental errors (e.g. gapwidth correction) to gather in the correction factor b_T.

For most materials a small vertical shift in the loss angle at low temperatures is observed. This may be caused by slip between the contact surfaces, but rather by the transducer reaching its specification limit at very high moduli ($G^* \approx 1$ [MPa]). At high temperatures and, accordingly, low viscosities, the apparatus is no longer able to measure the elastic contribution correctly; G' is then observed to remain constant, causing a decline in the loss angle with decreasing frequency. This is shown in the loss angle spectra of GE spiro PC and TMPC (see Appendix B).
For the determination of J_e^0, this latter phenomenon presents a problem to the extent that the slopes 1 and especially 2 in respectively $G''(\omega)$ and $G'(\omega)$ are not always reached. If slope 2 is not reached, this causes an underestimation of J_e^0.

§ 4.2 Steady shear experiments

Totally 45 creep and recovery experiments were performed, of which 19 successfully. Stresses between 0.94 and 72 [kPa] were applied. In the successful experiments a relation between stress and recoverable compliance was not found, therefore the results of these experiments were averaged and are summarized in Table 4.3. In Appendix C tables with all results are given. The experiments were evaluated using the methods that were described in section 3.3.2. Determination of J_e^0 from the final value of the recoverable strain in the recovery experiment proved to be the only successful method. In most cases however, recovery was not completely finished at the end of the experiment causing a slight underestimation of J_e^0.

Table 4.3
Averaged values of the recoverable compliance as calculated from the final value of the recoverable strain.

Steady shear experiments	$<J_e^0>$ 10^5 [Pa^{-1}]	*n*
PS678E	6.12 ± 0.79	3
PS96	1.42	1
PS330	1.31 ± 0.16	2
PS560	1.69 ± 0.42	4
CD2000	0.51 ± 0.03	3
Spiro PC 27 %	2.86 ± 0.9	2
Spiro PC 46 %	4.06 ± 2.97	2
Spiro PC 65 %	-	-
Spiro PC 86 %	5.79 ± 0.51	2
GE Spiro PC	-	-

The recoverable compliance could not be calculated successfully from the creep experiment, because the available methods are based on subtracting a viscous contribution from the absolute value of the total strain during creep. Although linear viscoelastic steady state was achieved in most cases (slope log $J(t) = 1$; constant shear rate), the elastic contribution was influenced by start-up transients unacceptably.
Changing this will require a very accurate apparatus, designed for high T_g polymers. In Appendix

D, an illustration of the influence of small stress transients is given.

Weissenberg [44] noted that, when an elastic liquid is subjected to simple shear flow, a pull along the lines of flow is present besides the shear stress. In a cone and plate rheometer that pull strangulates the flow, causing a pressure profile across the face of the instrument and a normal thrust forcing the faces apart. In this study it appeared that repeating experiments with one sample at the same stress level systematically resulted in a reduced elastic response, even at very low stress levels of 1 [kPa]. This is illustrated in Appendix D.

It was found that control of the normal force is critical to perform a well defined experiment. Pressing the cone into the cylindrical sample caused in some cases an unacceptable normal force that resulted in friction and/or dislocation of the optical encoder. Therefore the cone-plate geometry was replaced by a plate-plate system. Total absence of the normal force, however, may cause loss of contact surface, especially at high viscosities.

Other experimental problems that were experienced include heat leakage and a windmill effect caused by airflows in the bearing that have an influence on rotation, especially at low viscosities. This is illustrated in Appendix D where recovery curves of PC CD2000 at different temperatures are given.

To show that good results can be achieved with the DSM prototype at low temperatures, using the plate-plate system, a polydimethylsiloxane (PDMS) sample was tested. The strain curve is given in Appendix D.

§ 4.3 Molecular property effects

§ 4.3.1 The weight-average molecular weight M_w

The elastic response of the three narrowly distributed polystyrenes (Table 3.1) is presented in Figure 4.2. The recoverable compliance J_e^0 is plotted against the weight-average molecular weight M_w. Results of both oscillatory shear and steady shear experiments are shown. As Figure 4.2 shows, the experimental results agree reasonably well with values calculated from dynamic data (G' & G'') that was presented by Schausberger et al. [34, 35].

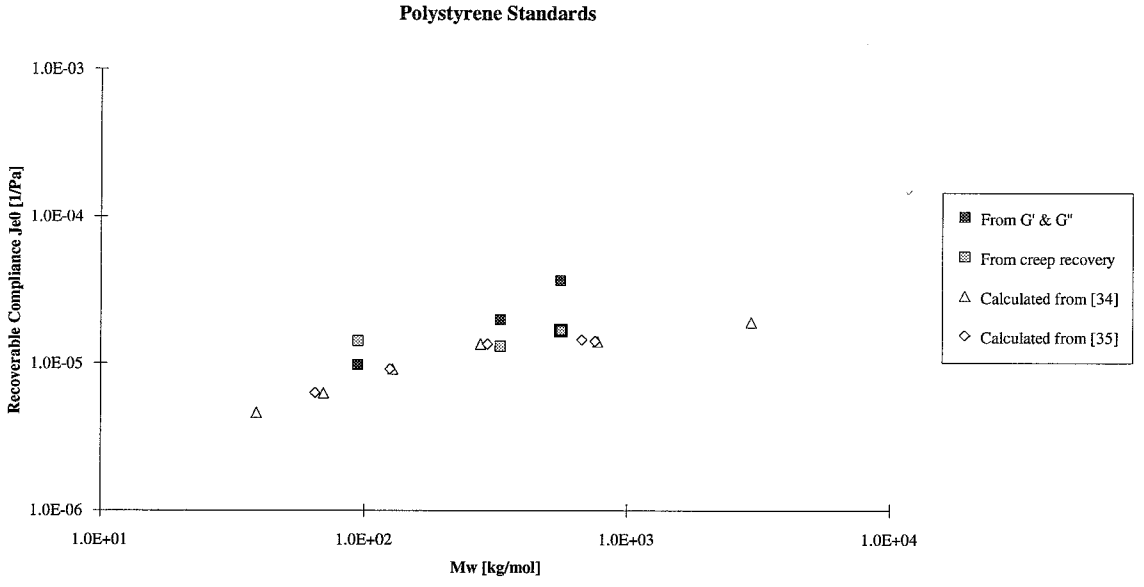

Figure 4.2
Elastic response as a function of the molecular weight. Square markers reperesent narrowly distributed PS standards, other markers represent literature values.

As expected J_e^0 does not show a profound dependence of M_w. The molecular weight is directly related to the viscosity ($\eta \propto M^{3,4}$) and thus causes the moduli to shift horizontally along the frequency axes. This does not affect the recoverable compliance. The value of J_e^0 that is found for PS560 is an overestimation.This can be explained as follows: during the oscillatory shear experiments excess material at the outer edge of the plates was removed, because it affects results significantly. For PS560 this was not possible, without tearing material out of the gap and therefore omitted. The resulting effect can be seen in the spectrum of the dynamic modulus of PS560 (Appendix B), which shows that some curves intersect above the reference temperature.

§ 4.3.2 The dispersion *D*

The effect of the molecular weight distribution on the elastic response is shown in Figure 4.3 where PS678E is compared to the nearly monodisperse polystyrene standards. As expected [1, 24], J_e^0 increases rapidly with polydispersity.
Where the dynamic and steady state values agree reasonably well for the nearly monodisperse polystyrenes, this is not the case for the broadly distributed PS678E.

When a sample has a narrow molecular weight distribution, all the chains show a similar degree of entanglement, so they are uniformly stressed during flow. In a sample of broad molecular weight distribution, with the same average molecular weight, longer chains are present. It is the long chains that accept a large amount of the total stress, assuming that it is the entanglements which resist deformation. The resulting above-average elastic response in those molecules is retarded by

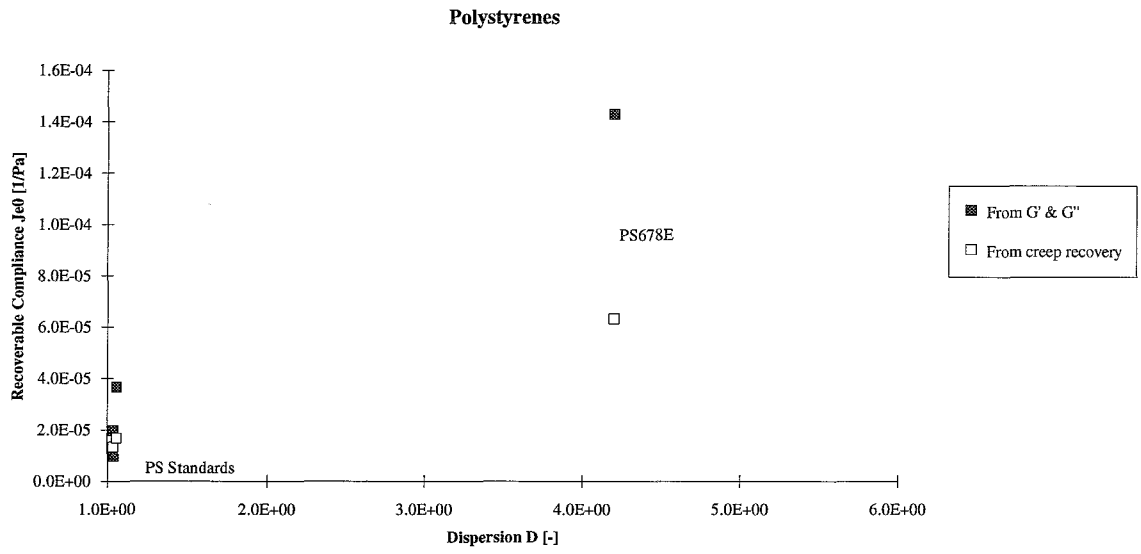

Figure 4.3
The elastic response as a function of the width of the molecular weight distribution.

viscous resistance as the smaller molecules conform. Thus a material of broad molecular weight distribution is expected to show more elastic response than a material of narrow molecular weight distribution, with a delay in the total time necessary to achieve maximum recovery [20].
It is this delay that causes the underestimation of J_e^0 for PS678E from recovery. Within the same experimental time window, the nearly monodisperse polystyrene can virtually reach maximum recovery, while the broadly distributed PS678E has only partially recovered.

An investigation by Schausberger [35] confirms these observations. In his study two polystyrene standards, with molecular weights of 65 and 669 [kg/mol] show J_e^0 values of $6.30 \cdot 10^{-6}$ and $1.45 \cdot 10^{-5}$ [Pa^{-1}] respectively. A bimodal *1:1* blend yields $J_e^0 = 6.01 \cdot 10^{-5}$ [Pa^{-1}]. It should be noted that the steady state viscosity η_0 for the two standards varies from $1.00 \cdot 10^3$ to $3.02 \cdot 10^6$ [Pa·s] where the blend shows $3.55 \cdot 10^5$ [Pa·s].

In order to avoid influences of a variation in M_e on the results presented in § 4.3.1 and § 4.3.2, the recoverable compliance can be multiplied by the plateau modulus. Based on the assumption that the value $J_e^0 \cdot G_N^0$ [-] is essentially universal for nearly monodisperse ($D \approx 1$) linear polymers, Wasserman et al. [24] reported values in the range of 1.8 to 2.5. In this study, values of 2.1, 3.6 and 6.9 were found in oscillatory shear for PS96, PS330 and PS560 respectively, where it should be noted that the dispersion D of these materials is not exactly equal (Table 3.1).
Schausberger [45] calculated a value of $J_e^0 \cdot G_N^0 = 2.8$ for $D = 1$ and predicted a proportional relation between D and $J_e^0 \cdot G_N^0$ on double logarithmic scales for polymers with a log-normal molecular weight distribution.

For nearly monodisperse polymers is has been stated [24] that the theoretical limit of the value $J_e^0 \cdot G_N^0$ is unity for $D \rightarrow 1$. This would mean that the low frequency behaviour for $D = 1$ can be described by a single Maxwell element. To test this assumption, the storage and loss moduli of the polystyrenes used in this study were fitted with a single Maxwell element, using the plateau modulus and the zero shear viscosity of each material.

The governing equations are given in Appendix E. The results for the different moduli (divided by the difference of T_g and the temperature of the mastercurve) are shown in Figure 4.4 and Figure 4.5 where respectively G' and G'' are plotted against the angular frequency. Obviously, the low frequency behaviour of PS678E can not be described by a single Maxwell element, but it also fails to describe the low frequency storage behaviour of the nearly monodisperse polystyrenes. Consequently, the assumption that for monodisperse polymers at low frequencies the recoverable compliance J_e^0 is equal to the reciprocal plateau modulus G_N^0 is not justified.

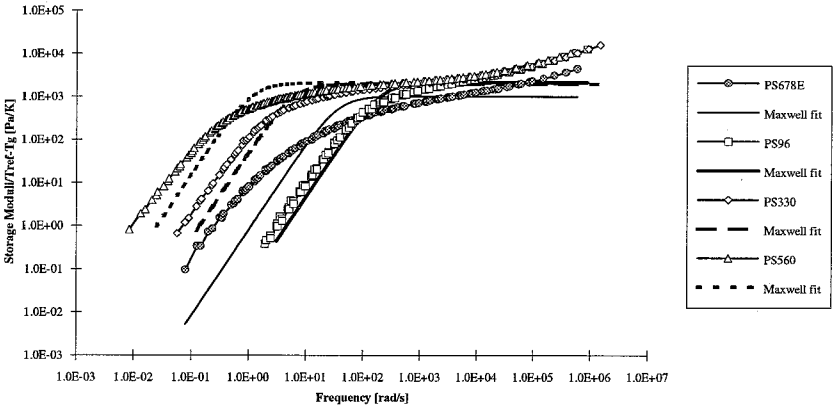

Figure 4.4
Mastercurves of the storage behaviour as a function of the frequency. Markers are experimental results, lines are single-Maxwell-element fits.

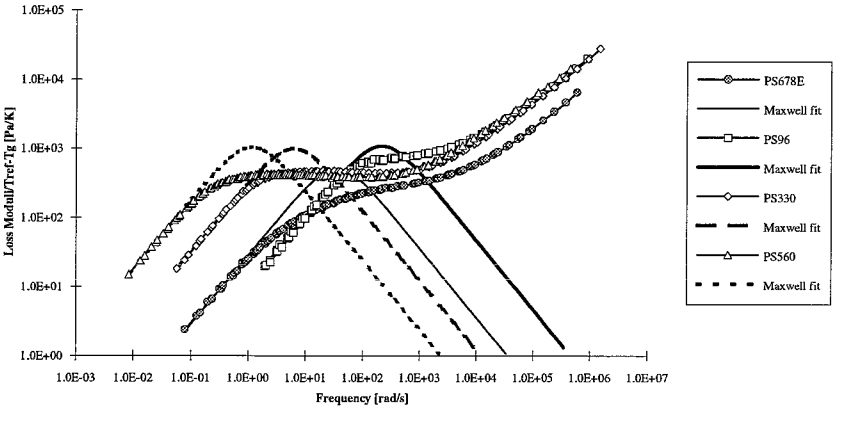

Figure 4.5
Mastercurves of the loss behaviour as a function of the frequency. Markers are experimental results, lines are single-Maxwell-element fits.

Figure 4.4 and Figure 4.5 also illustrate that a change in molecular weight mainly causes a frequency shift, that does not influence the recoverable compliance. A difference in dispersity

causes a vertical shift and a change of the shape of the spectrum that greatly affects the elastic response.

§ 4.3.3 The entanglement molecular weight M_e

The influence of the entanglement molecular weight M_e on the recoverable compliance of different copolycarbonates is shown is Figure 4.6.

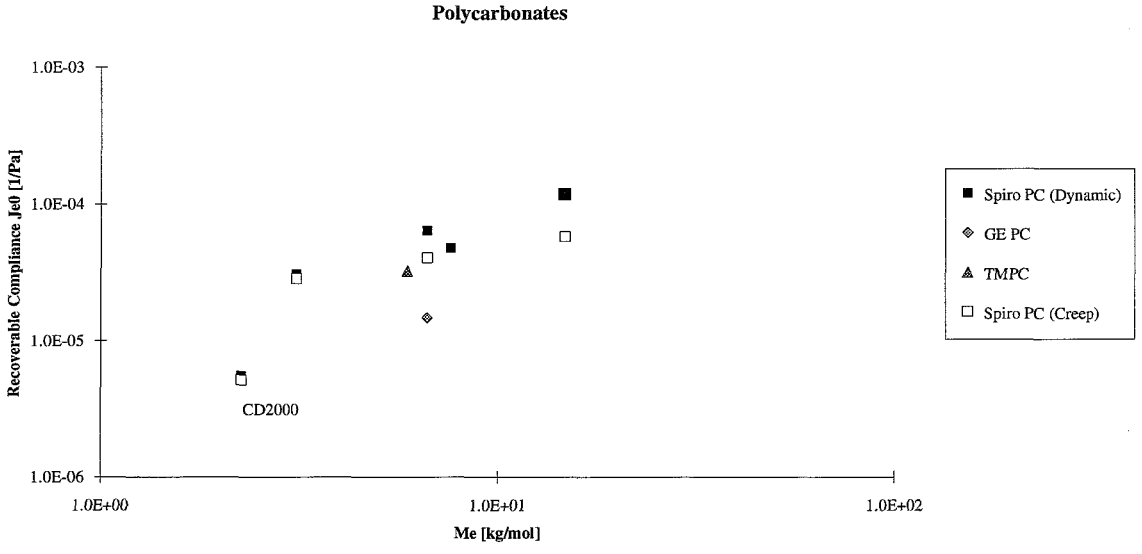

Figure 4.6
The elastic response as a function of the experimentally determined entanglement molecular weight M_e of different copolycarbonates.

A proportionality between M_e and J_e^0 appears to be present. However, a scatter of the results is observed. As shown in Table 3.1 not only the molecular weight M_w, but also the dispersion D varies significantly for the different copolycarbonates. This has a profound effect on the elastic response.

To determine the effect of M_e in a more unambiguous manner, materials with a more similar dispersion should be synthesized.

Chapter 5

Conclusions and recommendations

It was found that the entanglement molecular weight M_e of polycarbonate can be systematically varied by a factor of 10, by adding molecules with a restraining spiro-group in different percentages to Bisphenol-A polycarbonate molecules.

The recoverable compliance J_e^0 can be calculated from dynamic mechanical measurements in the melt state, if the limiting constant slopes of the moduli at low frequencies can be determined. This provides a method to assess the intrinsic elastic response of a material, even if only a small sample is available. However, since the dynamic properties are plotted on double logarithmic scales, the results have to be considered with care.
It also proved to be possible to estimate J_e^0 from steady shear recovery experiments. However, due to long relaxation times, especially in broadly distributed polymers, maximum recovery is not always reached within the experimental time window. Determining J_e^0 from creep experiments proved to be unsuccessful, due to start-up transients. This will require a more accurate constant-stress rheometer, specifically designed for high T_g polymers. Points of attention for the design of such an apparatus are control of the normal force, friction and the prevention of heat leakage.

The weight-average molecular weight M_w does not influence the recoverable compliance of polystyrene significantly. However, J_e^0 was found to increase rapidly with increasing polydispersity. A correlation between J_e^0 and was found to be present in copolycarbonates, although these results were affected by a variation in dispersion D.

The product of J_e^0 and G_N^0 is not a constant, but unique for every polymer, even if monodisperse. Consequently, the use of the rubbery plateau modulus instead of the compliance for the prediction of dimensional stability will lead to different results, depending on the type of polymer and the molecular weight distribution.

From this study it can be concluded, that the recoverable compliance J_e^0 can be used as a comparative measure for deducing the elastic response and thus the potential dimensional instability of materials with different molecular properties.
However, simple deformation was applied and therefore results are only valid for comparative purposes. To link the results to actual injection moulded products that inhibit complex spatial property distributions, more research is needed.

In this investigation, experiments in shear were performed. With simple extension under constant force, the recoverable compliance cannot be determined due to the quadratic increase of the stress with elongation. An elegant method that deals with this problem, which can be implemented quite easily is shown in § 3.4. By decreasing the load during creep with a cam, an extension test under virtually constant stress can be performed.

Control of the dimensional stability is crucial for the long-term performance of injection moulded products. It was shown that the molecular network structure of amorphous polymers affects the potential dimensional stability. It was shown elsewhere [29] that this molecular network structure also influences the ultimate toughness of amorphous polymers. The range in M_e of the copolycarbonates used in this study can fill up the difference between M_e of the polycarbonates and M_e of the polystyrenes that were studied previously. Therefore, additional mechanical tests with the copolycarbonates that were used here may provide interesting information.

Bibliography

[1] Ferry, J.D., *Viscoelastic Properties of Polymers (3rd edition)*, J. Wiley & Sons, Inc., New York, 1980.

[2] Meijer, H.E.H., et al., *Polymeerverwerking en Reologie, deel I & II*, Syllabus, Eindhoven University of Technology, The Netherlands, 1992.

[3] Wimberger-Friedl, R., *Orientation, Stress and Density Distributions in Injection-Moulded Amorphous Polymers Determined by Optical Techniques,* Doctoral Thesis, Eindhoven University of Technology, The Netherlands, 1991.

[4] Krevelen, D.W. van, *Properties of Polymers*, Elsevier, Amsterdam, 1990.

[5] Ward, I.M., *Mechanical Properties of Solid Polymers*, J. Wiley & Sons, Ltd., London, 1971.

[6] Arridge, R.G.C., *An Introduction to Polymer Mechanics*, Taylor & Francis, Ltd., London, 1985.

[7] Struik, L.C.E., *Internal Stresses, Dimensional Instabilities and Molecular Orientations in Plastics*, J. Wiley & Sons, Ltd., Chichester, 1990.

[8] Douven, L.F.A., *Towards the Computation of Properties of Injection Moulded Products: Flow- and Thermally Induced Stresses in Amorphous Thermoplastics*, Doctoral Thesis, Eindhoven University of Technology, The Netherlands, 1991.

[9] Schennink, G.G.J., *On the Dimensional Stability of Injection Moulded, Amorphous Thermoplastic Products*, Technical Report, # WFW 93.010, Institute for Continuing Education, Eindhoven University of Technology, The Netherlands, 1993.

[10] Struik, L.C.E., *Physical Ageing in Amorphous Polymers and other Materials*, Elsevier, Amsterdam 1978.

[11] Brown, R.P. (ed.), *Handbook of Plastics Test Methods*, J. Wiley & Sons, Inc., New York, 1988.

[12] Larson, R.G., *Constitutive Equations for Polymer Melts and Solutions*, Butterworths, Boston, 1980.

[13] Wimberger-Friedl, R., *Rheological Characterization of low M_w - Polycarbonates*, Internal Philips Report, # TN 328/86, 1986.

[14] Flory, P.J., *Statistical Mechanics of Chain Molecules*, J. Wiley & Sons, Inc., New York, 1969.

[15] Wu, S., *Chain Structure and Entanglement.* In: Journal of Polymer Science: Part B: Polymer Physics, **27**, 723, 1989.

[16] Treloar L.R.G., *The Physics of Rubber Elasticity*, Clarendon Press, Oxford, 1975.

[17] Wu, S., *Predicting Chain Conformation and Entanglement of Polymers from Chemical Structure*, In: Polymer Engineering and Science, **32**, # 32, 1992.

[18] Wu, S., *The Origin of Chain Entanglement: Correlations Between Entanglement and Chain Structure*, In: Polymer Engineering and Science, **33**, # 5, 1993.

[19] Oomens, C.W.J., *Constitutieve Modellen*, Syllabus, Eindhoven University of Technology, The Netherlands, 1992.

[20] Cogswell, F.N., *Polymer Melt Rheology*, George Godwin, Ltd., London, 1981.

[21] Coleman , B.D., et al., *Normal Stress Effects in Second-Order Fluids*, In: Journal of Applied Physics, **35**, # 1, 1964.

[22] Lodge, A.S., *Elastic Liquids*, Academic Press, Ltd., London, 1964.

[23] Prest, W.M., et al., *Rheological Properties of Poly(2,6-dimethylphenylene Oxide)-Polystyrene Blends*, In: Journal of Polymer Science: part A-2, **10**, 1639, 1972.

[24] Wasserman, S.H., et al., *Effects of Polydispersity on Linear Viscoelasticity in Entangled Polymer Melts.* In: Journal of Rheology, **36**, 543, 1992.

[25] Leaderman, H., *Elastic and Creep Properties of Filamentous Materials and Other High Polymers.*The Textile Foundatation, Washington D.C., 1943.

[26] Williams, M.L., et al., *The Temperature Dependence of Relaxation Mechanisms in Amorphous Polymers and Other Glass-forming Liquids*, In: Journal of the American Chemical Society, **77**, # 13, 1955.

[27] Bueche, F., *Physical Properties of Polymers*, Interscience, New York, 1962.

[28] Young, R.J., et al., *Introduction to Polymers*, Chapmann & Hall, London, 1991.

[29] Van der Sanden, M.C.M, *Ultimate Tougness of Amorphous Polymers*, Doctoral Thesis, Eindhoven University of Technology, The Netherlands, 1993.

[30] Beerens, M.N.M., *Precisie in Kunststoffen; (Dow Styron PS 678E) Maatvoering, Dimensiestabiliteit, Dubbele Breking en Krimp boven Tg: Invloeden van Procesparameters*, Internal Philips Report, # TN 050/92, 1992.

[31] Zoetelief, W.F., *On the Numerical Simulation of the Multilayer Injection Moulding Process,* Technical Report, # WFW 92.100, Institute for Continuing Education, Eindhoven University of Technology, The Netherlands, 1992.

[32] Vleeshouwers, S.M., *Modelling and Predicting Properties of Polymers in the Amorphous Glassy State*, Doctoral Thesis, Eindhoven University of Technology, The Netherlands, 1993.

[33] Sherby, O.D., et al., *Anelastic Creep of Polymethyl Methacrylate.* In: Journal of the Mechanics and Physics of Solids, **6**, 145, 1958.

[34] Schausberger, A., et al., *Linear elastico-viscous Properties of Molten Standard Polystyrenes. 1. Presentation of Complex Moduli; Role of Short Range Structural Parameters.* In: Rheologica Acta, **24**, 220, 1985.

[35] Schausberger, A., *A Simple Method of Evaluating the Complex Moduli of Polystyrene Blends.* In: Rheologica Acta, **25**, 596, 1986.

[36] Turi, E. A. (Ed.), *Thermal Characterization of Polymeric Materials*, Academic Press, New York, 1981.

[37] Janeschitz-Kriegl, H., *Polymer Melt Rheology and Flow Birefringence*, Springer Verlag, Berlin, 1983.

[38] Braam, W.G.M., *Scheidingsmethoden Chromatografie*, Wolters-Noordhoff, Groningen, 1985.

[39] Brandrup, J., et al. (Eds.), *Polymer Handbook*, J. Wiley & Sons, Inc., New York, 1975.

[40] Rodriguez, F., *Principles of Polymer Systems*, Hemisphere Publishing Corporation, New York, 1989.

[41] Wales, J.L.S., *The Application of Flow Birefringence to Rheological Studies of Polymer Melts*, Nijgh-Wolters-Noordhoff Universitaire Uitgevers B.V. ,Rotterdam, 1976.

[42] Schausberger, A., *A Description of the Linear Viscoelasticity of Molten Linear Monodisperse Polystyrenes with the Aid of a Generalized Discrete Relaxation Time Spectrum.* In: Rheologica Acta, **30**, 197, 1991.

[43] Cox, W.P., et al., *Correlation of Dynamic and Steady Flow Viscosities.* In: Journal of Polymer Science, **28**, 622, 1958.

[44] Weissenberg, K., *A continuum theory of rheological phenomena.* In: Nature, **159**, 310, 1947.

[45] Schausberger, A., *Unpublished Results.*

Appendix A

The Voigt model

The Kelvin or Voigt model is commonly used to describe creep behaviour in viscoelastic materials and is particularly useful in the case where the stress is held constant. In this appendix the stress-strain relations for a single Voigt element are derived. A single element, which is the basic component of a generalized multi-mode model, consists of a spring and a dashpot in parallel (Figure A.1).

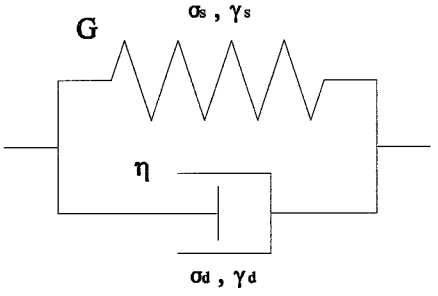

Figure A.1
Single Voigt element.

The total stress σ and strain γ are given by:

$$\sigma = \sigma_s + \sigma_d \tag{A.1}$$

$$\gamma = \gamma_s = \gamma_d \tag{A.2}$$

showing that the stresses in each component will add, whereas the strains are uniform.
The ideal spring stores all elastic energy and returns it completely after removal of external forces, following Hooke's law:

$$\sigma_s = G \cdot \gamma_s \tag{A.3}$$

with elastic modulus *G*.
The dashpot accounts for ideal viscous behaviour, governed by Newton's law:

$$\sigma_d = \eta \cdot \dot{\gamma}_d \tag{A.4}$$

where η is the viscosity and shear rate $\dot{\gamma}_d = \frac{d\gamma_d}{dt}$.
Thus, combining these four equations yields a simple differential equation of the form:

$$\sigma = G\gamma + \eta \cdot \dot{\gamma} \tag{A.5}$$

Using straightforward Laplace transforming will show that equation (A.5) has the solution:

$$\gamma = \frac{\sigma}{G}\left(1 - e^{-\frac{G}{\eta}t}\right) \tag{A.6}$$

For a single element, the ratio $\frac{\sigma}{G}$ is constant and equal to the maximum elastic strain γ_0.
Also the term $\frac{\eta}{G}$ will be constant for a given Voigt element and can be replaced by a characteristic time constant τ_0 called retardation time. Equation (A.6) can then be written as:

$$\gamma = \gamma_0\left(1 - e^{-\frac{t}{\tau_0}}\right) \tag{A.7}$$

For the case of recovery after creep, when the stress $\sigma = 0$, equation (A.6) becomes:

$$\gamma = \gamma_0 e^{-\frac{t}{\tau_0}} \tag{A.8}$$

As discussed in Chapter 2, real materials exhibit a range of relaxation times and moduli. A generalized Voigt model consisting of several elements in series, which results in a discrete spectrum of relaxation times and moduli, provides a more accurate way to describe material behaviour.

Where the Maxwell model describes the stress relaxation of a polymer to a first approximation and the Voigt model similarly describes creep, a next step is to find a combination of these two basic models that accounts for both phenomena. A relatively simple model that is able to do so, is known as the standard linear solid and consists of a spring and a Maxwell element[1] in series.
The more interested reader is referred to Ward [5] or Young et al. [28].

[1] A spring and a dashpot in series.

Appendix B

Dynamical spectra

In this appendix the results of the dynamic oscillatory shear experiments are summarized in the sequence given below. For each material mechanical spectra of loss angle δ and complex modulus G^* are given. Mastercurves of G', G'' and η^* are shown together in one plot for every material. A plot of the experimentally deduced shiftfactors and the different fitting methods is also included. Both a WLF fit (according to equation 2.28) and an Arrhenius fit (equation 2.29) are applied to the horizontal shiftfactor a_T, by least squares linear regression using all values.
The vertical shiftfactor b_T is modelled by a temperature density correction. For polystryrene two fitting procedures were applied, according to equations (3.1) and (3.2) (*'T(rho) corr. 1'* and *'T(rho) corr. 2'* respectively). The vertical shift of polycarbonate was fitted according to equation (3.1).

Material	*Page*
PS678E	37
PS96	39
PS330	41
PS560	43
PC CD2000	45
Spiro PC 27%	47
Spiro PC 46%	49
Spiro PC 65%	51
Spiro PC 86%	53
GE Spiro PC	55
TMPC	57

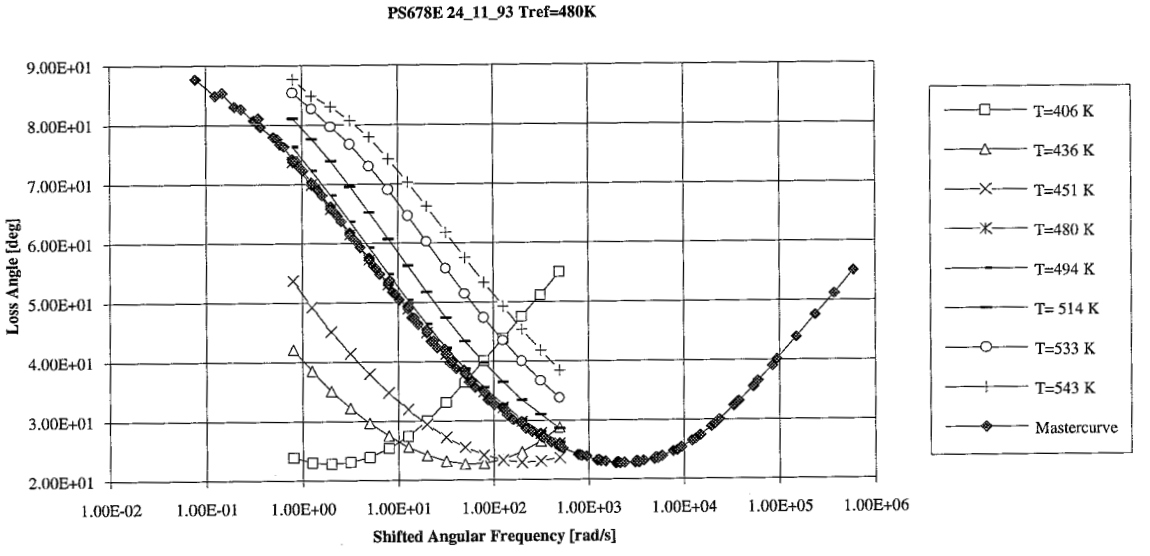
PS678E 24_11_93 Tref=480K
Loss Angle [deg]
9.00E+01
8.00E+01
7.00E+01
6.00E+01
5.00E+01
4.00E+01
3.00E+01
2.00E+01
1.00E-02
1.00E-01
1.00E+00
1.00E+01
1.00E+02
1.00E+03
1.00E+04
1.00E+05
1.00E+06
Shifted Angular Frequency [rad/s]
T=406 K
T=436 K
T=451 K
T=480 K
T=494 K
T= 514 K
T=533 K
T=543 K
Mastercurve

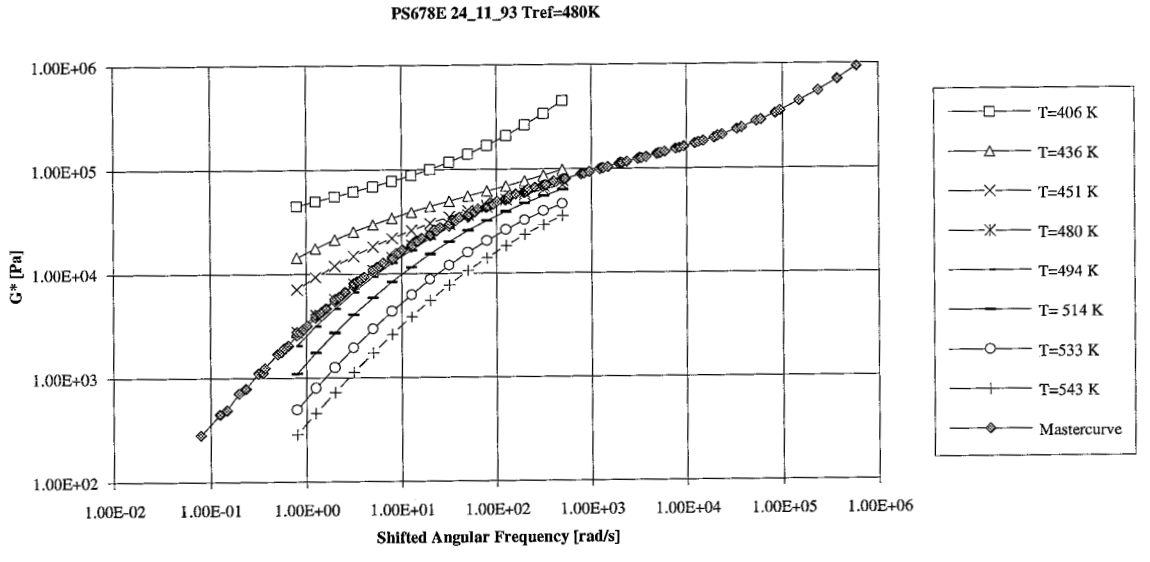
PS678E 24_11_93 Tref=480K
G* [Pa]
1.00E+06
1.00E+05
1.00E+04
1.00E+03
1.00E+02
1.00E-02
1.00E-01
1.00E+00
1.00E+01
1.00E+02
1.00E+03
1.00E+04
1.00E+05
1.00E+06
Shifted Angular Frequency [rad/s]
T=406 K
T=436 K
T=451 K
T=480 K
T=494 K
T= 514 K
T=533 K
T=543 K
Mastercurve

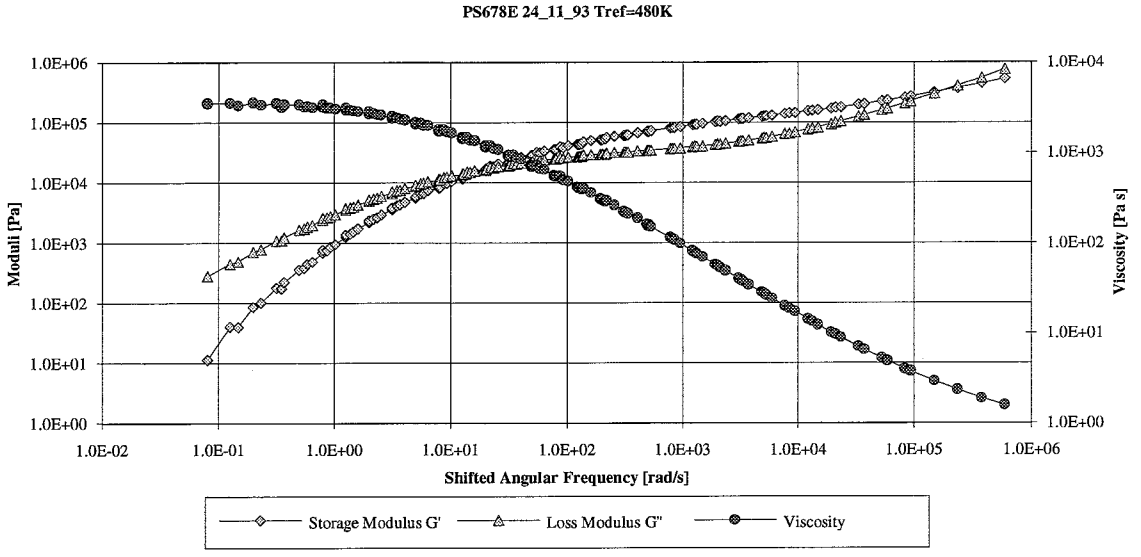
PS678E 24_11_93 Tref=480K
Moduli [Pa]
Viscosity [Pa s]
Shifted Angular Frequency [rad/s]
Storage Modulus G'
Loss Modulus G"
Viscosity

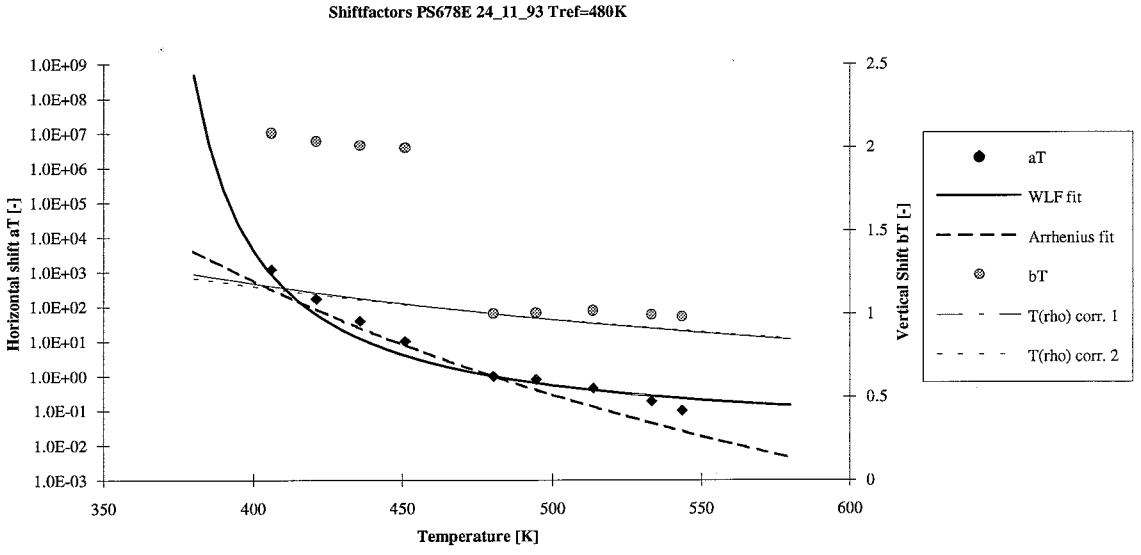
Shiftfactors PS678E 24_11_93 Tref=480K
Horizontal shift aT [-]
Vertical Shift bT [-]
Temperature [K]
aT
WLF fit
Arrhenius fit
bT
T(rho) corr. 1
T(rho) corr. 2

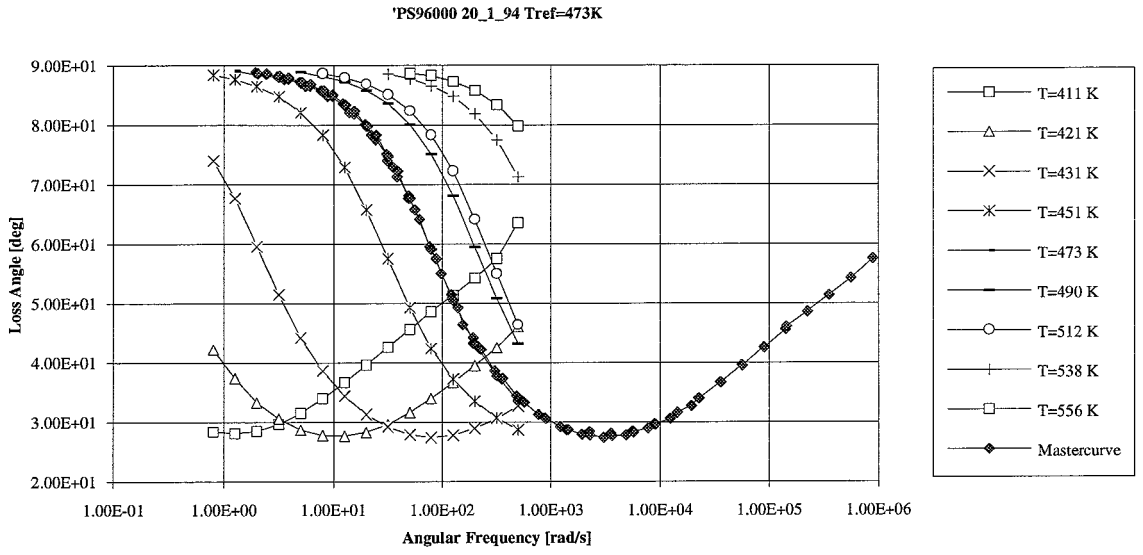
'PS96000 20_1_94 Tref=473K
Loss Angle [deg]
9.00E+01
8.00E+01
7.00E+01
6.00E+01
5.00E+01
4.00E+01
3.00E+01
2.00E+01
1.00E-01
1.00E+00
1.00E+01
1.00E+02
1.00E+03
1.00E+04
1.00E+05
1.00E+06
Angular Frequency [rad/s]
T=411 K
T=421 K
T=431 K
T=451 K
T=473 K
T=490 K
T=512 K
T=538 K
T=556 K
Mastercurve

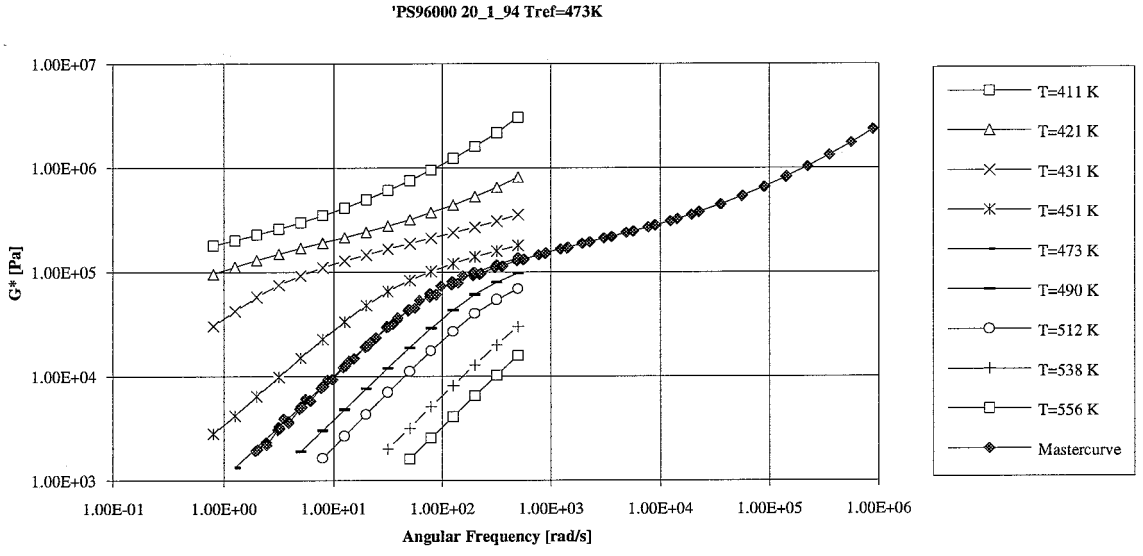
'PS96000 20_1_94 Tref=473K
G* [Pa]
1.00E+07
1.00E+06
1.00E+05
1.00E+04
1.00E+03
1.00E-01
1.00E+00
1.00E+01
1.00E+02
1.00E+03
1.00E+04
1.00E+05
1.00E+06
Angular Frequency [rad/s]
T=411 K
T=421 K
T=431 K
T=451 K
T=473 K
T=490 K
T=512 K
T=538 K
T=556 K
Mastercurve

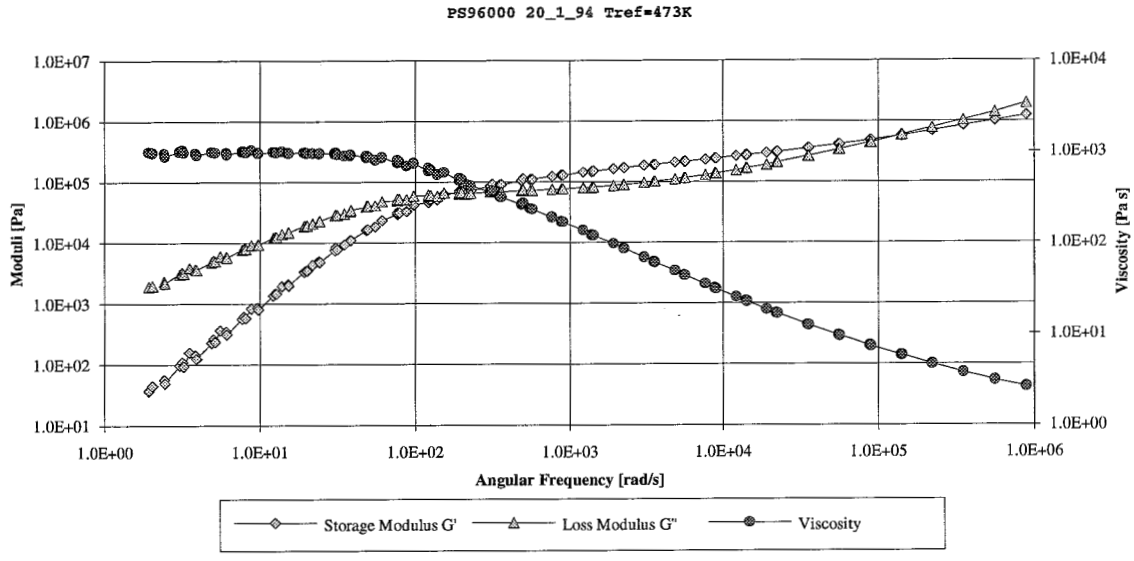
PS96000 20_1_94 Tref=473K
Moduli [Pa]
Viscosity [Pa s]
Angular Frequency [rad/s]
Storage Modulus G'
Loss Modulus G"
Viscosity

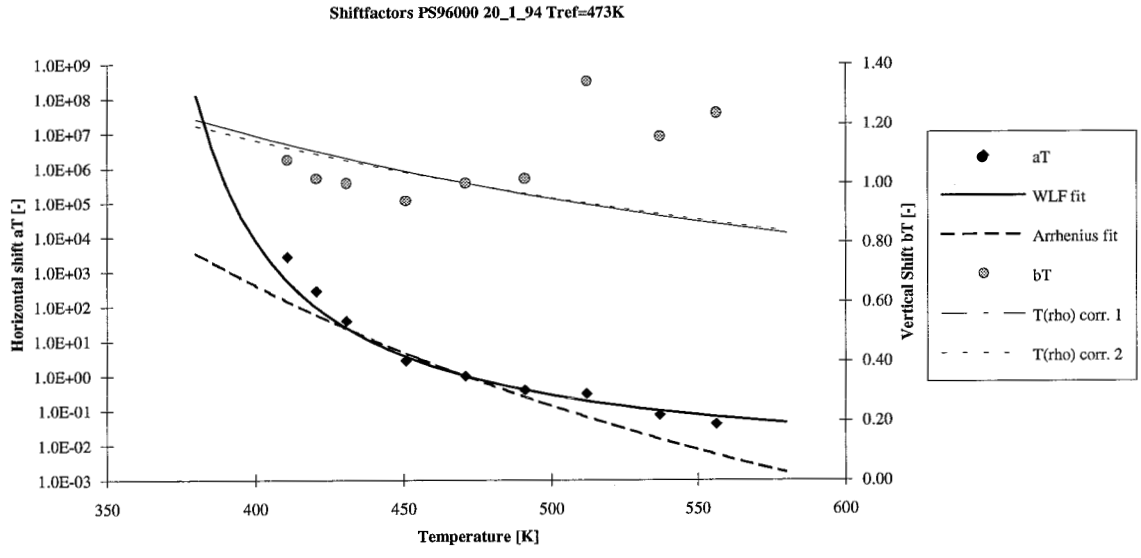
Shiftfactors PS96000 20_1_94 Tref=473K
Horizontal shift aT [-]
Vertical Shift bT [-]
Temperature [K]
aT
WLF fit
Arrhenius fit
bT
T(rho) corr. 1
T(rho) corr. 2

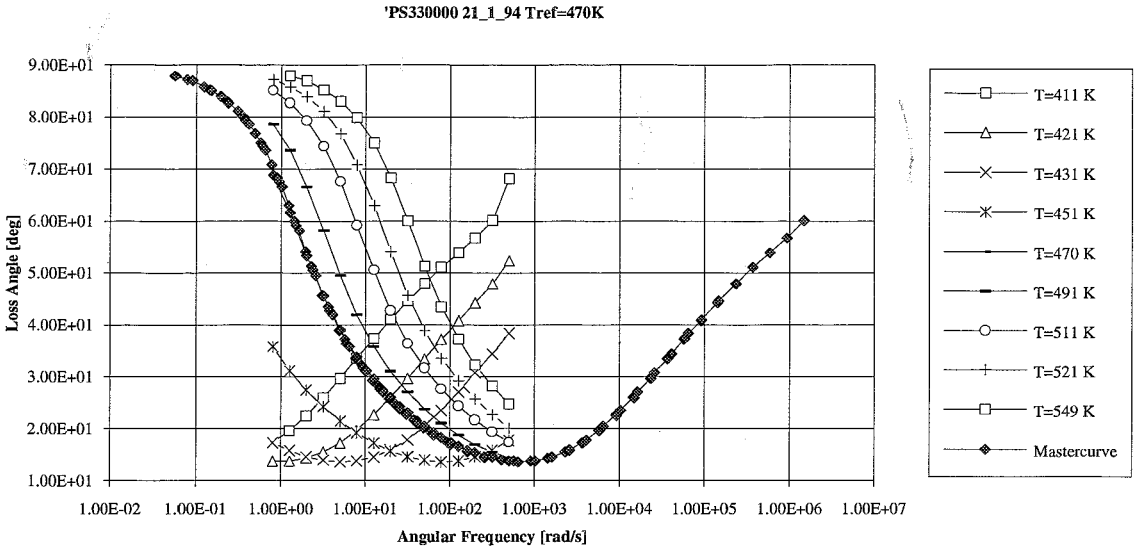
'PS330000 21_1_94 Tref=470K
Loss Angle [deg]
9.00E+01
8.00E+01
7.00E+01
6.00E+01
5.00E+01
4.00E+01
3.00E+01
2.00E+01
1.00E+01
1.00E-02
1.00E-01
1.00E+00
1.00E+01
1.00E+02
1.00E+03
1.00E+04
1.00E+05
1.00E+06
1.00E+07
Angular Frequency [rad/s]
T=411 K
T=421 K
T=431 K
T=451 K
T=470 K
T=491 K
T=511 K
T=521 K
T=549 K
Mastercurve

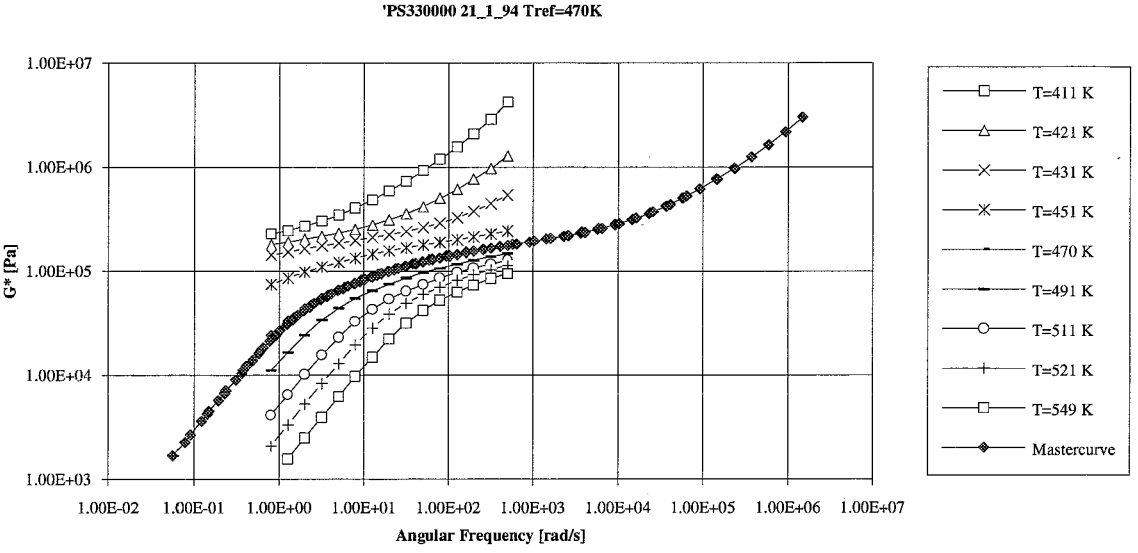
'PS330000 21_1_94 Tref=470K
G* [Pa]
1.00E+07
1.00E+06
1.00E+05
1.00E+04
1.00E+03
1.00E-02
1.00E-01
1.00E+00
1.00E+01
1.00E+02
1.00E+03
1.00E+04
1.00E+05
1.00E+06
1.00E+07
Angular Frequency [rad/s]
T=411 K
T=421 K
T=431 K
T=451 K
T=470 K
T=491 K
T=511 K
T=521 K
T=549 K
Mastercurve

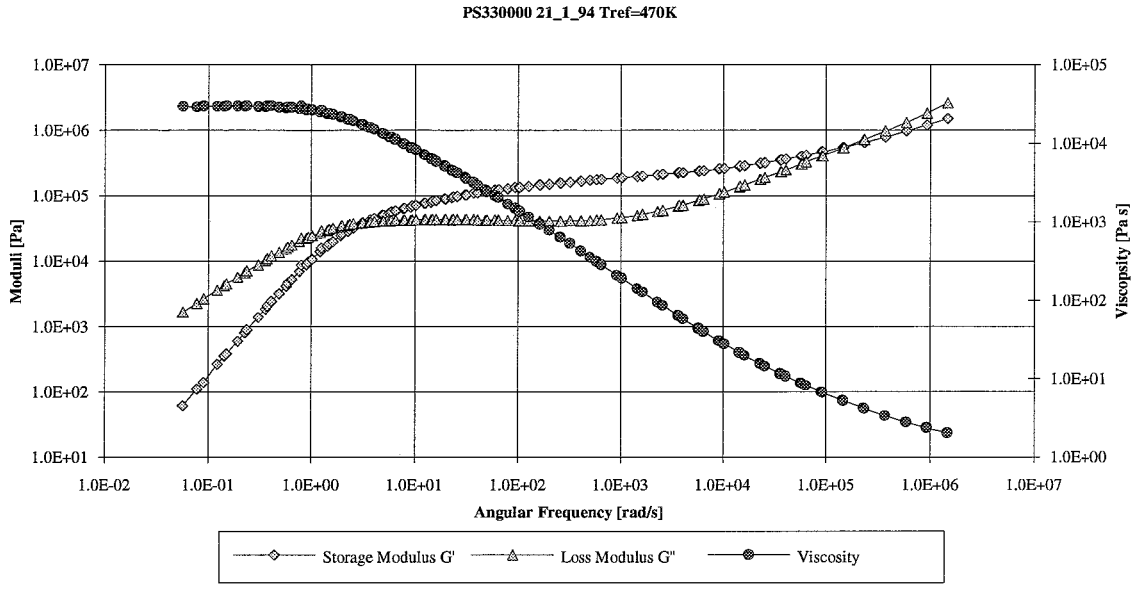
PS330000 21_1_94 Tref=470K
Moduli [Pa]
Viscopsity [Pa s]
Angular Frequency [rad/s]
1.0E+07
1.0E+06
1.0E+05
1.0E+04
1.0E+03
1.0E+02
1.0E+01
1.0E+05
1.0E+04
1.0E+03
1.0E+02
1.0E+01
1.0E+00
1.0E-02
1.0E-01
1.0E+00
1.0E+01
1.0E+02
1.0E+03
1.0E+04
1.0E+05
1.0E+06
1.0E+07
Storage Modulus G'
Loss Modulus G"
Viscosity

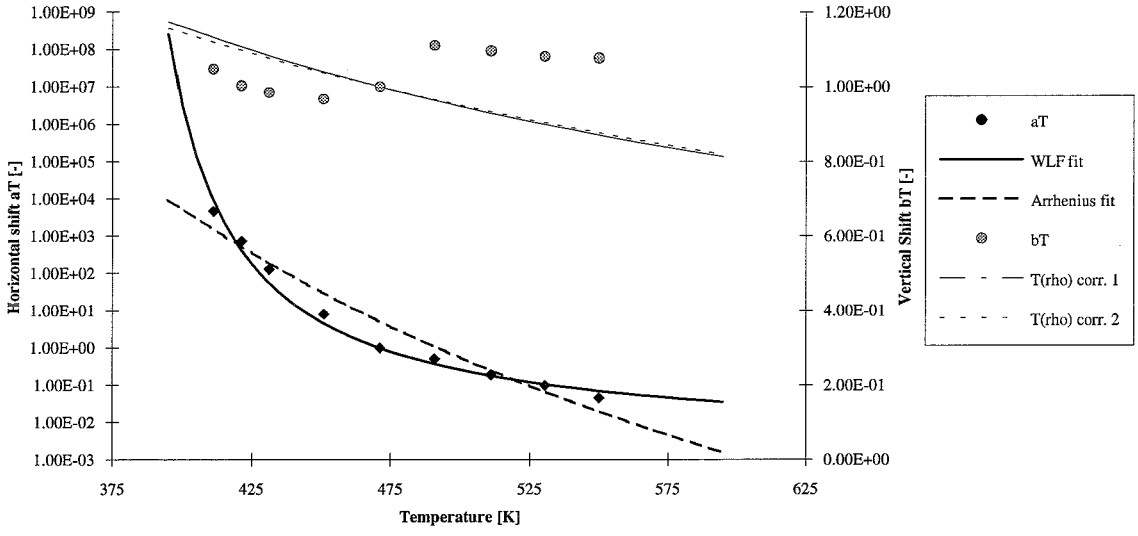
Shiftfactors PS330000 21_1_94 Tref=470K
Horizontal shift aT [-]
Vertical Shift bT [-]
Temperature [K]
1.00E+09
1.00E+08
1.00E+07
1.00E+06
1.00E+05
1.00E+04
1.00E+03
1.00E+02
1.00E+01
1.00E+00
1.00E-01
1.00E-02
1.00E-03
1.20E+00
1.00E+00
8.00E-01
6.00E-01
4.00E-01
2.00E-01
0.00E+00
375
425
475
525
575
625
aT
WLF fit
Arrhenius fit
bT
T(rho) corr. 1
T(rho) corr. 2

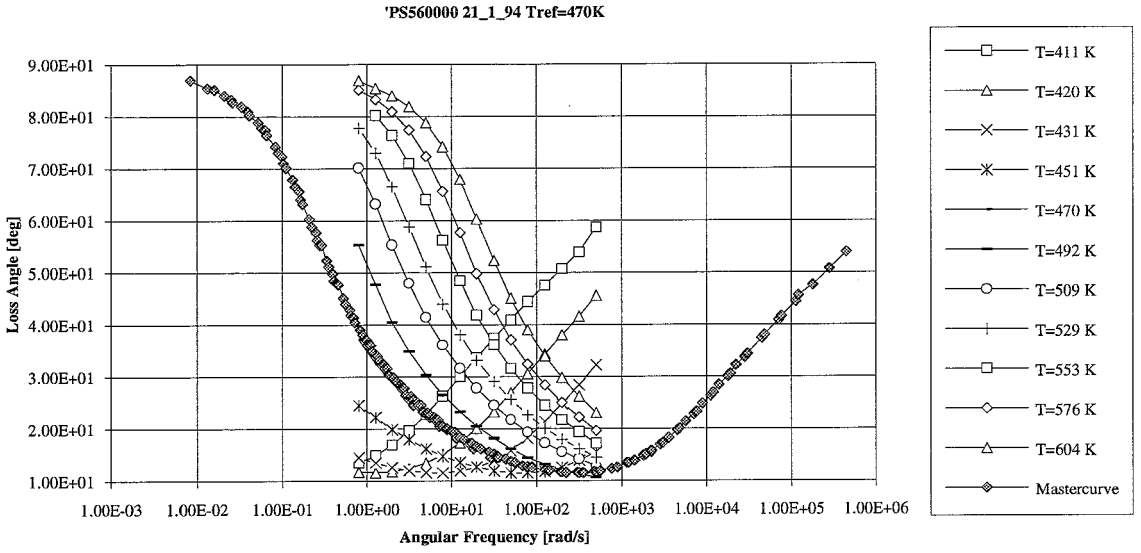
'PS560000 21_1_94 Tref=470K
Loss Angle [deg]
9.00E+01
8.00E+01
7.00E+01
6.00E+01
5.00E+01
4.00E+01
3.00E+01
2.00E+01
1.00E+01
1.00E-03
1.00E-02
1.00E-01
1.00E+00
1.00E+01
1.00E+02
1.00E+03
1.00E+04
1.00E+05
1.00E+06
Angular Frequency [rad/s]
T=411 K
T=420 K
T=431 K
T=451 K
T=470 K
T=492 K
T=509 K
T=529 K
T=553 K
T=576 K
T=604 K
Mastercurve

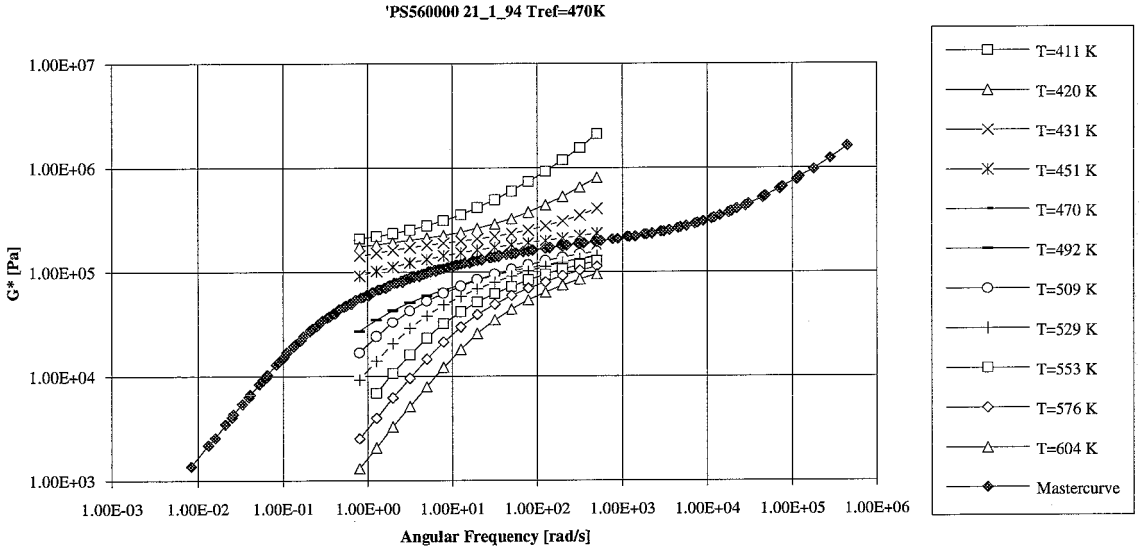
'PS560000 21_1_94 Tref=470K
G* [Pa]
1.00E+07
1.00E+06
1.00E+05
1.00E+04
1.00E+03
1.00E-03
1.00E-02
1.00E-01
1.00E+00
1.00E+01
1.00E+02
1.00E+03
1.00E+04
1.00E+05
1.00E+06
Angular Frequency [rad/s]
T=411 K
T=420 K
T=431 K
T=451 K
T=470 K
T=492 K
T=509 K
T=529 K
T=553 K
T=576 K
T=604 K
Mastercurve

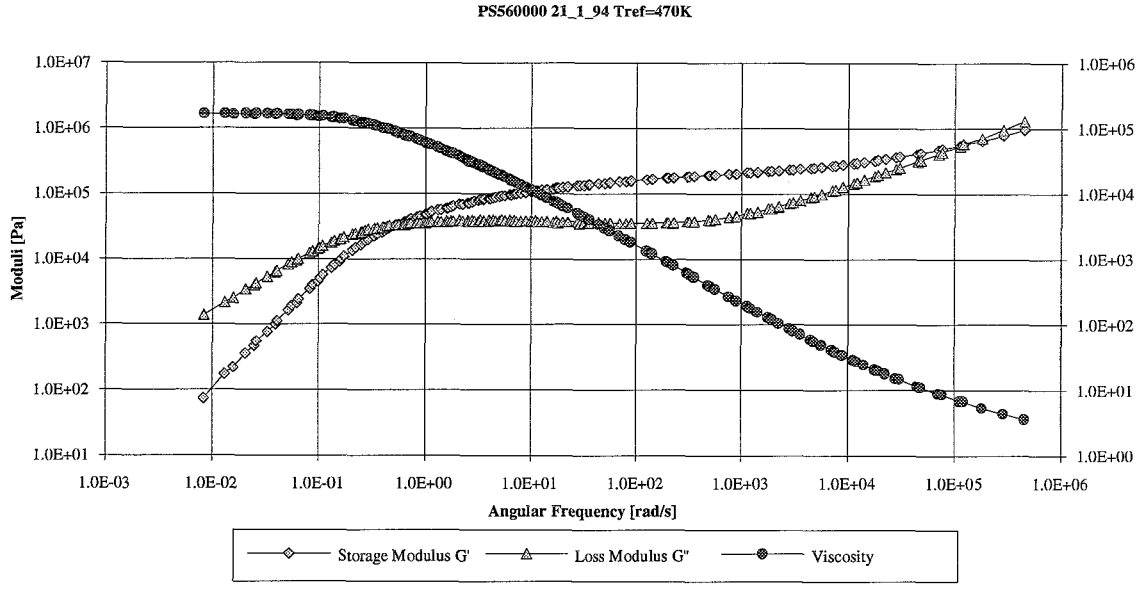
PS560000 21_1_94 Tref=470K
Moduli [Pa]
1.0E+07
1.0E+06
1.0E+05
1.0E+04
1.0E+03
1.0E+02
1.0E+01
1.0E+06
1.0E+05
1.0E+04
1.0E+03
1.0E+02
1.0E+01
1.0E+00
1.0E-03
1.0E-02
1.0E-01
1.0E+00
1.0E+01
1.0E+02
1.0E+03
1.0E+04
1.0E+05
1.0E+06
Angular Frequency [rad/s]
Storage Modulus G'
Loss Modulus G"
Viscosity

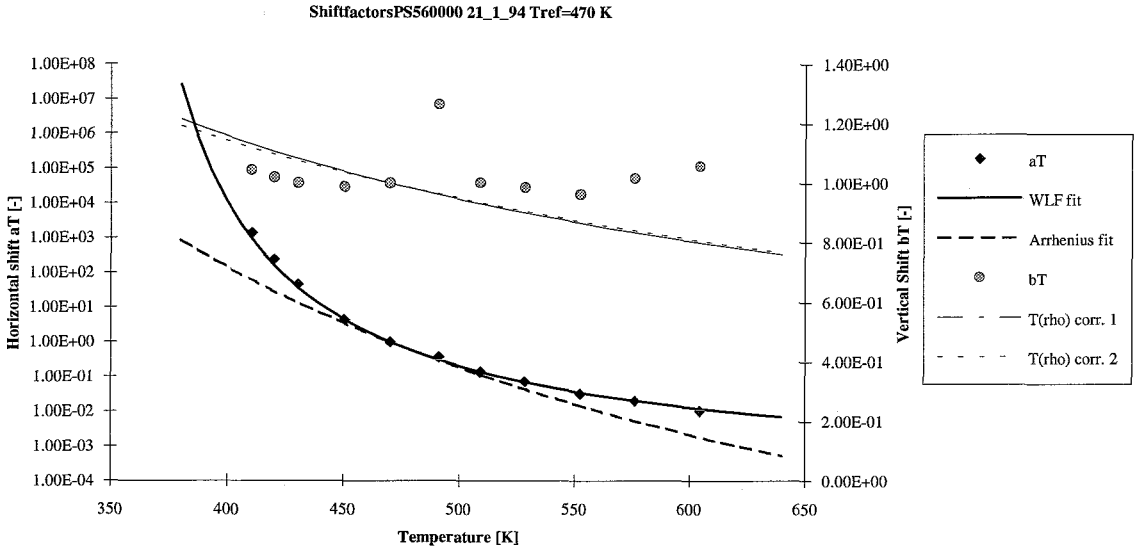
ShiftfactorsPS560000 21_1_94 Tref=470 K
Horizontal shift aT [-]
1.00E+08
1.00E+07
1.00E+06
1.00E+05
1.00E+04
1.00E+03
1.00E+02
1.00E+01
1.00E+00
1.00E-01
1.00E-02
1.00E-03
1.00E-04
Vertical Shift bT [-]
1.40E+00
1.20E+00
1.00E+00
8.00E-01
6.00E-01
4.00E-01
2.00E-01
0.00E+00
350
400
450
500
550
600
650
Temperature [K]
aT
WLF fit
Arrhenius fit
bT
T(rho) corr. 1
T(rho) corr. 2

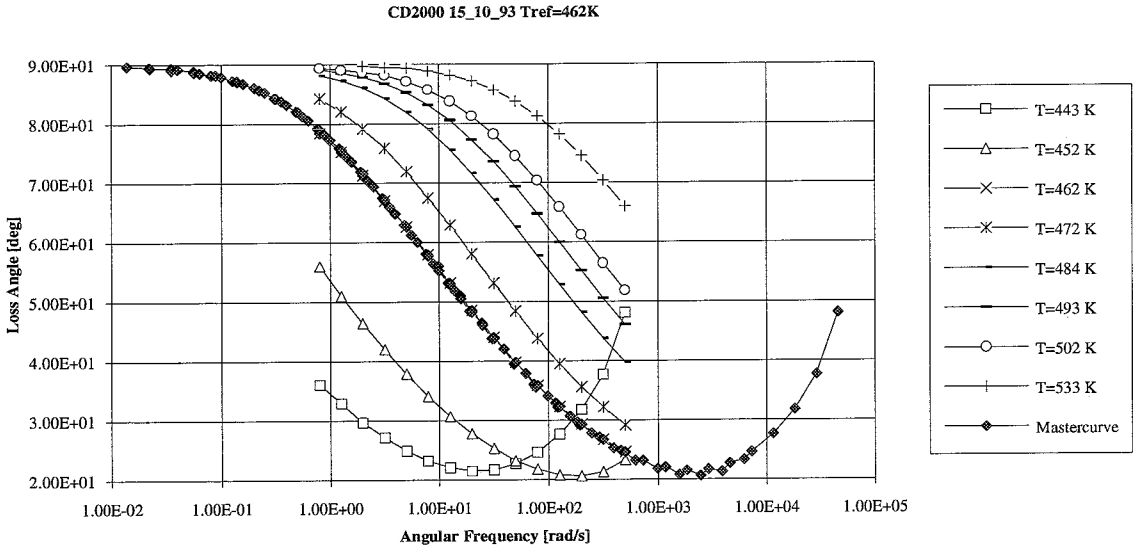
CD2000 15_10_93 Tref=462K
Loss Angle [deg]
9.00E+01
8.00E+01
7.00E+01
6.00E+01
5.00E+01
4.00E+01
3.00E+01
2.00E+01
1.00E-02
1.00E-01
1.00E+00
1.00E+01
1.00E+02
1.00E+03
1.00E+04
1.00E+05
Angular Frequency [rad/s]
T=443 K
T=452 K
T=462 K
T=472 K
T=484 K
T=493 K
T=502 K
T=533 K
Mastercurve

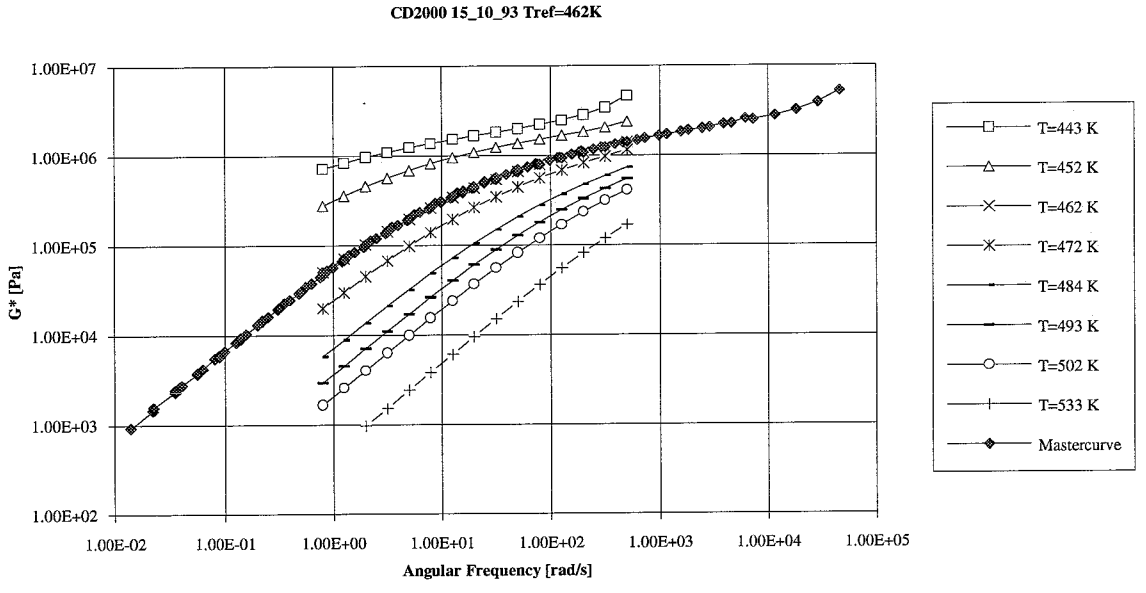
CD2000 15_10_93 Tref=462K
G* [Pa]
1.00E+07
1.00E+06
1.00E+05
1.00E+04
1.00E+03
1.00E+02
1.00E-02
1.00E-01
1.00E+00
1.00E+01
1.00E+02
1.00E+03
1.00E+04
1.00E+05
Angular Frequency [rad/s]
T=443 K
T=452 K
T=462 K
T=472 K
T=484 K
T=493 K
T=502 K
T=533 K
Mastercurve

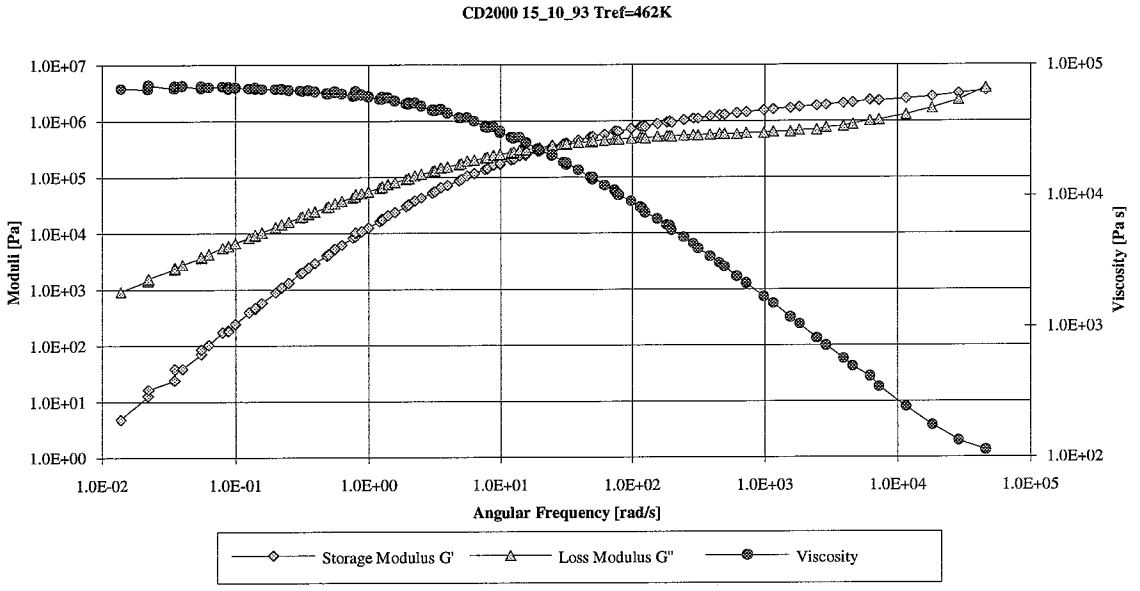
CD2000 15_10_93 Tref=462K
Moduli [Pa]
Viscosity [Pa s]
Angular Frequency [rad/s]
Storage Modulus G'
Loss Modulus G"
Viscosity

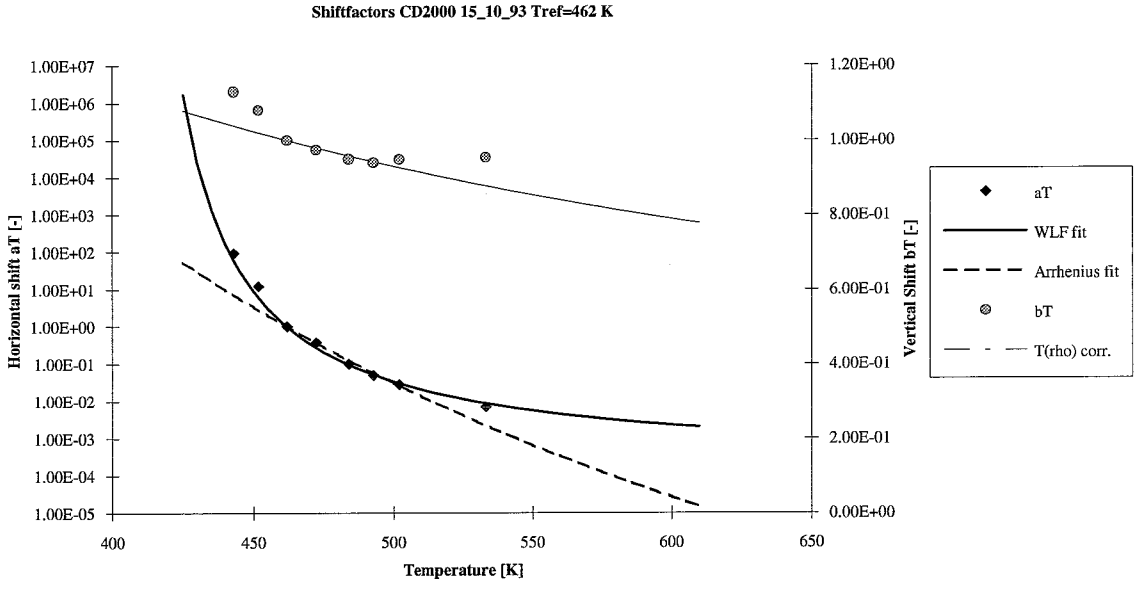
Shiftfactors CD2000 15_10_93 Tref=462 K
Horizontal shift aT [-]
Vertical Shift bT [-]
Temperature [K]
aT
WLF fit
Arrhenius fit
bT
T(rho) corr.

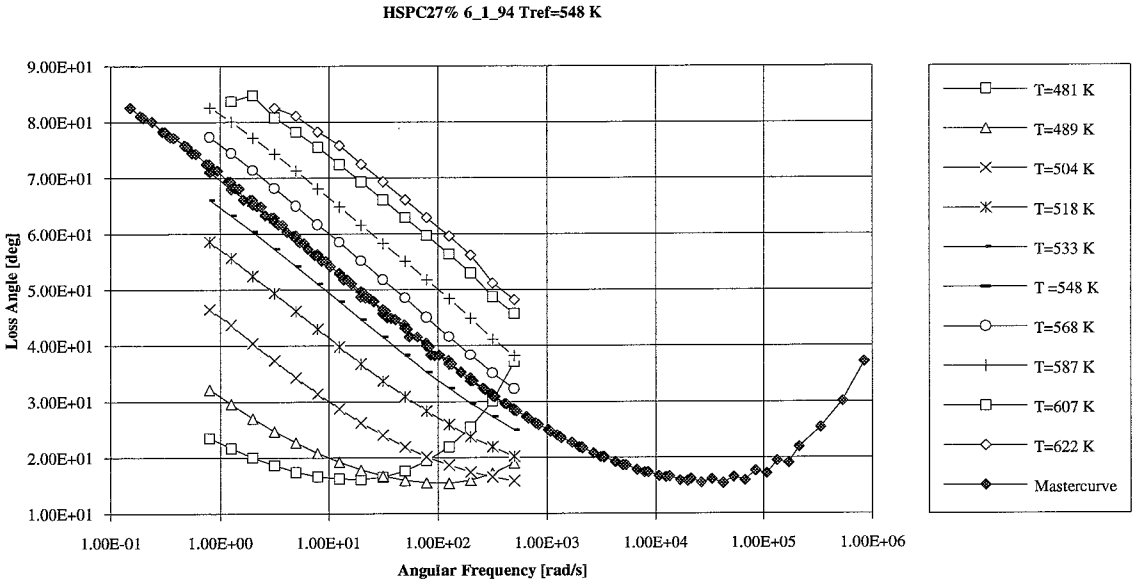
HSPC27% 6_1_94 Tref=548 K
Loss Angle [deg]
9.00E+01
8.00E+01
7.00E+01
6.00E+01
5.00E+01
4.00E+01
3.00E+01
2.00E+01
1.00E+01
1.00E-01
1.00E+00
1.00E+01
1.00E+02
1.00E+03
1.00E+04
1.00E+05
1.00E+06
Angular Frequency [rad/s]
T=481 K
T=489 K
T=504 K
T=518 K
T=533 K
T =548 K
T=568 K
T=587 K
T=607 K
T=622 K
Mastercurve

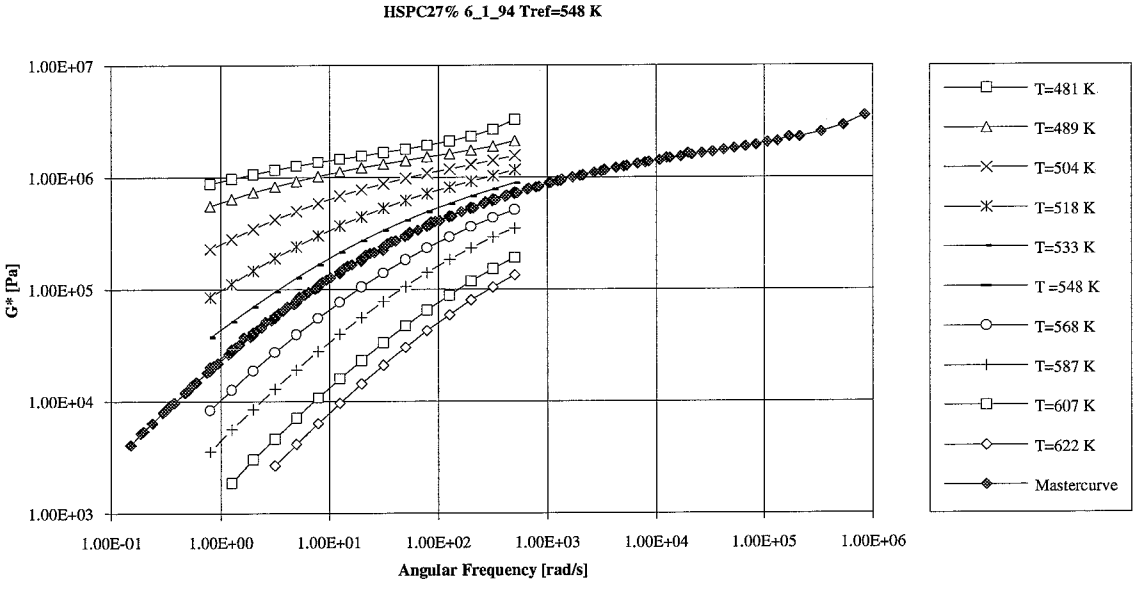
HSPC27% 6_1_94 Tref=548 K
G* [Pa]
1.00E+07
1.00E+06
1.00E+05
1.00E+04
1.00E+03
1.00E-01
1.00E+00
1.00E+01
1.00E+02
1.00E+03
1.00E+04
1.00E+05
1.00E+06
Angular Frequency [rad/s]
T=481 K
T=489 K
T=504 K
T=518 K
T=533 K
T =548 K
T=568 K
T=587 K
T=607 K
T=622 K
Mastercurve

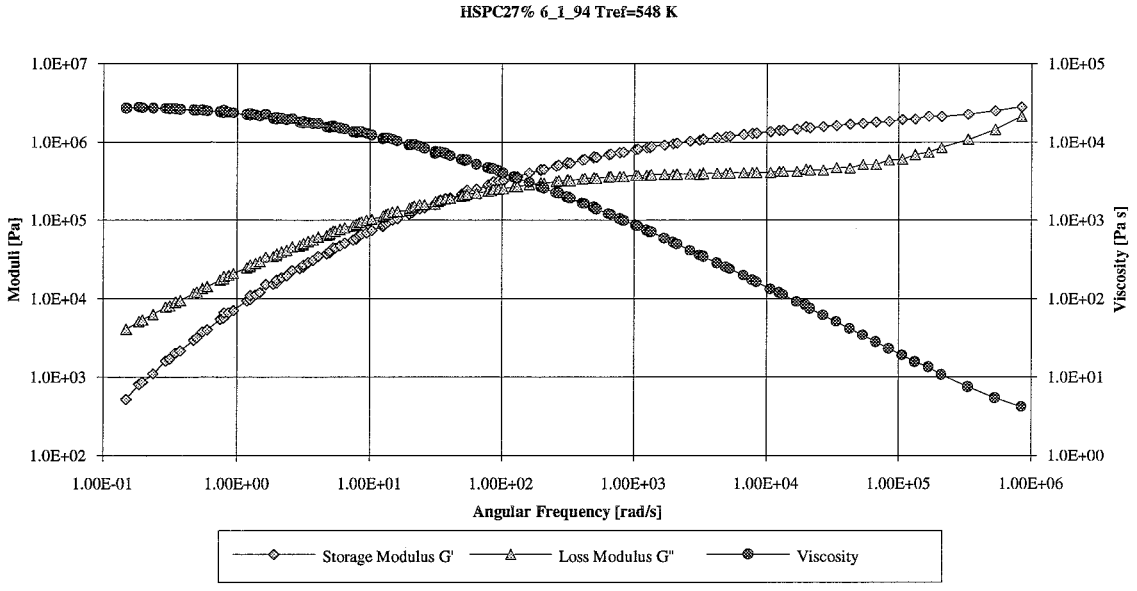
HSPC27% 6_1_94 Tref=548 K
Moduli [Pa]
Viscosity [Pa s]
Angular Frequency [rad/s]
Storage Modulus G'
Loss Modulus G"
Viscosity

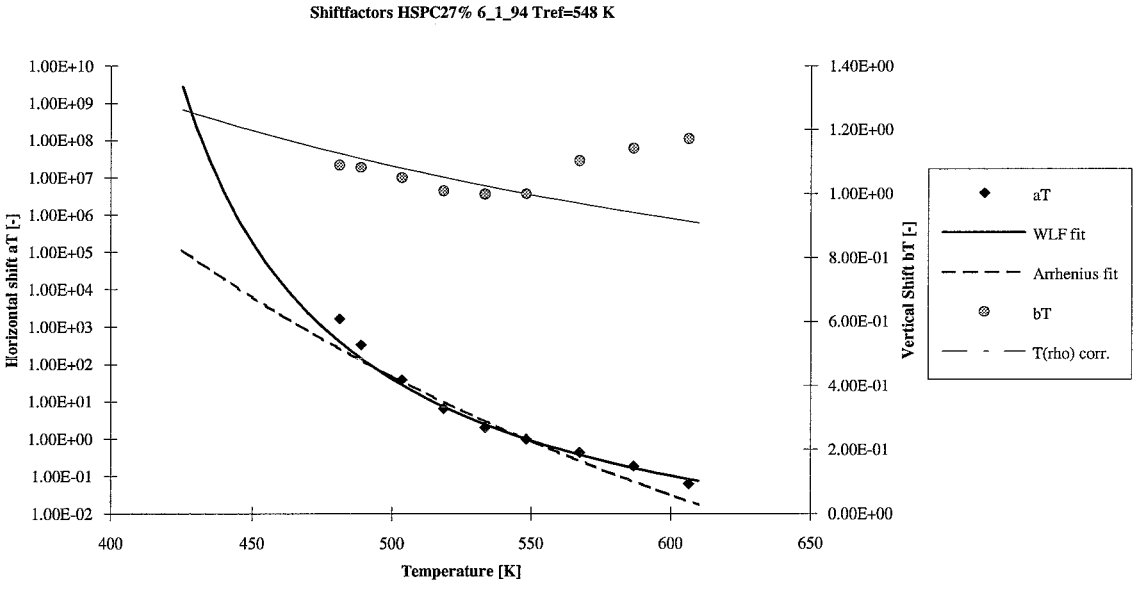
Shiftfactors HSPC27% 6_1_94 Tref=548 K
Horizontal shift aT [-]
Vertical Shift bT [-]
Temperature [K]
aT
WLF fit
Arrhenius fit
bT
T(rho) corr.

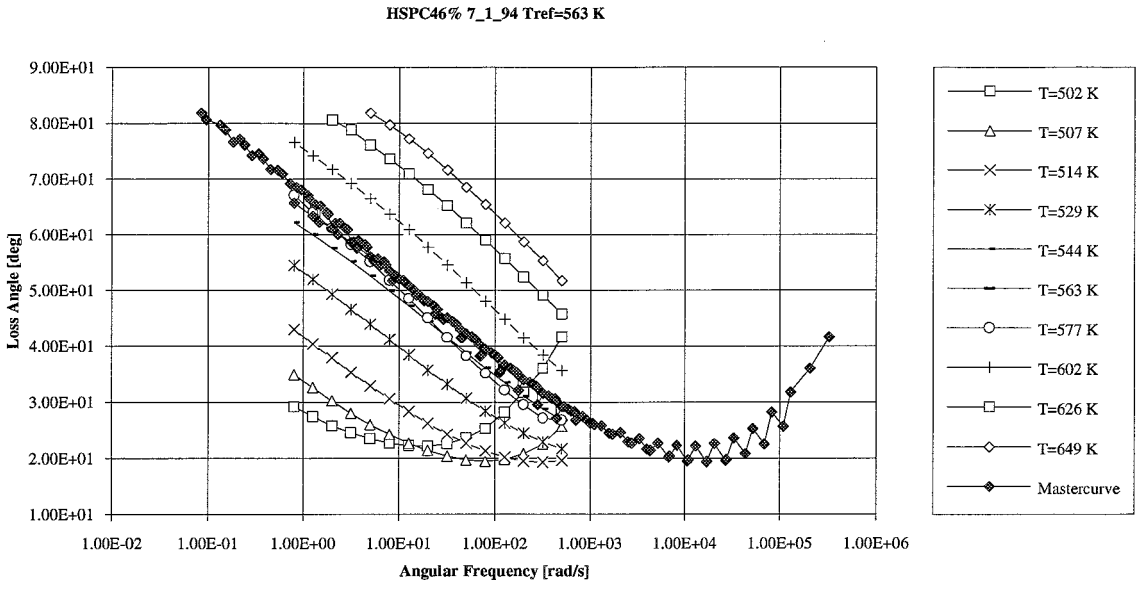
HSPC46% 7_1_94 Tref=563 K
Loss Angle [deg]
9.00E+01
8.00E+01
7.00E+01
6.00E+01
5.00E+01
4.00E+01
3.00E+01
2.00E+01
1.00E+01
1.00E-02
1.00E-01
1.00E+00
1.00E+01
1.00E+02
1.00E+03
1.00E+04
1.00E+05
1.00E+06
Angular Frequency [rad/s]
T=502 K
T=507 K
T=514 K
T=529 K
T=544 K
T=563 K
T=577 K
T=602 K
T=626 K
T=649 K
Mastercurve

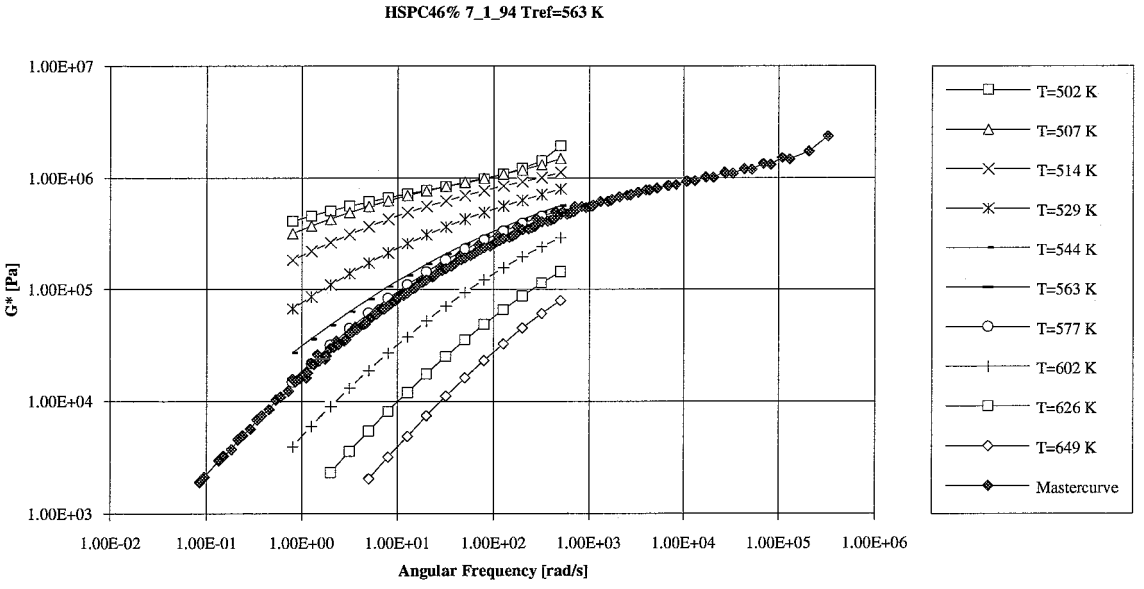
HSPC46% 7_1_94 Tref=563 K
G* [Pa]
1.00E+07
1.00E+06
1.00E+05
1.00E+04
1.00E+03
1.00E-02
1.00E-01
1.00E+00
1.00E+01
1.00E+02
1.00E+03
1.00E+04
1.00E+05
1.00E+06
Angular Frequency [rad/s]
T=502 K
T=507 K
T=514 K
T=529 K
T=544 K
T=563 K
T=577 K
T=602 K
T=626 K
T=649 K
Mastercurve

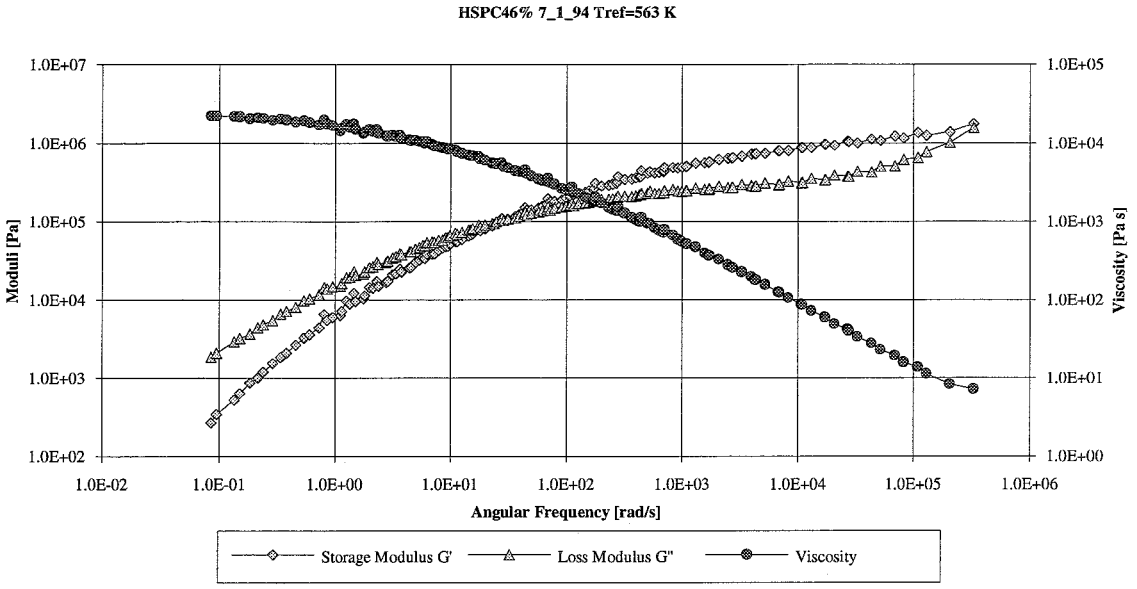
HSPC46% 7_1_94 Tref=563 K
Moduli [Pa]
Viscosity [Pa s]
Angular Frequency [rad/s]
Storage Modulus G'
Loss Modulus G"
Viscosity

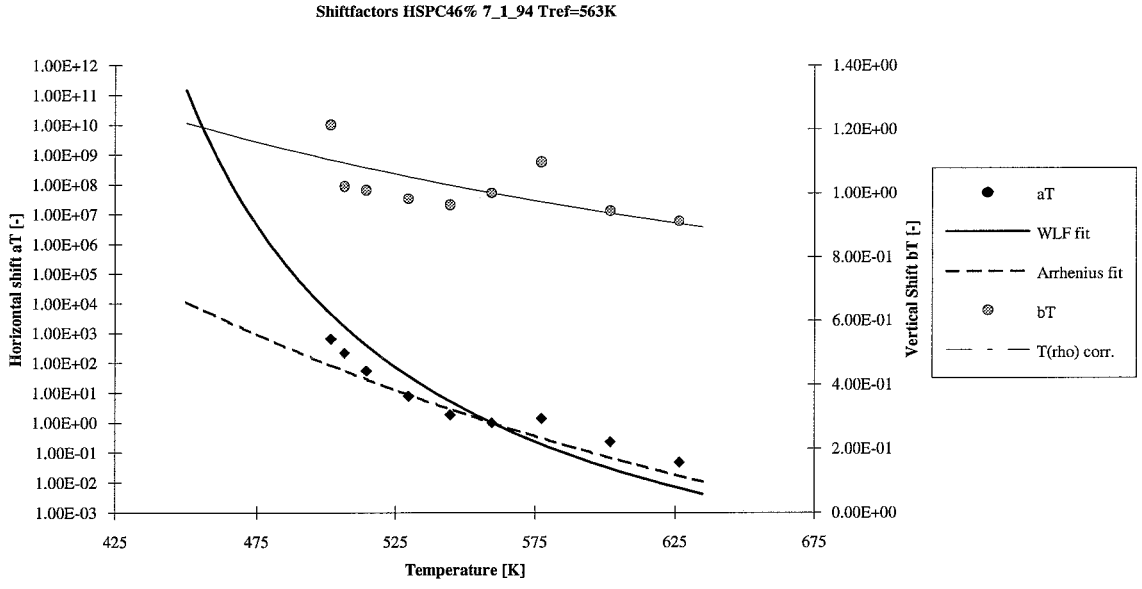
Shiftfactors HSPC46% 7_1_94 Tref=563K
Horizontal shift aT [-]
Vertical Shift bT [-]
Temperature [K]
aT
WLF fit
Arrhenius fit
bT
T(rho) corr.

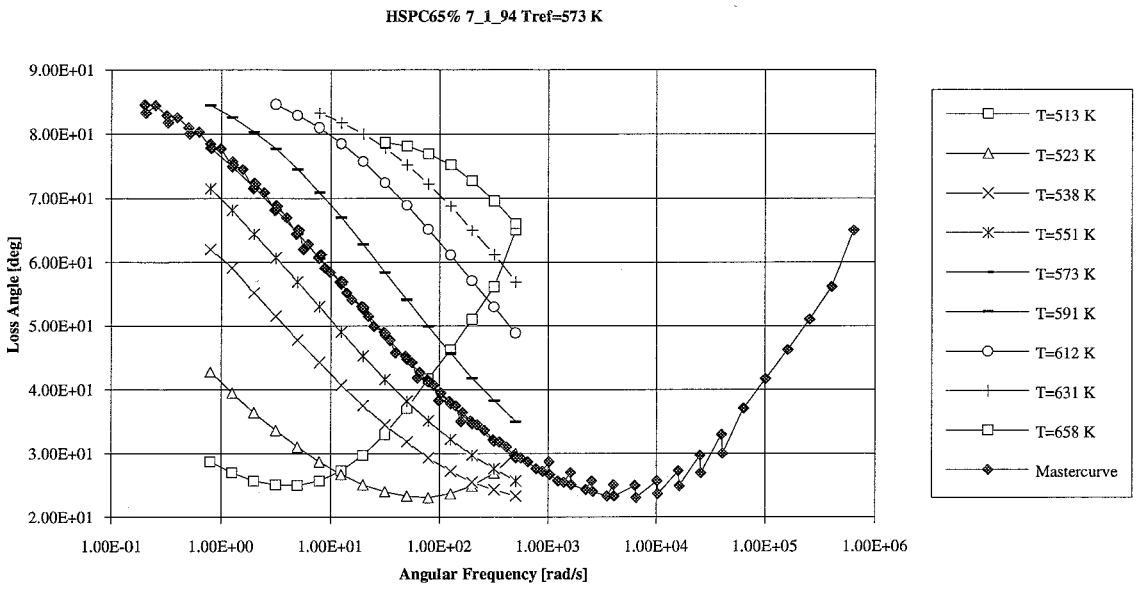
HSPC65% 7_1_94 Tref=573 K
Loss Angle [deg]
9.00E+01
8.00E+01
7.00E+01
6.00E+01
5.00E+01
4.00E+01
3.00E+01
2.00E+01
1.00E-01
1.00E+00
1.00E+01
1.00E+02
1.00E+03
1.00E+04
1.00E+05
1.00E+06
Angular Frequency [rad/s]
T=513 K
T=523 K
T=538 K
T=551 K
T=573 K
T=591 K
T=612 K
T=631 K
T=658 K
Mastercurve

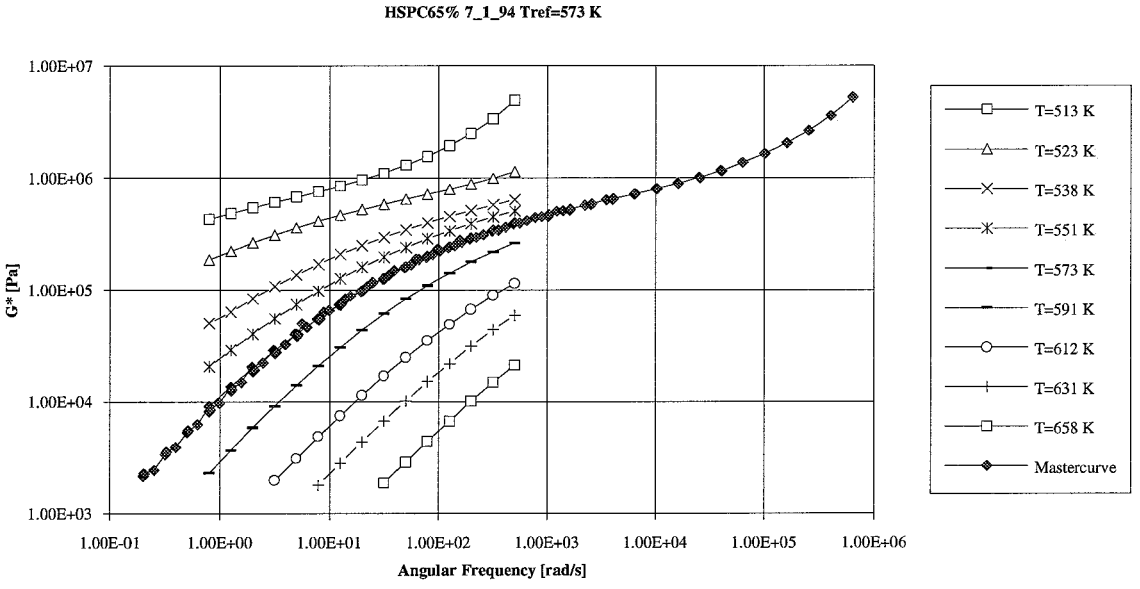
HSPC65% 7_1_94 Tref=573 K
G* [Pa]
1.00E+07
1.00E+06
1.00E+05
1.00E+04
1.00E+03
1.00E-01
1.00E+00
1.00E+01
1.00E+02
1.00E+03
1.00E+04
1.00E+05
1.00E+06
Angular Frequency [rad/s]
T=513 K
T=523 K
T=538 K
T=551 K
T=573 K
T=591 K
T=612 K
T=631 K
T=658 K
Mastercurve

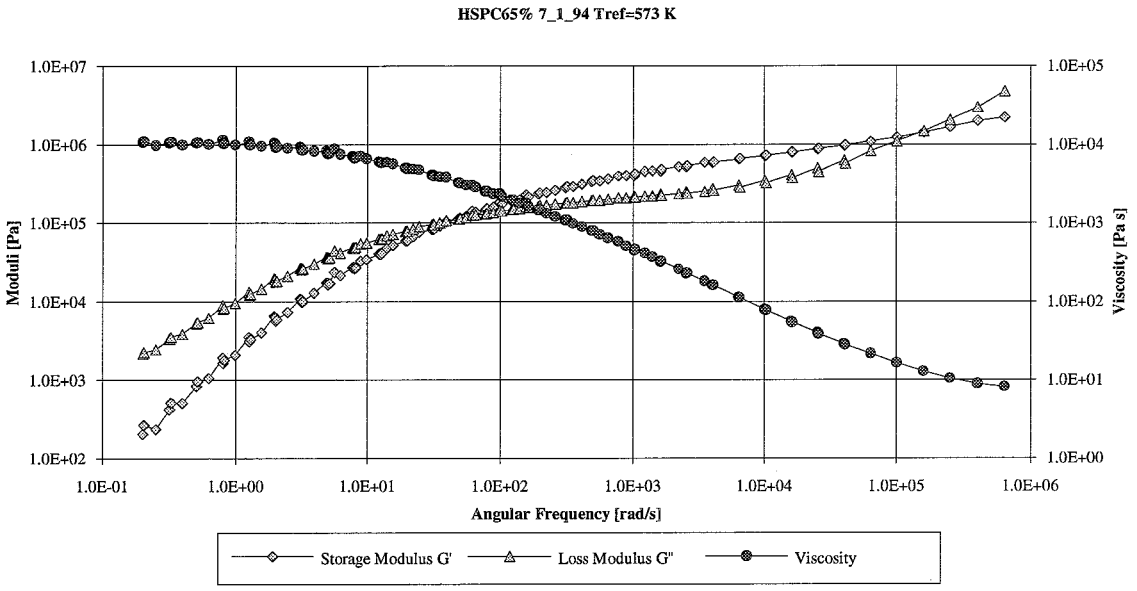
HSPC65% 7_1_94 Tref=573 K
Moduli [Pa]
Viscosity [Pa s]
Angular Frequency [rad/s]
Storage Modulus G'
Loss Modulus G"
Viscosity

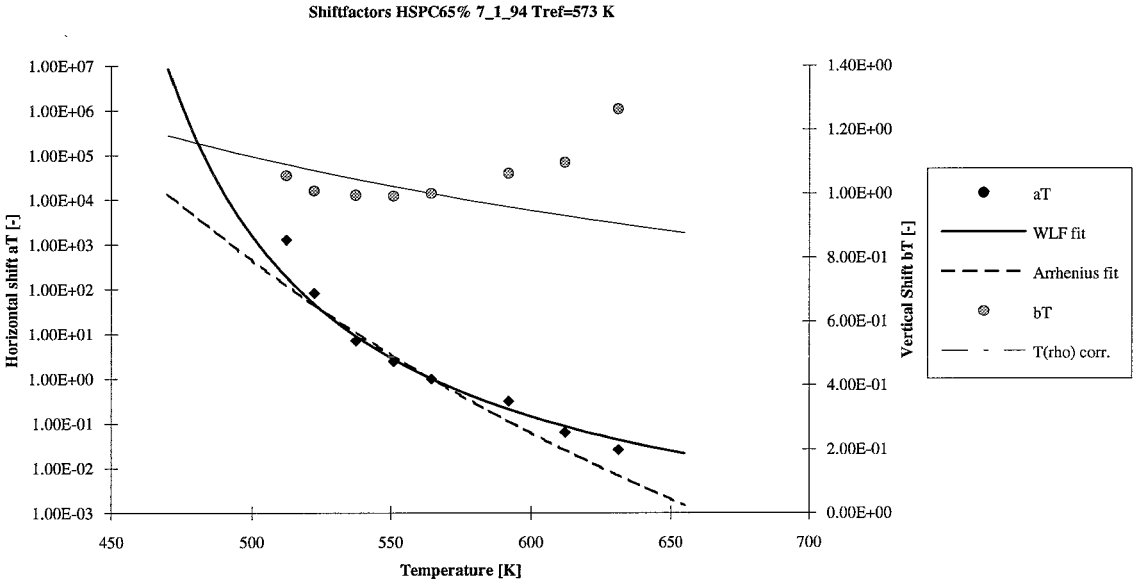
Shiftfactors HSPC65% 7_1_94 Tref=573 K
Horizontal shift aT [-]
Vertical Shift bT [-]
Temperature [K]
aT
WLF fit
Arrhenius fit
bT
T(rho) corr.

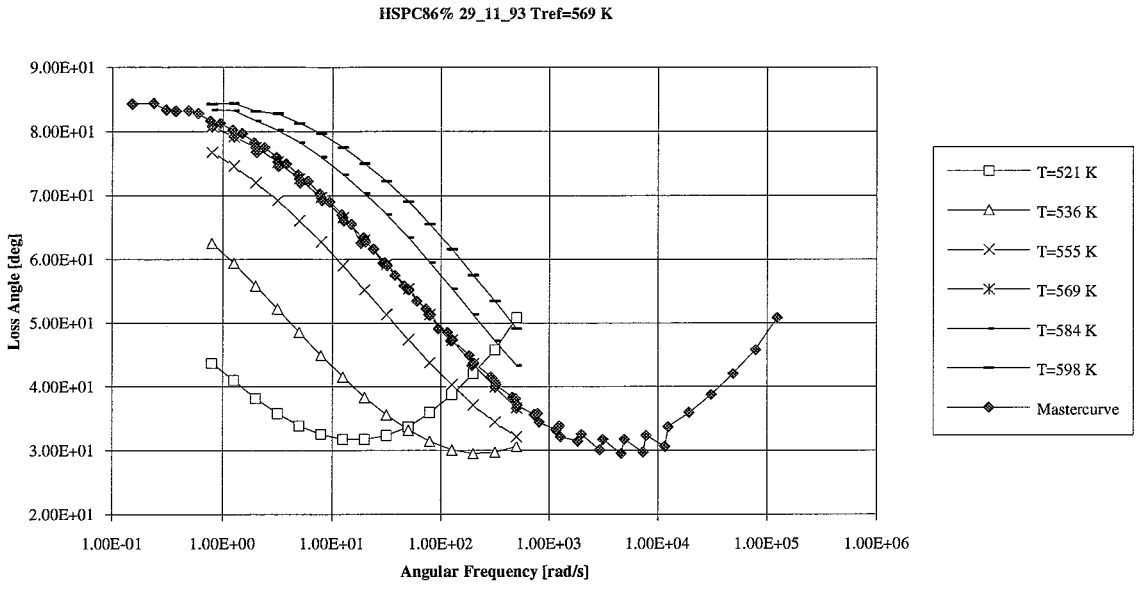
HSPC86% 29_11_93 Tref=569 K
9.00E+01
8.00E+01
7.00E+01
6.00E+01
5.00E+01
4.00E+01
3.00E+01
2.00E+01
Loss Angle [deg]
1.00E-01
1.00E+00
1.00E+01
1.00E+02
1.00E+03
1.00E+04
1.00E+05
1.00E+06
Angular Frequency [rad/s]
T=521 K
T=536 K
T=555 K
T=569 K
T=584 K
T=598 K
Mastercurve

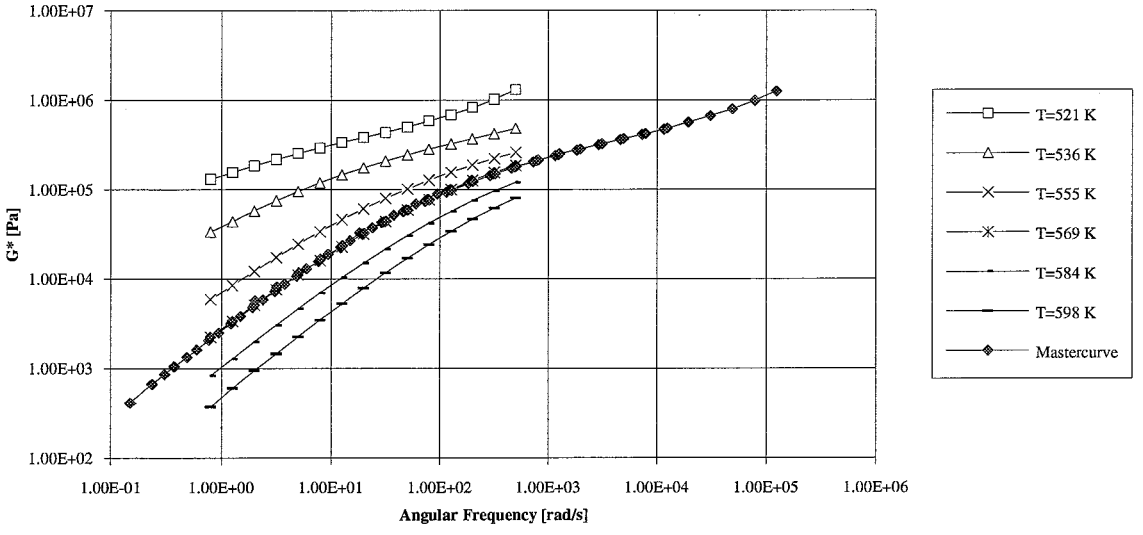
HSPC86% 29_11_93 Tref=569 K
1.00E+07
1.00E+06
1.00E+05
1.00E+04
1.00E+03
1.00E+02
G* [Pa]
1.00E-01
1.00E+00
1.00E+01
1.00E+02
1.00E+03
1.00E+04
1.00E+05
1.00E+06
Angular Frequency [rad/s]
T=521 K
T=536 K
T=555 K
T=569 K
T=584 K
T=598 K
Mastercurve

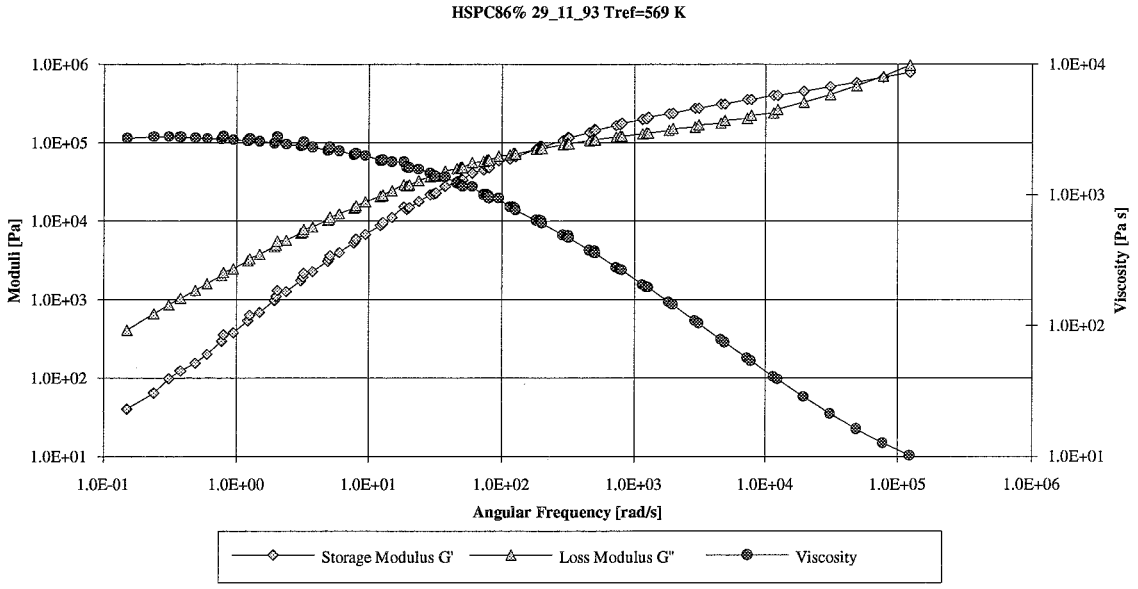
HSPC86% 29_11_93 Tref=569 K
1.0E+06
1.0E+05
1.0E+04
1.0E+03
1.0E+02
1.0E+01
Moduli [Pa]
1.0E+04
1.0E+03
1.0E+02
1.0E+01
Viscosity [Pa s]
1.0E-01
1.0E+00
1.0E+01
1.0E+02
1.0E+03
1.0E+04
1.0E+05
1.0E+06
Angular Frequency [rad/s]
Storage Modulus G'
Loss Modulus G"
Viscosity

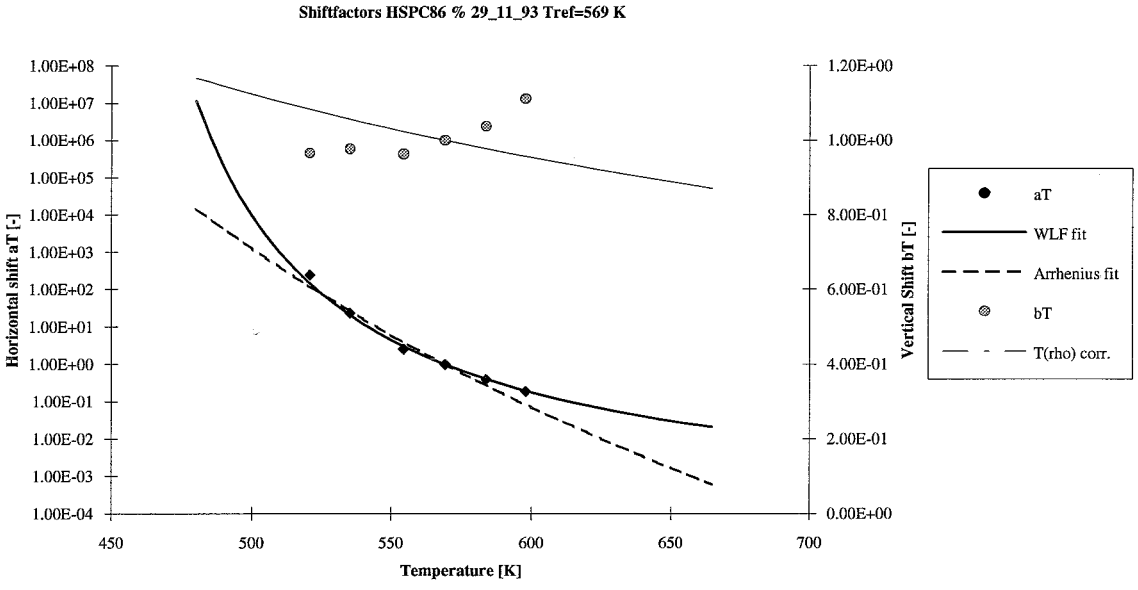
Shiftfactors HSPC86 % 29_11_93 Tref=569 K
1.00E+08
1.00E+07
1.00E+06
1.00E+05
1.00E+04
1.00E+03
1.00E+02
1.00E+01
1.00E+00
1.00E-01
1.00E-02
1.00E-03
1.00E-04
Horizontal shift aT [-]
1.20E+00
1.00E+00
8.00E-01
6.00E-01
4.00E-01
2.00E-01
0.00E+00
Vertical Shift bT [-]
450
500
550
600
650
700
Temperature [K]
aT
WLF fit
Arrhenius fit
bT
T(rho) corr.

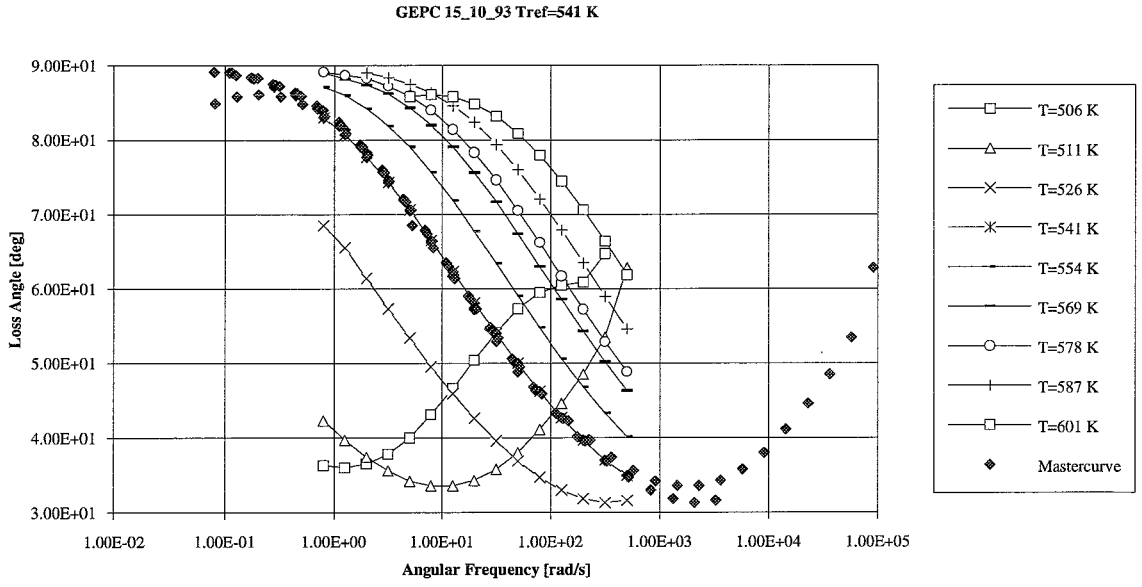
GEPC 15_10_93 Tref=541 K
9.00E+01
8.00E+01
7.00E+01
6.00E+01
5.00E+01
4.00E+01
3.00E+01
Loss Angle [deg]
1.00E-02
1.00E-01
1.00E+00
1.00E+01
1.00E+02
1.00E+03
1.00E+04
1.00E+05
Angular Frequency [rad/s]
T=506 K
T=511 K
T=526 K
T=541 K
T=554 K
T=569 K
T=578 K
T=587 K
T=601 K
Mastercurve

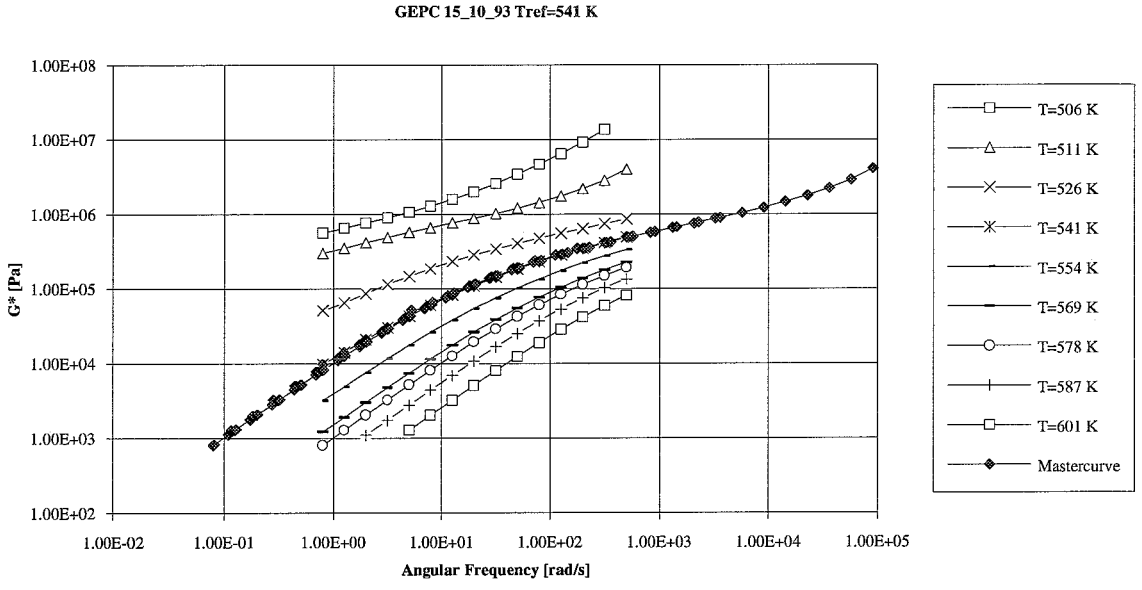
GEPC 15_10_93 Tref=541 K
1.00E+08
1.00E+07
1.00E+06
1.00E+05
1.00E+04
1.00E+03
1.00E+02
G* [Pa]
1.00E-02
1.00E-01
1.00E+00
1.00E+01
1.00E+02
1.00E+03
1.00E+04
1.00E+05
Angular Frequency [rad/s]
T=506 K
T=511 K
T=526 K
T=541 K
T=554 K
T=569 K
T=578 K
T=587 K
T=601 K
Mastercurve

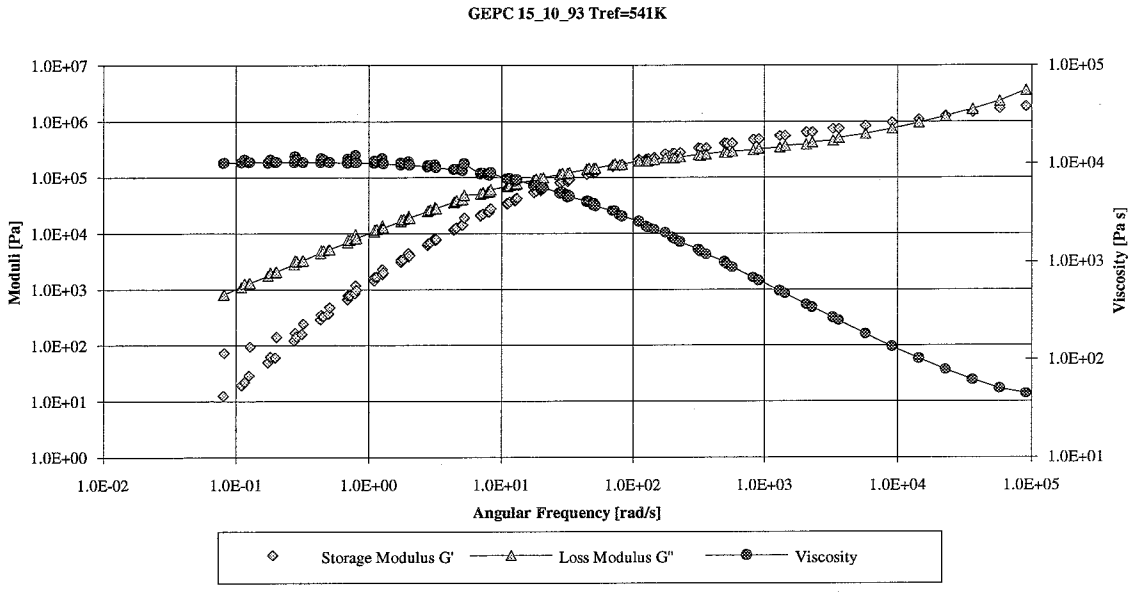
GEPC 15_10_93 Tref=541K
Moduli [Pa]
Viscosity [Pa s]
Angular Frequency [rad/s]
1.0E+07
1.0E+06
1.0E+05
1.0E+04
1.0E+03
1.0E+02
1.0E+01
1.0E+00
1.0E-02
1.0E-01
1.0E+00
1.0E+01
1.0E+02
1.0E+03
1.0E+04
1.0E+05
Storage Modulus G'
Loss Modulus G"
Viscosity

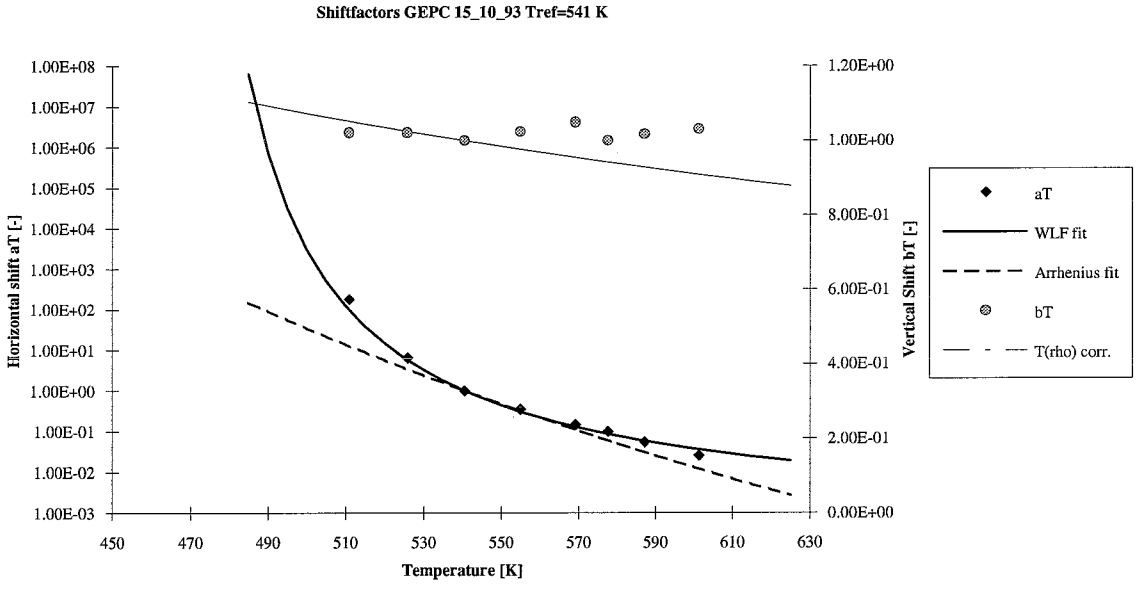
Shiftfactors GEPC 15_10_93 Tref=541 K
Horizontal shift aT [-]
Vertical Shift bT [-]
Temperature [K]
1.00E+08
1.00E+07
1.00E+06
1.00E+05
1.00E+04
1.00E+03
1.00E+02
1.00E+01
1.00E+00
1.00E-01
1.00E-02
1.00E-03
1.20E+00
1.00E+00
8.00E-01
6.00E-01
4.00E-01
2.00E-01
0.00E+00
450
470
490
510
530
550
570
590
610
630
aT
WLF fit
Arrhenius fit
bT
T(rho) corr.

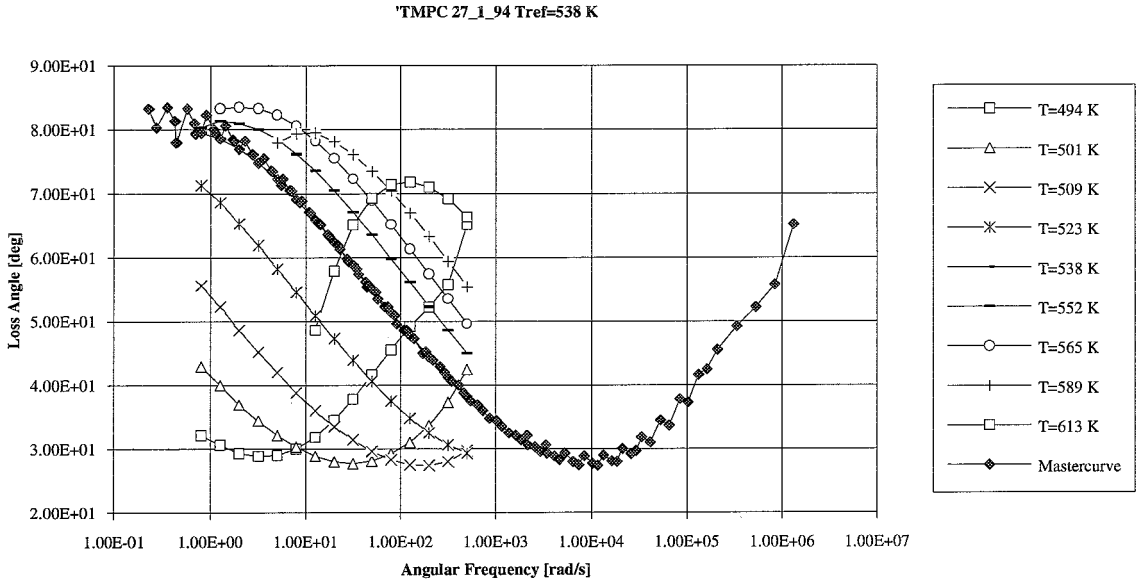
'TMPC 27_1_94 Tref=538 K
Loss Angle [deg]
9.00E+01
8.00E+01
7.00E+01
6.00E+01
5.00E+01
4.00E+01
3.00E+01
2.00E+01
1.00E-01
1.00E+00
1.00E+01
1.00E+02
1.00E+03
1.00E+04
1.00E+05
1.00E+06
1.00E+07
Angular Frequency [rad/s]
T=494 K
T=501 K
T=509 K
T=523 K
T=538 K
T=552 K
T=565 K
T=589 K
T=613 K
Mastercurve

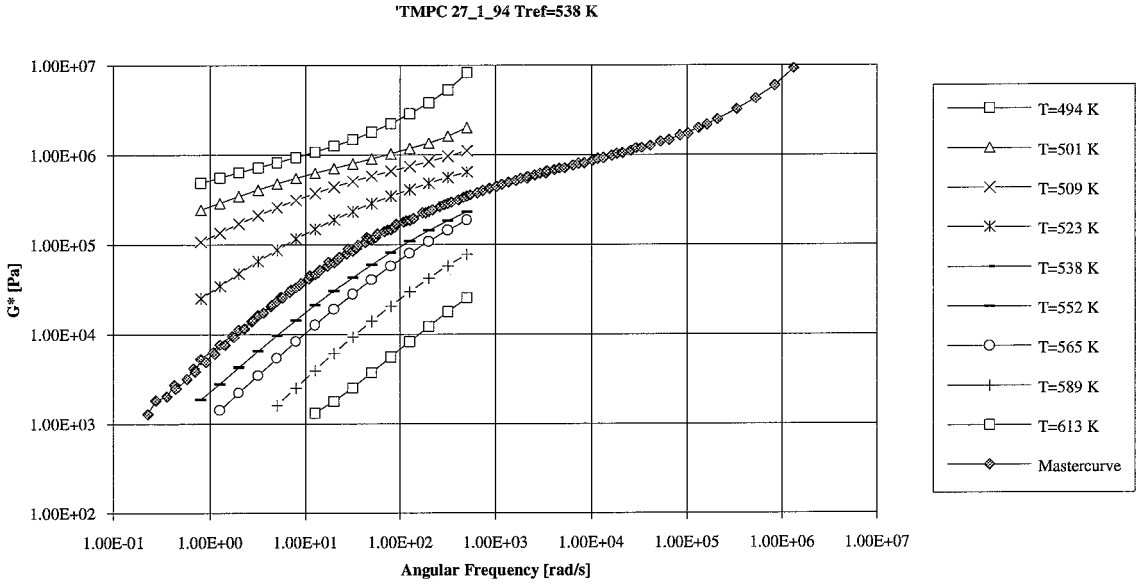
'TMPC 27_1_94 Tref=538 K
G* [Pa]
1.00E+07
1.00E+06
1.00E+05
1.00E+04
1.00E+03
1.00E+02
1.00E-01
1.00E+00
1.00E+01
1.00E+02
1.00E+03
1.00E+04
1.00E+05
1.00E+06
1.00E+07
Angular Frequency [rad/s]
T=494 K
T=501 K
T=509 K
T=523 K
T=538 K
T=552 K
T=565 K
T=589 K
T=613 K
Mastercurve

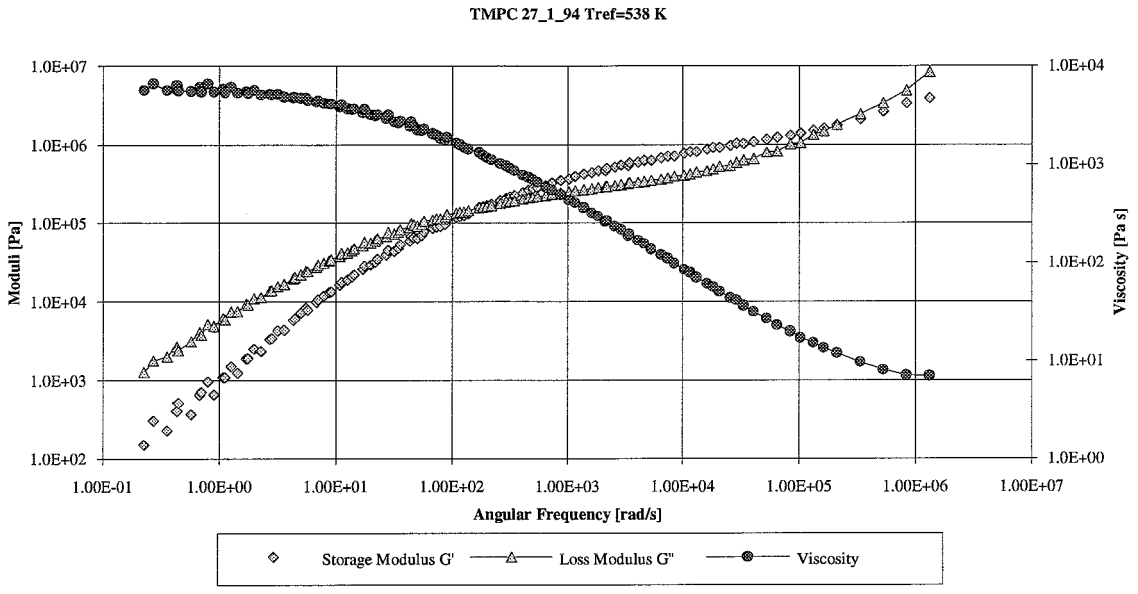
TMPC 27_1_94 Tref=538 K
Moduli [Pa]
Viscosity [Pa s]
Angular Frequency [rad/s]
Storage Modulus G'
Loss Modulus G"
Viscosity

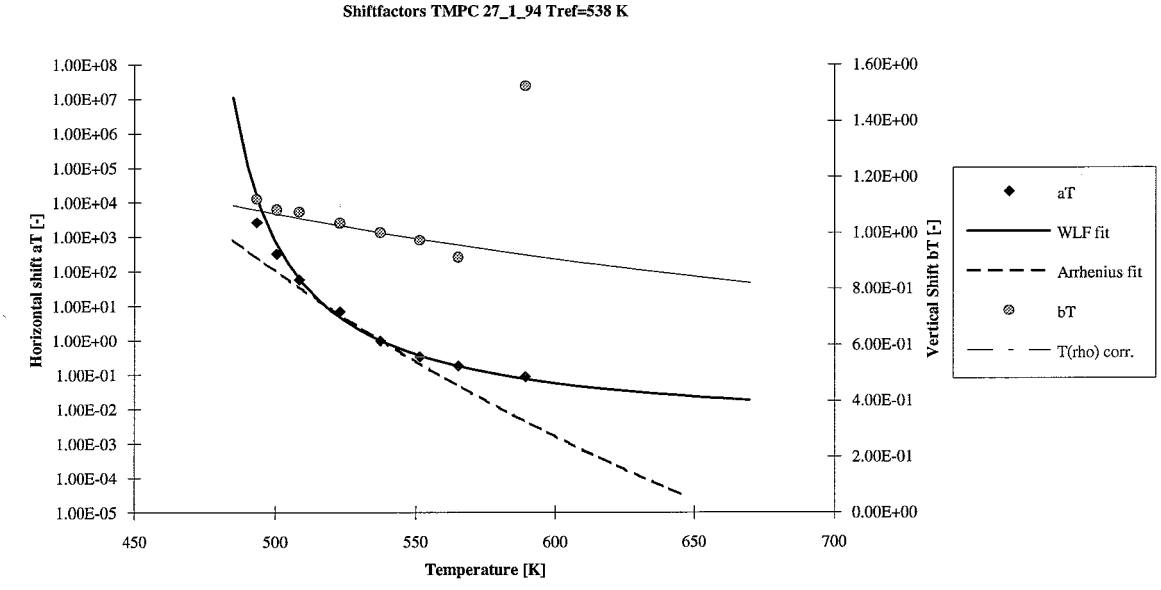
Shiftfactors TMPC 27_1_94 Tref=538 K
Horizontal shift aT [-]
Vertical Shift bT [-]
Temperature [K]
aT
WLF fit
Arrhenius fit
bT
T(rho) corr.

Appendix C

Creep and recovery results

In this appendix tables are given with results of all steady shear experiments for polystyrene and polycarbonate respectively. Empty cells indicate that unambiguous results could not be determined. Results of the useable experiments are shaded, these values are averaged and given in Chapter 4. The results are discussed in § 4.2 and details on the used methods are given in § 3.3.2.1 and § 3.3.2.2 for recovery and creep respectively.

Start-up transients occurring during creep do not prevent the recoverable compliance to be determined from the recovery experiment, if steady-state is achieved.

The cone-plate geometry caused for the apparatus unacceptable normal forces, therefore it was replaced by a plate-plate system.

Materials	σ	T	t_creep	t_rec	γmax	Recovery		Regression J(t)		"Sherby-Dorn"	Remarks
	[kPa]	[K]	[s]	[s]	[-]	$J_e^0\ 10^{-5}$ [Pa^{-1}]	η_0 [Pa s]	$J_e^0\ 10^{-5}$ [Pa^{-1}]	η_0 [Pa s]	$J_e^0\ 10^{-5}$ [Pa^{-1}]	
PS678E	4.68	403	1000	1000		7.03		2.89	4.24e6		start-up erroneous
	4.68	403	1000	1000		5.66		4.76	4.9e6		same sample as previous
	4.68	403	1000	2000		5.66					slope log(J)<1
	18.7	403	1000	1000		4.21					γ(t) discontinuous
PS96	4.68	414	891	1782							encoder out of specification
	4.68	414	1000	1000	5.08	1.42	9.3e5	0.416	9.26e5		start-up erroneous
	9.37	414	1259	1259							slope log(J)>1
	1.25	440	1000	1000	69.7						plate-plate; slip?!
	0.63	435	1000	1000							plate-plate; slip?!
PS330	1.25	435	1000	1585	1.48	2.92		5	1.39e6	3.5	plates; surface indicates slip
	6.25	435	1000	1000	4.03	1.42					plates; start-up erroneous
	8.57	424	1000	1000	0.76	1.19					
	17.1	424	1258	1258	3.8	0.68					plates; γ(t) discontinuous
	34.3	424	631	631	0.2	0.43					plates; creep stopped
PS560	9.37	423	1202	1202							creep stopped
	28.11	434	1202	1202							encoder out of specification
	6.25	435	1000	1000	0.838	1.6	6.7e7	2.08	1.11e7	1.9	plate-plate
	12.5	435	1000	1000		1.73					plate-plate; creep stopped followed by an upswing; recovery smooth
	17.1	424	1259	1259		1.2					
	34.3	424	1259	1259		2.23					

Materials	σ	T	t_creep	t_rec	γmax	Recovery		Regression J(t)		"Sherby-Dorn"	Remarks
	[kPa]	[K]	[s]	[s]	[-]	J_e^0 10^{-5} [Pa^{-1}]	η_0 [Pa s]	J_e^0 10^{-5} [Pa^{-1}]	η_0 [Pa s]	J_e^0 10^{-5} [Pa^{-1}]	
CD2000	0.937	438	1000	1000	0.171	0.537	5.6e6				
	4.68	438	1000	1000		0.241	1.2e7				same sample; slope log(J)<1
	4.68	448	1000	1000	5.2	0.483	9.0e5				
	18.7	448	1000	1000	17.4	0.523					
	0.937	463	1000	1000	11.2	0.268					windmill-effect
	4.68	463	1000	1000	67.8						windmill-effect; γ>1 rotation
PC 27%	0.937	493	1000	2000	0.44	3.49	2.3e6	4.72	2.38e6	4.02	recovery finished
	0.937	493	1000	2000	0.29	5.37	3.4e6	1.52	3.43e6		same sample; start-up ?!
	18.7	493	1000	1000							same sample
	18.7	493	1000	1000	1.79	2.22				2.46	
PC 46%	4.68	508	1000	2000	0.212	1.96					start-up erroneous
	4.68	508	1000	2000	1.09	2.04					same sample; constriction ?!
	18.7	508	1000	2000	21.8	6.16					
PC 65%	1.25	523	1000	1000	25.9						plate-plate; T ?!; slip ?!
	6.25	523	1000	1585							plates; slope log(J)>1
	12.5	523	1000	1000							plates; γ>3 rotations; slip ?!
PC 86%	1.46	515	1000	1000	0.093	3.28					plates; T ?!; γ(t) discontinuous
	7.28	515	1000	1000	0.289						plates; T ?!; slip ?!
	14.6	515	1000	1000	0.818	6.15					plates; T ?!;
	14.6	526	1000	1000	2.75	5.43					plates; T ?!;
	14.6	526	1000	1000							recovery file lost
GE PC	1.46	515	1000	1000	28.1						plates; T ?!; slope log(J)>1
	1.46	515	1000	1000	12.4	33.1					plates; surface indicates slip
	14.6	515	1000	1000	109	1.35					plates; γ>1 rotation
	72.3	515	1000	1000	88.8	9.32					plates; surface indicates slip

Appendix D

Creep and recovery plots

In this appendix some illustrative plots of the steady shear experiments are given. The results are discussed in § 4.2 in more detail.

Figure D.1 shows the influence of stress transients during creep. The dip in the creep curve is caused by a small knot in the load string, at the moment it passed the second air bearing (see Figure 3.4).

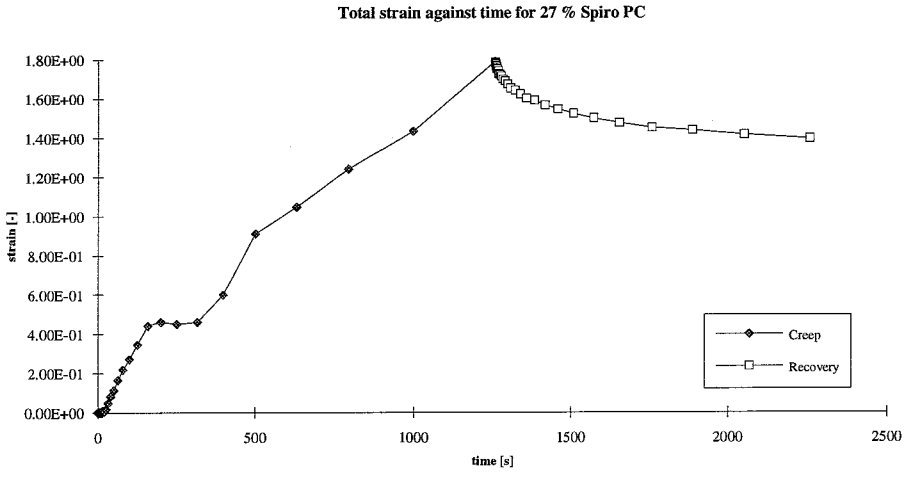

Figure D.1
The total strain during creep and recovery (T = 493 [K]; $\sigma = 1.87 \cdot 10^4$ [Pa])

Figure D.2 shows that repeating an experiment with one sample results in a reduced elastic response, even at low stress levels.

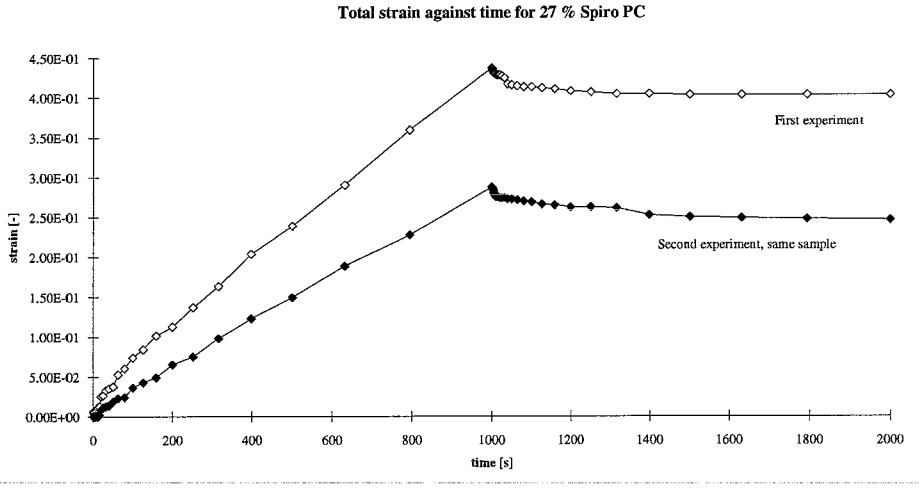

Figure D.2
The total strain during creep and recovery (T = 493 [K]; $\sigma = 9.37 \cdot 10^2$ [Pa])

Figure D.3 shows the influence of airflows in the air bearing causing a windmill effect. At high temperatures and low creep stress the recovery is overruled by an opposite rotation. At high stress, recovery does not stop because of this effect.

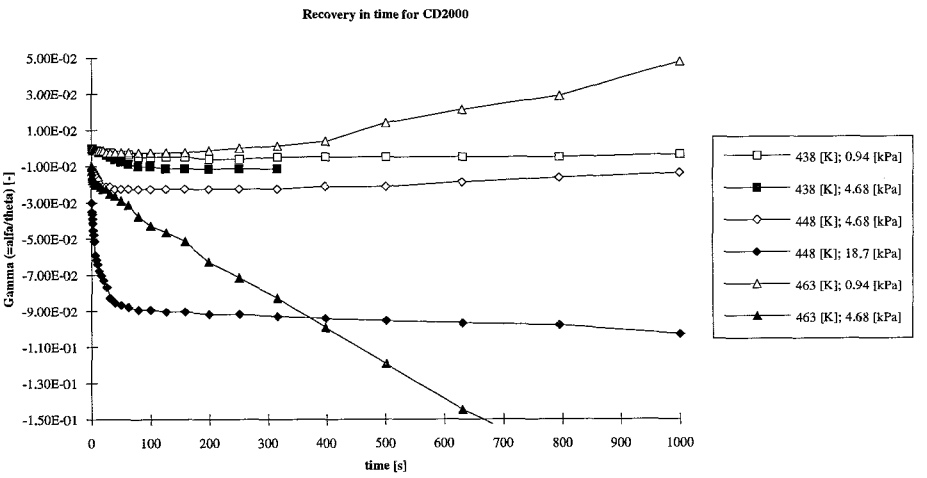

Figure D.3
Recovery for CD2000 at different temperatures and different stresses.

Figure D.4 shows a smooth strain curve for PDMS, a low T_g polymer. No start-up transients are observed and the creep quickly reaches steady-state.

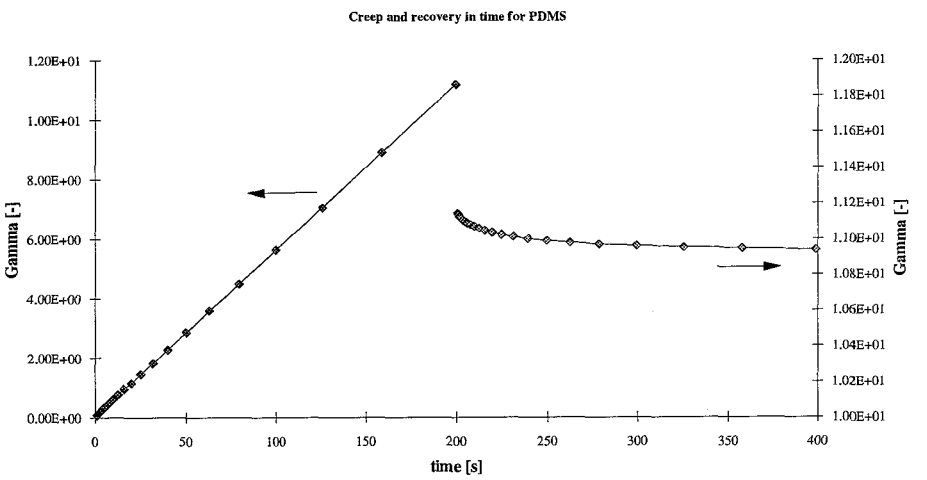

Figure D.4
Total strain curve for PDMS at roomtemperature and at a stress below 1 [kPa].

Appendix E

A single Maxwell element

As shown in Figure E.1, a single Maxwell element consists of a spring and a dashpot in series. In this appendix the equations governing the storage and loss behaviour of a single Maxwell element are given. Ideally, the behaviour of a true monodisperse polymer is governed by a single relaxation time and modulus.

Figure E.1
Single Maxwell element

For a Maxwell model, the total stress and strain are related as follows [5]:

$$\frac{d\gamma}{dt} = \frac{1}{G}\frac{d\sigma}{dt} + \frac{\sigma}{\eta} \tag{E.1}$$

where γ is the total strain, σ the total stress, G the relaxation modulus and η the viscosity. If the relaxation time is defined as $\tau = \eta/G$, equation E.1 can be written as:

$$\sigma + \tau\frac{d\sigma}{dt} = G\tau\frac{d\gamma}{dt} \tag{E.2}$$

when the stress is defined as:

$$\sigma = \sigma_0 e^{i\omega t} = (G' + iG'')\gamma \tag{E.3}$$

with storage modulus G' and loss modulus G'', substitution of equation (E.3) in (E.2) yields:

$$\sigma_0 e^{i\omega t} + i\omega\tau\sigma_0 e^{i\omega t} = \frac{G\tau i\omega\sigma_0 e^{i\omega t}}{G' + iG''} \tag{E.4}$$

From equation (E.4) it follows that:

$$G' + iG'' = \frac{Gi\omega\tau}{1 + i\omega\tau} \tag{E.5}$$

and relations for G' and G'' respectively become:

$$G' = \frac{G\omega^2\tau^2}{1 + \omega^2\tau^2} \tag{E.6}$$

$$G'' = \frac{G\omega\tau}{1 + \omega^2\tau^2} \tag{E.7}$$

Thus by substituting the plateau modulus G_N^0 for G and the zero shear viscosity η_0 for η, the storage and loss behaviour of a monodisperse polymer can be modelled to a first approximation.

From equations (E.6) and (E.7) it follows that:

$$\frac{G'}{G''^2} = (1 + \omega^2\tau^2)\ \frac{1}{G} \tag{E.8}$$

For vanishing shear and $G = G_N^0$ equation (E.8) yields:

$$J_e^0 = \lim_{\omega \to 0} \frac{G'}{G''^2} = \frac{1}{G_N^0} \tag{E.9}$$

which means that theoretically the product of G_N^0 and J_e^0 is equal to 1, if a monodisperse polymer is modelled with a single Maxwell element.

More details on experimental patterns for the storage and loss behaviour are given by Ward [5].

Acknowledgements

For their help and guidance during this project, I would like to thank my coach Reinhold Wimberger-Friedl and Hans de Bruin. I am grateful to Paul Tas and Wim Zoetelief for helping me with the oscillatory shear experiments and the shifting procedure. Marnix van Gurp and Jo Palmen of DSM Research are gratefully acknowledged for their hospitality and kind help. Finally, I would like to thank my parents for all their material and moral support throughout my college life.

Eindhoven, March 1994.